SYNTHESIS OF HOLLOW SILICA NANOPARTICLES AND THEIR STRUCTURE CONTROL FOR OPTICAL PROPERTIES

中空シリカナノ粒子の合成および光学特性付与に向けた構造制御

WALAIPORN SUTHABANDITPONG

ワライポン スタバンディトポン

DOCTOR OF PHILOSOPHY DISSERTATION

FRONTIER MATERIALS

MARCH 2016

NAGOYA INSTITUTE OF TECHNOLOGY

JAPAN

SYNTHESIS OF HOLLOW SILICA NANOPARTICLES AND THEIR STRUCTURE CONTROL FOR OPTICAL PROPERTIES

中空シリカナノ粒子の合成および光学特性付与に向けた構造制御

WALAIPORN SUTHABANDITPONG

ワライポン スタバンディトポン

DOCTOR OF ENGINEERING

FRONTIER MATERIALS

NAGOYA INSTITUTE OF TECHNOLOGY

JAPAN

MARCH 2016

SYNTHESIS OF HOLLOW SILICA NANOPARTICLES AND THEIR STRUCTURE CONTROL FOR OPTICAL PROPERTIES

中空シリカナノ粒子の合成および光学特性付与に向けた構造制御

WALAIPORN SUTHABANDITPONG

ワライポン スタバンディトポン

23513314

RECOMMENDED FOR ACCEPTANCE
BY THE ADVANCE CERAMICS RESEARCH CENTER OF
THE DEPARTMENT OF FRONTIER MATERIALS
ADVISER: PROF. MASAYOSHI FUJI

A DISSERTATION SUBMITTED IN PARTIAL FULFILLMENT OF
THE REQUIREMENTS FOR THE DEGREE OF DOCTOR OF ENGINEERING PROGRAM
IN FRONTIER MATERIALS ENGINEERING
DEPARTMENT OF FRONTIER MATERIALS
NAGOYA INSTITUTE OF TECHNOLOGY
JAPAN

MARCH 2016

ABSTRACT

Silica nanoparticles have many interesting properties; for example, a high surface area, high mechanical strength, thermal and chemical stability, permeability, and a low refractive index and especially optical properties. Therefore, these particles are effectively applied for fillers in light diffuser films as type of volumetric diffuser. The light diffuser film is an important part of backlight unit of the liquid crystal display (LCD). The film generally employs fillers as function of distributing the incident light and contributing the brightness. Therefore, structure of fillers is one of the main roles for improving performance of light diffuser films. For this reason, hollow structures of silica nanoparticles have shown a great promise to reduce light absorption of them in the diffuser films. Meanwhile, morphologies and surface properties of hollow silica nanoparticles probably affect the formation of good light diffuser film, which requires for LCDs. According to the assumptions, this work is only used of different structures of silica nanoparticles to fabricate, investigate, develop and innovative approach in producing films with high optical properties which are applied for light diffuser film. All films in the study are fabricated by a bar coating machine and cured by a UV-photo surface processor. The study is mainly organized as follows

Chapter 1 introduces general background of silica especially silica nanoparticles and hollow silica nanoparticles. It mainly focuses on optical properties of the particles to apply for fabricating light diffuser films. Meanwhile, the important of a light diffuser film in backlight unit of LCDs is briefly introduced. Moreover, light scattering involving optical properties of particles in the films is described. Based on the attempt to fabricate light diffuser films with varying morphologies of silica in nanoscale and

simplify the coating process, the goal of this study is conceptualized.

Chapter 2 describes a facile method to prepare the highly loaded silica dispersions. The method was the matching refractive indices of the silica nanoparticles and a UV-curable acrylate monomer. The obtained dispersions exhibit a long-term stability of silica dispersions during dark storage. This is due to the reduction of particle-particle attraction forces. Such dispersions were further coated on cleaned glass substrates for fabricating the thin solid silica UV-cured films. The amount of silica nanoparticles in the films was varied from 1 to 30 vol %. The coated films were investigated their optical properties by a UV-Vis-NIR spectrophotometer. The total transmittances of the films are close to the bare glass which indicates the films transparency. The increment of silica nanoparticles in the films does not significantly affect their transmittances but it improves the diffuse transmittance. The reasonable explanation is an enhancement of the multiple scattering in the films through the particles. The increased amount of silica nanoparticles also leads to the formation of the aggregated particles with a larger size and homogeneous dispersion as evidenced from the FE-SEM images. Remarkably, the thin solid silica film containing 30 vol% silica nanoparticles exhibits the highest diffuse transmittance in this experiment, which is about 20%. These indicated that the amount and distribution of the silica nanoparticles strongly affect the improved optical properties of the thin solid silica UV-cured film.

Chapter 3 applies spherical silica nanoparticles containing dense structures to modify UV-cured acrylate films. The films were prepared by coating suspension of silica-acrylate on cleaned glass substrates. The effect of the particle content on the optical properties of the modified films was investigated. The light diffusing ability of the films was also studied using an apparatus equipped with a laser lamp. Based on the

visible absorption data, the transmittance of all modified films coated substrates is lower than that of the unmodified film. The transmittance of the modified films decreases with the increasing silica content. The increasing silica content also improves the haze and light diffusing ability of the modified films. The highest haze of about 0.26 and the largest range of scattered light were achieved using the film modified with 30 vol% particles. These nanoparticles show a good potential to improve the optical properties of the UV-cured acrylate film, especially the light diffusing property that may be utilized in electronic display technologies.

Chapter 4 uses silica nanoparticles containing hollow structures to improve optical properties and light diffusing ability of UV-cured acrylate film. The hollow particles calcined at temperature of 400 °C were dispersed in a UV-curable acrylate monomer solution. The obtained dispersion was then coated on a cleaned glass substrate. The amount of the particles in the coated films was varied from 5 to 20 vol%. The optical properties and the light diffusing ability of the films were studied and then compared to those of the cleaned glass. As a result, the films become opaque when the amount of the particles increases. Although the opacity of the films was observed, the total transmittance of those was still high and close to that of cleaned glass substrate. Interestingly, a film based on 20 vol% hollow silica nanoparticles gives the highest total transmittance (93%) and diffuse transmittance (40%) when comparing to other films in this experiment. Meanwhile, the increased amount of the particles leads to the formation of aggregated particles with a larger size and homogenous dispersion as evidenced from the FE-SEM images. It also improves the optical properties of the films; for instance, diffuse transmittance and light diffusing ability. According to these results in the study, it can be concluded that the films based on the hollow silica nanoparticles as fillers have

potentially in application as light diffuser films in the LCD industry.

Chapter 5 controls the morphologies and surface properties of hollow silica nanoparticles with varying pH of HCl in the core-template removal process. The obtained particles were then dispersed in a UV-curable acrylate monomer. The dispersions containing different hollow particles were employed to fabricate silica/UV-cured polymer composite films. The high pH of HCl produces the thinner shell and larger window cavities of the hollow silica nanoparticles. Moreover, it provides the higher specific surface area of those. Meanwhile, the film embedded with hollow silica nanoparticles, which contain larger size of hollow interiors, thinner shells, larger window cavities and high specific surface area, exhibits higher total transmittance (~80%), higher diffuse transmittance (~80%) and better light diffusing ability when comparing to other composite films. Its properties still maintain at longer wavelength. Therefore, the distinct morphologies and surface properties of the hollow silica nanoparticles significantly affect the optical properties and the morphologies of the resulting films. In addition, the hollow silica nanoparticles with hierarchical structures are one of the effective inorganic fillers for light diffuser films which probably reduce the number of backlight unit in the LCD industry leading to energy saving and subsequently light-weight LCD screens.

Finally, Chapter 6 presents the overall concluding remarks of the present work and the directions for the future research. The techniques presented in all studies of this dissertation provide an informative foundation for the structures of silica nanoparticles, which affect optical properties of silica films. It is a template and a saving energy approach for the various future applications in the field of optical materials, especially light diffuser films for backlight unit in the LCD industry.

TABLE OF CONTENTS

LIST OF FIGURES

CHAPTER 1

CHAPTER 2

CHAPTER 3

CHAPTER 4

CHAPTER 5

LIST OF TABLES

CHAPTER 1

CHAPTER 2

CHAPTER 4

NOMENCLATURES

BET	Brunauer-Emmett-Teller method
BJH	Bareett-Joyner-Halenda method
CLSM	Confocal Laser Scanning Microscope
DLS	Dynamic Light Scattering
FE-SEM	Field Emission Scanning Electron Microscope
HSiNPs	Hollow silica nanoparticles
SiNPs	Silica nanoparticles
SSiNPs	Spherical silica nanoparticles
LCD	Liquid Crystal Display
TEM	Transmission Electron Microscope
TGA	Thermogravimetric analysis
UV-Vis	UV-Vis spectrophotometer
XRD	X-Ray Diffraction

CHAPTER 1

GENERAL INTRODUCTION

Nowadays, nanotechnology is extensively applied for various major scientific and technological fields; for example, electronic, medication, environment, agriculture, and energy [1-3]. This involvement includes the structure of particles on the nanometer scale. The nanoparticles often exhibit novel physical, chemical, biological and other properties, which are different from individual atoms and bulk samples of the same material. Therefore, nanoparticles are one of the new tasks to develop new classes of advanced materials for supporting future technologies.

The variety of inorganic nanoparticles including silica, silicon nitride, silicon carbide, alumina, titania, zinc oxide and etc., have been extensively applied for diverse electronics to enhance mechanical, thermal, electrical and optical properties, and new functionality [4-7]. Among these nanoparticles, silica nanoparticles are much attractively considered as fillers in light diffuser films of backlight unit in the liquid crystal display (LCD) industry [8, 9]. This is due to their good light transmittance and diffusion capacity. While the structure of silica nanoparticles is one of the important factors for achieving high optical properties of light diffuser films which is suitable for the LCD industry. With these reasons, this study had mainly focused on the synthesis hollow silica nanoparticles and their structure control for optical properties.

In this chapter, general properties of silica and light diffuser films are basically introduced. Until now many researchers have reviewed or published the synthesis, properties and applications in the LCD industry of silica. The work has briefly reviewed some recent developments in preparation, and properties of silica nanoparticles and hollow silica nanoparticles, including application of them for light diffuser films.

1.1 Silica

Silica, also known as silicon dioxide (SiO_2), is a chemical compound of the two most abundant elements in the Earth's crust, which are silicon and oxygen [10]. Its appearance is both in the form of an amorphous and a variety of crystalline. There are three main crystalline forms of silica; for instance, quartz, tridymite and cristobalite. Silica with a high purity grade is called as fused silica and is primarily used in the electronic industry [1, 11-13]. It is also applied as a refractory material and a substance in casting industry. This is due to its properties that are very high refractive index, good electric insulation, thermal stability and abrasion resistance. Some general properties of fused silica are shown in the table below [10].

Table 1.1 General properties of fused silica

Properties	
Density (g/cm^3)	2.2
Thermal conductivity ($Wm^{-1}K$)	1.4
Melting point (°C)	1600

Some of its properties are usually size dependent because a number of atoms residing on silica surface will increase while the particle size of silica will decrease [14]. When the size is smaller than 5 nm, more than half of the Si atoms are present on the surface [15]. Therefore, the surface should have one or more silanol groups (≡Si-OH) leading to increase silanol groups per grams of silica. The number of silanol groups is interrelated to the specific surface area of silica. According to these reasons, the

decrease in the nano-sized silica probably provides distinctive properties, which are different from its basic properties. Meanwhile, morphologies of silica nanoparticles are also controlled to tune them for diverse applications.

1.1.1 Silica nanoparticles

Silica nanoparticles have many interesting properties, including a high surface area, high mechanical strength, thermal and chemical stability, permeability, and a relatively low refractive index [1-3, 12, 16-18]. They also contain unique features: low light absorption in the ultraviolet-visible (UV-vis) and near-infrared (NIR) regions, dielectric electrons, and low toxicity. Therefore, the nanoparticles are of great interest to various applications in many major chemical fields; for example, electronic, optic, sensing, insulating, sorption, separation, catalysis, solar cell and medication. One of the prominent applications of silica nanoparticles is filler or reinforcement in advanced composite materials [1]. The most important feature of silica-polymer nanocomposite is the ability to attain homogeneous filler dispersion, which affects the overall performance of the nanocomposite. The type of used polymer matrix is also one of the main roles for the performance of a nanocomposite. Recently, many approaches have been developed for preparing silica-polymer nanocomposite for wide applications in adhesion, biomaterial, protective coatings, microelectronics, optical materials, and especially light diffuser films [19- 30]. The incorporation of silica nanoparticles in polymer films not only enhances mechanical properties of the film but also reduce its thermal degradation at high temperature [31]. Furthermore, it can improve insulation properties of the film.

1.1.2 Hollow silica nanoparticles

Hollow silica nanoparticles compose of hollow interiors and solid shells [32]. The hollow interiors act as storage basin or micro-reactor while the solid shells provide controlled release pathways or substantial reaction [33]. According to their advanced structures, these nanoparticles have a great promise for various applications such as adsorbents, delivery carriers, catalysts, biomedical detectors, building blocks for photonic crystals, and optical displays [34-36]. Moreover, silica containing a hollow structure probably allows light penetration through it hollow interior that result in a lower light absorption as compared to silica with a dense structure. This can be illustrated by Fig. 1.1.

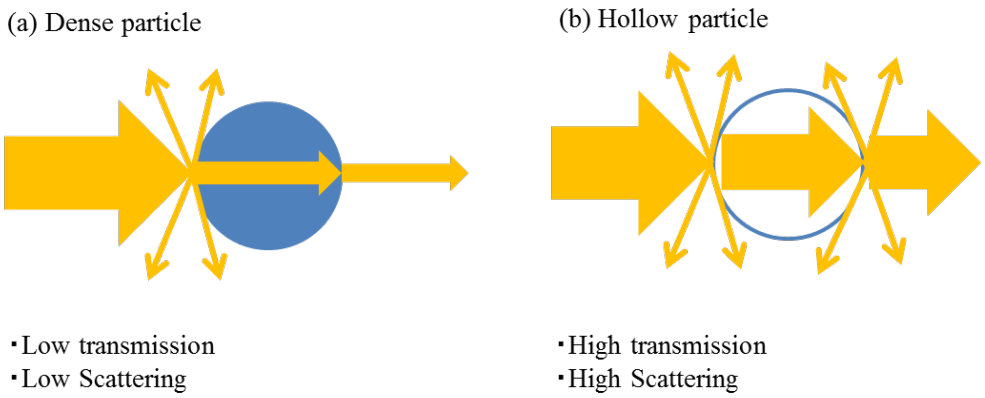

Fig. 1.1 Interaction of light and silica with: (a) dense structure and (b) hollow structure.

Moreover, the light is nonspecifically adsorbed by pore on a solid shell of silica and may occur light scattering and refraction latterly [36]. This is due to the difference refractive index between the air in the hollow interior and the solid shell. Therefore, large hollow interiors of hollow silica nanoparticles are probably required for light

penetration and scattering. Meanwhile, thinner shells of the hollow silica nanoparticles are necessary for low light absorption and more light refraction. These can improve optical properties of the hollow silica nanoparticles and subsequently provide advanced functional materials. The design of shell structures of hollow silica nanoparticles, including diameter, shape, thickness, surface roughness, morphology, and pore size, is precisely controlled by numerous synthesis processes. Therefore, many approaches have been exploited to synthesize hollow silica nanoparticles with respect to meso-structure shells, which exhibit unique properties of both macroporous and mesoporous structures in one single piece [33]. The well-known approaches are sol-gel and template methods [32, 33]. The template method can be typically divided into two types; for example, hard (e.g. polymer, silica or carbon spheres) [37-40] and soft templates (e.g. micelles or vesicles) [41, 42]. Comparing to sol-gel method, the template method has attracted much attention because the diameter and shape of hollow silica nanoparticles are simply controlled by those of used templates [43-46]. It can also design shell thickness of the hollow silica nanoparticles by ratio of silica source and template, reaction time, and etc [47, 48]. Therefore, both hollow interior size and shell thickness of hollow silica nanoparticles being two independent variables in optical designs of the optical displays can be tuned by the essible choices from the template method.

1.2 Light diffuser film

A light diffuser film or plate, also known as optical diffuser, plays key optical component in backlight unit of various LCD devices, such as TVs, overhead projectors, handheld game consoles, and mobile phones [30, 49-52]. The backlight unit supply light

to LCD panels since they cannot emit the light themselves [50]. A typical configuration of the backlight unit comprises of a light emitter (usually cold cathode fluorescent lamps (CCFLs) or a light-emitting diode (LED) matrix), a light guide plate (LGP), a reflection film, one/two diffuser film(s) and one/two brightness enhancement film(s) (BEFs) [50, 53, 54]. All those mentioned components are shown in Fig. 1.2. The light diffuser film has a function of scattering and homogenizing the incident light from sources over a wide angle. As a result, the images are suitable and wide view-angle images to displays [28-30].

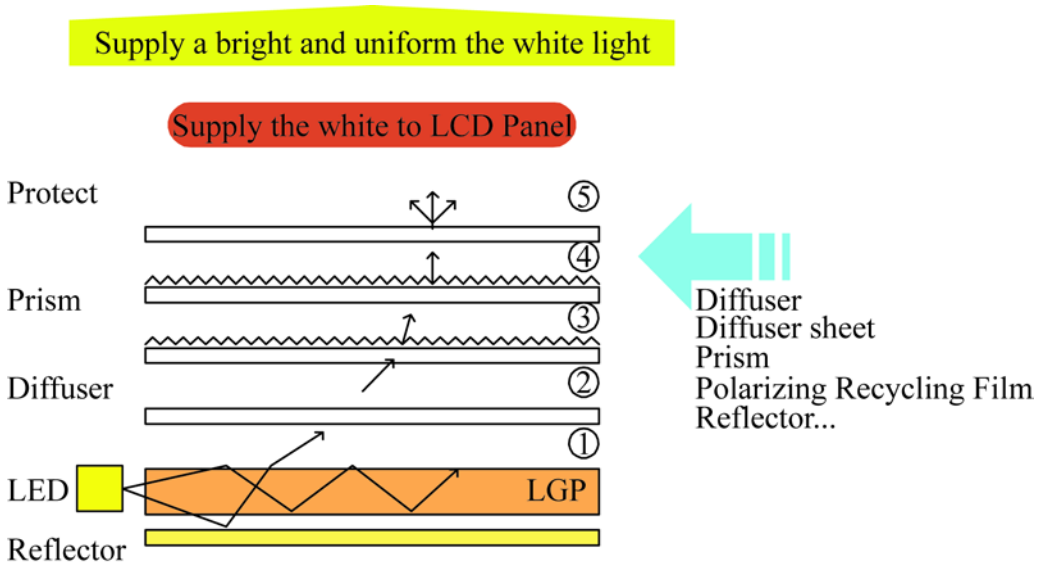

Fig. 1.2 Typical configuration of the backlight unit [54].

Generally, there are two main types of light diffuser films that achieve the high efficient light diffusers used in backlight unit of LCDs. The first type is surface-relief diffuser film, which relies on microstructures of the surface layers to scatter light [49]. The second type is called volumetric diffuser film, which mainly depends on the difference in refractive indices between light diffusing particles (LDPs) or fillers and

binding resin. The surface-relief diffuser film commonly contains higher light transmittance than the volumetric diffuser film because of no light absorption by particles. However, the most methods used for fabricating the microstructures on the surface-relief, including microlens [55, 56], pyramids [57, 58], hemisphere [59] and other microstructures [60, 61], require complicated processes using expensive equipments [29, 30, 49, 50]. Since the volumetric diffuser film is not only fabricated by a versatile method but also capable of distributing the incident light and contributing the brightness in the viewing, this kind of diffuser film currently dominate the diffuser market [50].

The volumetric diffuser film comprises of three major components which are light diffusing particles (LDPs) or fillers, binding resin, and a transparent substrate [29, 50]. It is basically fabricated by coating a mixture of fillers and binder resin on a substrate. After solvent evaporation, the surface of coating layer becomes rough due to the fillers [62]. The surface roughness affects an outer haze while the difference in refractive indices between the fillers and the binder resin has an influence on an inner haze. The haze values are defined as the ratio between diffuse transmittance and total transmittance (Haze = $T_{diffuse}/T_{total}$). A summation of the outer haze and the inner haze is total haze. This diffuser film is more possible to scatter and homogenize the incident light from sources to avoid the occurrence of local concentrated light when either the outer or the inner haze of the film increases. Accordingly, fillers have significantly influence on optical performance and light diffusing ability of the film. Many efforts have been developed on optical materials to fabricate volumetric diffuser films. One of the dominant researches is the study of Wang et al [28] who worked on the fabrication of volumetric diffuser films using silicone emulsions as a substrate and micro-scale

water drop as fillers. Another interesting study is from Guo et al [29] who presented organic-inorganic hybrid materials as fillers to achieve good light diffusing film with high both of transmittance and haze. The organic-inorganic fillers were prepared via the electrostatic attraction between positively charged polymethyl methacrylate (PMMA) spheres and negatively charged SiO_2 nanoparticles before blending with polyacrylate latex to produce strawberry-like PMMA/SiO_2 composite microspheres. This previous study is similar to the research of Hu et al [52] who also prepared the PMMA microspheres incorporated with a small amount of inorganic nanoparticles to prepare fillers used in multifunctional optical diffuser films. The multifunctional optical diffusers based on hybrid polysiloxane@CeO_2@PMMA microspheres were successfully prepared by UV curing process. The hybrid microspheres improved properties of the diffusers; for example, heat resistance, mechanical, UV-shielding, fluorescence, well NIR absorption and anti-aging ability, which had a potential application in absorbing materials and night vision LCD monitor products. Moreover, Ahn and co-worker [30] used hemispherical PMMA as filler for fabricating an optical diffuser with electrospray coating process. Meanwhile, Zhao et al [63] enhanced the light diffusion property of polycarbonate composites by TiO_2 coated silicate micro-spheres for light diffusion applications.

In addition, diverse applications of light diffuser films, Li et al [50] had conducted a study of the correlations of optical properties of light diffuser films as functions of the coating thickness/particle diameter ratio and beads/resin weight ratio. These correlations were empirically developed as a power law model and an exponential model, respectively. The developed correlations may effectively reduce the time required for designing light diffuser films in the backlight unit. Moreover, the group of Mingyan et

al [64] presented a mathematical model of direct type LED backlight. The model was the optimization and was designed as the micro-structures on the surface of the diffuser plate, which were the critical factors in manufacturing diffuser plates of good optical properties. Meanwhile, mechanical and thermal properties of light diffuser films are essential for their application. The research works done by Sun et al [30] prepared nano-silica reinforced hybrid light-diffusing films. The films prepared by light-diffusing agent (organosilicone resin, KMP-590) and nano-silica exhibited the excellent optical, thermal stability and mechanical properties, which might be suitable for anti-glare LED application.

1.3 Light scattering

The nature of light interacted with fillers and important features in a light diffuser film are governed by light scattering in the systems [65, 66]. Therefore, understanding the occurrence of the light scattering is essential for developing and optimizing the cost and performance of backlight unit in the LCD industry.

Light scattering is generally occurred when light passes through a material with different refractive indices. Meanwhile, the difference between particle size and incident light wavelength also produces the light scattering. Common aspects of light scattering are basically discussed with the following subject headlines which are Rayleigh scattering and Mie scattering.

1.3.1 Rayleigh scattering

Rayleigh scattering is named after the British physicist Lord Rayleigh (also known as John William Strutt). This subject describes the dominant elastic scattering of light or

electromagnetic radiation which involves particles much smaller than the incident wavelength [67]. The particles are individual atoms or molecules. Moreover, this type of scattering occurs if light passes through a transparent solid and liquid. Remarkably, the Rayleigh scattering is most seen in gases. The sample of Rayleigh scattering from air molecules that causes of the blue sky. It can be illustrated in Fig. 1.3.

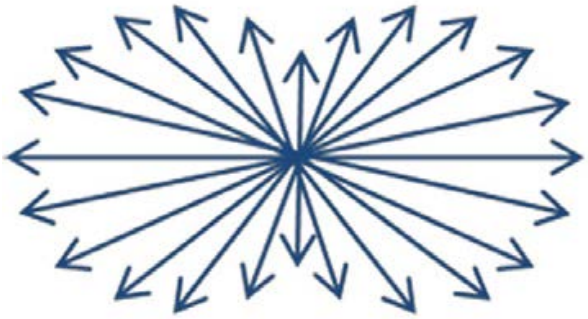

Fig 1.3 Rayleigh scattering from air molecules [29].

The Rayleigh scattering defines that light scattering depends on size of the particles and wavelength of the incident light [29, 68]. The intensity of the scattering is inversely proportional to the fourth power of the wavelength, which can be expressed by the following formula

$$I \propto \frac{1}{\lambda^4} \tag{1.1}$$

From the above formula, I is an intensity of the light scattering and λ is wavelength of the incident light. Accordingly, the intensity rapidly drops when the wavelength increases or the particle diameter decreases.

1.3.2 Mie scattering

Mie scattering named after the German physicist Gustav Mie describes for light scattering, which particle size is similar to or larger than a wavelength of the incident light [29, 65, 66, 69]. Meanwhile, the intensity of Mie scattering is independent to the particle size. Moreover, the direction of the light scattering is towards that of the incident light as illustrated in Fig. 1.4.

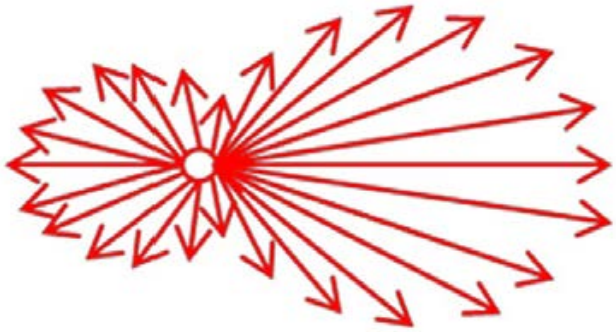

Fig 1.4 Schematic diagram of the direction of light scattering based on Mie scattering [29].

The Mie scattering is prominently of a single or isolated particle, which is called single scattering or dependent scattering [70]. Since the single scattering is independent of neighboring particles therefore the total scattering of a material embedded with isolated particles is calculated by a summation of light scattering by each individual particle. However, real particles in a film often approach another one. Therefore, the light scattering of each particle or cluster, being known as dependent scattering or multiple scattering, is dependent to the other ones. In the case of the multiple scattering, each particle is more illuminated by both the incident light and the secondary scattering than from other particles, as a result, the optical properties of the film increases. To

understand the complex of the light scattering in an actual film, many efforts have been devoted to study on the multiple scattering based on Mie scattering. For example, Kubelka and Munk further investigated the light scattering of the entire paint film embedded with millions of millions of particles. They reported a simplified form of multiple light scattering behaviors in aggregated particles, which will be widely applied for semitransparent materials.

1.4 Objective of this work and thesis organization

The objective of this work is to develop novel and facile method to fabricate light diffuser films with high optical properties using silica. Meanwhile, the effect of silica structure on optical properties of the light diffuser films also involves in this study.

The dissertation is organized as follows:

In Chapter 2, the details on preparation of highly loaded silica nanoparticles dispersions by matching refractive indices of silica nanoparticles and a binder resin for fabricating silica films are given. The optical properties of the silica films were analyzed. Based on the results, the effect of the silica loading on the optical properties of the films was also discussed.

In Chapter 3, it describes the application of spherical silica nanoparticles with dense structures for modifying UV-cured acrylate films. The aim of this experiment is to improve optical properties and light diffusing ability of the films. The films were prepared by coating dispersions of the particles in UV-curable acrylate monomer on cleaned glass substrates with a bar coating machine. The light diffusing ability is related to a haze value of the prepared films. The haze value was then measured at the

wavelength of 532 nm, which corresponded to the incident wavelength of a laser lamp used for studying the light diffusing ability. Moreover, the influence of silica content on optical properties of the films was investigated. The morphologies of the films were further studied to understand the formation of those.

In Chapter 4, it presents the characterization and utilization of silica nanoparticles with hollow structures for fabricating light diffuser films. Meanwhile, the quantitative effect of hollow silica nanoparticles on optical properties and light diffusing ability of the films is also given. A facile method to prepare the films was coating dispersions of the particles in a UV-curable acrylate monomer on a cleaned glass substrate by a bar coating machine. The effect of silica content on optical properties of the fabricated films was disscussed. The light diffusing ability of the films was also characterized. The results can be implied the performance of the films for being a light diffuser film.

Then Chapter 5 explicates a method for controlling structure of hollow silica nanoparticles that is varying of pH of acid in the core-template removal process. The hollow particles were firstly synthesized using calcium carbonate as an inorganic core-template and tetraethoxysilane as silica sources. The obtained particles which have different structures (e.g. shell thickness, hollow interior) were applied for fabricating light diffuser films. The optical properties of the films were characterized. The effect of hollow silica structure on morphologies of the films was studied because it related to light diffusing ability of those.

Finally, in Chapter 6, the concluding remarks of the present work were stated and the future directions of this research work were recommended.

References

[1] I.A. Rahman and V. Padavettan, Synthesis of silica nanoparticles by sol-gel: size-dependent properties, surface modification, and applications in silica-polymer nanocomposites-A review, *J Nanomater.* (2012) Article ID 132424.

[2] A. Liberman, N. Mendez, W.C. Trogler and A.C. Kummel, Synthesis and surface functionalization of silica nanoparticles for nanomedicine, *Surf Sci Rep.* **69** (2014) 132-158.

[3] M. Auffan, J. Rose, J.Y. Bottero, G.V. Lowry, J.P. Jolivet and M.R. Wiesner, Towards a definition of inorganic nanoparticles from an environmental, health and safety perspective, *Nat. Nanotechnol* **4** (2009) 634-641 .

[4] K. Ohashi, K. Nakai, S. Kitayama and T. Kawaguchi, Mechanisms of hydrogen evolution and stabilization of UV-cured urethane acrylate resin for coating of optical fiber, *Polym. Degrad. Stab.* **22** (1988) 223-232.

[5] G. Harbers, S.J. Bierhuizen and M.R. Krames, Performance of high power light emitting diodes in display illumination applications, *J. Display Technol.* **3** (2007) 98-108.

[6] Y. Du, L.E. Luna, W.S. Tan, M.F. Rubner and R.E. Cohen, Hollow silica nanoparticles in UV-visible antireflection coatings for poly(methyl methacrylate) substrates, *ACS Nano* **4** (2010) 4308-4316.

[7] Z. Wu, J. Walish, A. Nolte, L. Zhai, R.E. Cohen and M.F. Rubner, Deformable antireflection coatings from polymer and nanoparticle multilayers, *Adv. Mater.* **18** (2006) 2699-2702.

[8] Y. Jung, T.H. Yeo, W. Yang, Y. Kim, K. Woo and J. Moon, Direct photopatternable organic-inorganic hybrid materials as a low dielectric constant passivation layer for thin film transistor liquid crystal displays, *J. Phys. Chem. C* **115** (2011) 25056-25062.

[9] S. Song, Y. Sun, Y. Lin and B. You, A facile fabrication of light diffusing film with LDP/polyacrylates composites coating for anti-glare LED application, *Appl. Surf. Sci.* **273** (2013) 652-660.

[10] R. Nandanwar, P. Singh and F.Z. Haque, Synthesis and properties of silica nanoparticles by sol-gel method for the application in green chemistry, *Mat. Sci. Res. India.* **10** (2013) 85-92.

[11] A. Gupta, S. Hartner and H. Wiggers, Optical and electrical properties of silicon nanoparticles, in: *Proc. Nanoelectronics Conference (INEC)*, Hong Kong, 2010, http://dx.doi.org/10.1109/INEC.2010.5424734.

[12] W. Wang, J.C. Martin, X. Fan, A. Han, Z. Luo and L. Sun, Silica nanoparticles and frameworks from rice husk biomass, *ACS Appl. Mater. Interfaces* **4** (2012) 977-981.

[13] C. Huan and S.S. Qing, Silicon nanoparticles: Preparation, properties, and applications, *Chin. Phys. B* **23** (2014) 088102 .

[14] K.J. Klabunde, 2001, *Nanoscale Materials in Chemistry*, Wiley-Interscience, NY, USA.

[15] L.L. Hench and J. K. West, The Sol-Gel process, *Chemical Reviews* **90** (1990) 33-72.

[16] S. Xu, S. Hartvickson and J.X. Zhao, Increasing surface area of silica nanoparticles with a rough surface, *ACS Appl. Mater. Interfaces* **3** (2011) 1865-1872.

[17] C.H. Ho, Y.H. Hsiao, D.H. Lien, M.S. Tsai, D. Chang, K.Y. Lai, C.C. Sun and J.H. He, Enhanced light-extraction from hierarchical surfaces consisting of p-GaN microdomes and SiO_2 nanorods for GaN-based light-emitting diodes, *Appl. Phys. Lett* **103** (2013) 161104.

[18] T. Ribeiro, C. Baleizão and J.P.S. Farinha, Functional films from silica/polymer nanoparticles, *Materials* **7** (2014) 3881-3900.

[19] T.J. Wood, L.J. Ward and J.P.S. Badyal, Super-adhesive polymer-silica nanocomposite layers, *ACS Appl. Mater. Interfaces* **5** (2013) 9678-9683.

[20] Y. Yamamoto, S. Fujii, K. Shitajima, K. Fujiwara, S. Hikasa and Y. Nakamura, Soft polymer-silica nanocomposite particles as filler for pressure-sensitive adhesives, *Polymer* **70** (2015) 77-87.

[21] C.J. Wu, A.K. Gaharwar, P.J. Schexnailder and G. Schmidt, Development of biomedical polymer-silicate nanocomposites: A materials science perspective, *Materials* **3** (2010) 2986-3005.

[22] Y.Z.K. Lahijania, M. Mohseni and S. Bastani, Characterization of mechanical behavior of UV cured urethane acrylate nanocomposite films loaded with silane treated nanosilica by the aid of nanoindentation and nanoscratch experiments, *Tribology International* **69** (2014) 10-18.

[23] P. Manoudis, S. Papadopoulou, I. Karapanagiotis, A. Tsakalof, I. Zuburtikudis and C. Panayiotou, Polymer-Silica nanoparticles composite films as protective coatings for stone-based monuments, *Journal of Physics: Conference Series* **61** (2007) 1361-1365.

[24] Y. Jung, T.H. Yeo, W. Yang, Y. Kim, K. Woo and J. Moon, Direct photopatternable organic-inorganic hybrid materials as a low dielectric constant passivation layer for thin film transistor liquid crystal displays, *J. Phys. Chem. C* **115** (2011) 25056-25062.

[25] E. Logakis, D. Fragiadakis and P. Pissis, Low-k polyimide/silica nanocomposites for microelectronics applications, in: *Proc 25th INTERNATIONAL CONFERENCE ON MICROELECTRONICS (MIEL 2006)*, BELGRADE, SERBIA AND MONTENEGRO (2006).

[26] B.J. Scott, G. Wirnsberger and G.D. Stucky, Mesoporous and mesostructured materials for optical applications, *Chem. Mater.* **13** (2001) 3140-3150.

[27] A. M. Kauffman, A simple immersion method to determine the refractive index of thin silica films, *Thin Solid Films* **1** (1967) 131-136.

[28] J.H. Wang, S.Y. Lien, J.R. Ho, T.K. Shih, C.F. Chen, C.C. Chen and W.T. Whang, Optical diffusers based on silicone emulsions, *Opt. Mater* **32** (2009) 374-377.

[29] S. Guo, S. Zhou, H. Li and B. You, Light diffusing films fabricated by strawberry-like PMMA/SiO_2 composite microspheres for LED application, *J. Colloid Interface Sci.* **448** (2015) 123-129.

[30] X. Sun, N. Li, J. Hang, L. Jin, L. Shi, Z. Cheng and D. Shang, Nano-silica reinforced hybrid light-diffusing films with enhanced mechanical and thermal properties, *Optica Applicata* **45** (2015) 393-404.

[31] S.S. Ray and M. Okamoto, Polymer/layered silicate nanocomposites: A review from preparation to processing. *Prog. Polym. Sci.* **28** (2003) 1539-1641.

[32] C. Takai, H. Watanabe, T. Asai and M. Fuji, Determine apparent shell density for evaluation of hollow silica nanoparticle, *Colloids and Surfaces A: Physicochem. Eng. Aspects* **404** (2012) 101-105.

[33] R.V.R. Virtudazo, M. Fuji, C. Takai and T. Shirai, Fabrication of unique hollow silicate nanoparticles with hierarchically micro/mesoporous shell structure by a simple double template approach, *Nanotechnology* **23** (2012) 485608.

[34] X.Y. Lai, J. Li, B.A. Korgel, Z.H. Dong, Z.M. Li, F.B. Su, J.A. Du and D. Wang, General synthesis and gas-sensing properties of multiple-shell metal oxide hollow microspheres, *Angew. Chem. Int. Ed.* **50** (2011) 2738-2741.

[35] J.F. Chen, H.M. Ding, J.X. Wang and L. Shao, Preparation and characterization of porous hollow silica nanoparticles for drug delivery application, *Biomaterials* **25** (2004) 723-727.

[36] Y. Guo, R.A. Davidson, K.A. Peck and T. Guo, Encapsulation of multiple large spherical silica nanoparticles in hollow spherical silica shells, *J. Colloid Interface Sci.* **445** (2015) 112-118.

[37] X. Du and J.H. He, Spherical silica micro/nanomaterials with hierarchical structures: Synthesis and applications, *Nanoscale* **3** (2011) 3984-4002.

[38] G.X. Yang, S.L. Gai, F.Y. Qu and P.P. Yang, SiO_2@YBO_3:Eu^{3+} Hollow mesoporous spheres for drug delivery vehicle, *ACS Appl. Mater. Interfaces* **5** (2013) 5788-5796.

[39] Y. Su, R. Yan, M.H. Dan, J.X. Xu, D. Wang, W.Q. Zhang and S.X. Liu, Synthesis of hierarchical hollow silica microspheres containing surface nanoparticles employing the quasi-hard template of Poly (4-vinylpyridine) microspheres, *Langmuir* **27** (2011) 8983-8989.

[40] F.P. Chang, Y. Hung, J.H. Chang, C.H. Lin and C.Y. Mou, Enzyme encapsulated hollow silica nanospheres for intracellular biocatalysis, *ACS Appl. Mater. Interfaces* **6** (2014) 6883-6890.

[41] Z.G. Teng, X.D. Su, Y.Y. Zheng, J. Sun, G.T. Chen, C.C. Tian, J.D. Wang, H. Li, Y.N. Zhao and G.M. Lu, Mesoporous silica hollow spheres with ordered radial mesochannels by a spontaneous self-transformation approach, *Chem. Mater.* **25** (2013) 98-105.

[42] D.Y. Li, Z.C. Guan, W.H. Zhang, X. Zhou, W.Y. Zhang, Z.X. Zhuang, X.R. Wang and C.J. Yang, Synthesis of uniform-size hollow silica microspheres through interfacial polymerization in monodisperse water-in-oil droplets, *ACS Appl. Mater. Interfaces* **2** (2010) 2711-2714.

[43] R.V.R. Virtudazo, H. Tanaka, H. Watanabe, M. Fuji and T. Shirai, Facile preparation in synthesizing nano-size hollow silicate particles by encapsulating colloidal-hydroxyapatite nanoparticles, *J. Mater. Chem.* **21** (2011) 18205-18207.

[44] X.W. Lou, C.L. Yuan, and L.A. Archer, Double-walled SnO_2 nano-cocoons with movable magnetic cores, *Adv. Mater.* **19** (2007) 3328-3332.

[45] M. Fuji, T. Shin, H. Watanabe and T. Takei, Shape-controlled hollow silica nanoparticles synthesized by an inorganic particle template method, *Adv. Powder Technol.* **23** (2012) 562-565.

[46] R.A. Caruso, A. Susha and F. Caruso, Multilayered titania, silica, and laponite nanoparticle coatings on polystyrene colloidal templates and resulting inorganic hollow spheres, *Chem. Mater.* **13** (2001) 400-409.

[47] F. Caruso, Hollow capsule processing through colloidal templating and selfassembly, *Chem. Eur. J.* **6** (2000) 413-419.

[48] D.K. Yi, S.S. Lee, G.C. Papaefthymiou and J.Y. Ying, Nanoparticle architectures template by SiO_2/Fe_2O_3 nanocomposites, *Chem. Mater.* **18** (2006) 614-619.

[49] J. Zhuang, D. Wu, Y. Zhang, H. Xu, Z. Zhao and X. He, Investigation on optical property of diffuser with 3D microstructures, *Optik* **125** (2014) 7186-7190.

[50] H.P. Kuo, M.Y. Chuang and C.C. Lin, Design correlations for the optical performance of the particle-diffusing bottom diffusers in the LCD backlight unit, *Powder Technol.* **192** (2009) 116-121.

[51] C.T. Pan, M.F. Chen, P.J. Cheng, Y.M. Hwang, S.D. Tseng and J.C. Huang, Fabrication of gapless dual-curvature microlens as a diffuser for a LED package, *Sens. Actuators, A* **150** (2009) 156-167.

[52] J. Hu, Y. Zhou and X. Sheng, Optical diffusers with enhanced properties based on novel polysiloxane@CeO_2@PMMA fillers, *J. Mater. Chem. C* **3** (2015) 2223-2230.

[53] A. Kanemitsu, T. Sakamoto and H. Iyama, Light Diffuser Plates for LCD-TV Backlight Systems, R&D Report "*Sumitomo Kagaku*", **1** (2007).

[54] Basic structure of LCD module, [Online]. Available from: http://hicel.en. ec21. com/Technical_Summary_of_Backlight_Unit--3029629_3029633.html. [2015, December 25].

[55] P. Ruffieux, T. Scharf, I. Philipoussis, H.P. Herzig, R. Voelkel and K.J. Weible, Two step process for the fabrication of diffraction limited concave microlens arrays, *Opt. Express* **16** (2008) 19541-19549.

[56] S.I. Chang and J.B. Yoon, Microlens array diffuser for a light-emitting diode backlight system, *Opt. Lett.* **31** (2006) 3016-3018.

[57] S. Ahn and G. Kim, An electrosprayed coating process for fabricating hemispherical PMMA droplets for an optical diffuser, *Appl. Phys. A* **97** (2009) 125-131.

[58] C.F. Lin, Y.B. Fang and P.H. Yang, Optimized Micro-Prism diffusion film for slim-type bottom-lit backlight units, *J. Disp. Technol.* **7** (2011) 3-9.

[59] L. Liwei, T.K. Shia and C.J. Chiu, Silicon-processed plastic micropyramids for brightness enhancement applications, *J Micromech Microeng.* **10** (2000) 395-400.

[60] E. Hein, D. Fox and H. Fouckhardt, Glass surface modification by lithography-free reactive ion etching in an Ar/CF_4 -plasma for controlled diffuse optical scattering, *Surf. Coat. Technol.* **205** (2011) S419-S424.

[61] K.S. Lee, B. Jeon and S.W. Cha, Development of a multilayered optical diffusion sheet using microcellular foaming technology, *Polym.-Plast. Technol. Eng.* **50** (2011) 102-111.

[62] B.T. Liu and Y.T. Teng, A novel method to control inner and outer haze of an anti-glare film by surface modification of light-scattering particles, *J. Colloid Interface Sci.* **350** (2010) 421-426.

[63] Y. Zhao, P. Ding, C. Ba, A. Tang, N. Song, Y. Liu and L. Shi, Preparation of TiO2 coated silicate micro-spheres for enhancing the light diffusion property of polycarbonate composites, *Displays* **35** (2014) 220.

[64] L. Mingyan, W. Daming, Z. Yajun and Z. Jian, Optimization and design of LCD diffuser plate with micro-semisphere structure, *Procedia Eng.* **16** (2011) 306.

[65] W. Hergert and T. Wriedt (eds.), 2012, *The Mie Theory: Basics and Applications, Springer*, DOI: 10.1007/978-3-642-28738-1_2.

[66] M.P. Diebold, 2014, *Application of Light Scattering to Coatings*; Springer, DOI: 10.1007/978-3-319-12015-7.

[67] A.T. Young, Rayleigh scattering, *Applied Optics* **20 (4)** (1981) 553-535.

[68] S.E. Yancey, W. Zhong, J.R. Heflin and A.L. Ritter, The influence of void space on antireflection coatings of silica nanoparticle self-assembled films, *J. Appl. Phys* **99** (2006) 034313.

[69] R. Barchini, J.G. Gordon II and M.W. Hart, Multiple light scattering model applied to reflective display materials, *Jpn. J. Appl. Phys.* **37** (1998) 6662.

[70] A. Rastar, M.E. Yazdanshenas, A. Rashidi and S.M. Bidoki, Theoretical review of optical properties of nanoparticles, *J. Eng. Fiber Fabr.* **8** (2013) 85-96.

CHAPTER 2

PREPARATION OF HIGHLY LOADED SILICA NANOPARTICLE DISPERSIONS BY MATCHING REFRACTIVE INDICES OF THE SILICA AND A BINDER RESIN FOR FABRICATING SILICA FILMS WITH HIGH OPTICAL PROPERTIES

2.1 Introduction

The diversity of UV-curable monomers and oligomers, including acrylates, acrylated urethanes, epoxies and vinyl ethers, allow the UV-coating formulator many choices in achieving the desired properties [1]. A liquid resin rapidly transforms into a solid material under intense UV illumination within seconds at ambient temperature by the formation of a highly crosslinked polymer [2]. Due to its high crosslink density, the UV-cured polymer exhibits a better adhesive property [3], hardness [4, 5], mechanical property [5, 6], elastic property [6] and excellent abrasion resistance [5]. Consequently, the UV-cured polymer has been used in various industries as adhesive materials [3], jet-printed ink [7] and hard transparent coatings for optical materials [5, 8].

So far, optical materials have been extensively used in our daily life for various applications such as lens, automobile parts, and screen panel displays in many electronic devices [9-12]. The brightness and resolution are needed for achieving highly effective images. However, the issues of contrast ratio, resistance capacitance (RC) time delay, pixel resolution, reflection, glare, and transmittance (or brightness) are crucial problems especially when the liquid crystal display (LCD) panel size is enlarged. Due to the low quality of the final image, the transmittance and glare of the LCD panel must be improved in order to achieve both a higher brightness and better resolution. To solve these problems, the coating technology using various materials has been developed to increase the transmittance and reduce the glare of the LCD. Recently, a light diffusing film, a material with a high transmittance and light diffusivity [13], has been extensively investigated. This type of film has also an excellent anti-glare property so it is widely applied in LED light systems. The organic/inorganic hybrids have been extensively used for fabricating light diffusing films because of their unique and enhanced

mechanical, thermal, electrical and optical properties [14, 15]. A variety of inorganic colloidal particles including titanium dioxide, copper oxide, aluminum hydroxide, alumina and silica have been combined with an organic polymer [15, 16] to produce the hybrid materials. Among these materials, organic-silica hybrid materials are of great interest due to their high transmission, low refractive index, easy preparation and low cost [14, 17-18]. Konjhodzic et al. were able to produce a low refractive index film using mesoporous silica and a nonionic triblock copolymer, $HO(CH_2CH_2O)_{20}(CH_2CH(CH_3)O)_{70}(CH_2CH_2O_{20})H$ [19]. This hybrid film with a sufficient thickness showed an ultralow refractive index and birefringence. Yu et al. prepared a polyimide-silica hybrid thin film using a soluble fluorine-containing polyimide and monodispersed colloidal silica [20]. This film had an excellent optical transparency in both the UV and visible regions. Its refractive index and thermal stability were controlled by the silica content. Early attempts to fabricate an optical coating using nanoparticles resulted in fragile surfaces [21], but researchers recently tried to develop optical thin film coatings using nanoparticles and a UV-cured polymer to enhance the abrasion resistance. Krogman et al. studied the refractive index of sub-100 nm thin films by varying the metal oxide nanoparticle loading in an aqueous colloidal solution and UV-curable monomer [22]. The mechanical and optical performances of the resulting anti-reflective films coated on the plastic substrates were investigated. The results revealed that the thin films prepared by silica and ceria nanoparticles dispersed in a UV-curable monomer exhibited an optical transparency and anti-reflective property. Similarly, a high quality image through the light diffusing film of a display requires a quantitative description of light scattering in a high amount of dispersed particles in the colloid [15]. It is due to the polymer matrix that is assumed to

be transparent and homogeneous [23]. Therefore, the light scattering is assumed to be only due to the particles. When the light travels through a large amount of particles, the light scattering more readily occurs [23]. However, the particles usually tend to appear in aggregated cluster forms. The particles also do not have enough separation, thus the scattered light of each particle or cluster is dependent on the other ones, and multiple scattering occurs. The multiple scattering affects the increasing diffuse transmittance in the film. It should be concluded that the enhanced optical properties of the polymer film with particles is attributed to the amount, dispersibility and aggregated size distribution of the particles [14]. Especially, preparation of an optical film using a colloid of dispersed particles in a polymer must control the stability of the dispersant to force the particles to remain separated and, in turn, on the sign and magnitude of the total interparticle potential energy, V_T [24]. The general equation for describing V_T can be expressed as [25]:

$$V_T = V_{vdW} + V_{elect} + V_{steric} \tag{2.1}$$

where V_{vdW} is the attractive potential energy due to long-range van der Waals interactions between the particles, V_{elect} is the repulsive potential energy resulting from electrostatic interactions between the like-charged particle surfaces, and V_{steric} is the repulsive potential energy resulting from long-chain molecules adsorbed onto the particle surface. The stability of the dispersion is achieved when the repulsive forces are high enough to overcome the attractive van der Waal attractive forces [24]. The parameters involved in the electrostatic repulsion are well described by the DLVO theory (as developed by Derjaguin, Landau, Verwey and Overbeek). The electrostatic repulsion between the particles depends on the dielectric constant of the medium,

therefore it is less effective in the majority of nonaqueous media than in water because of the lower ionic concentration and the lower dielectric constant [24]. Steric barriers between particles and dispersing medium are also another way to induce a colloidal stability [25]. The long-range van der Waals interactions between particles must be mitigated during colloidal processing to achieve the dispersion stability [26]. One approach is to render this force negligible by matching the refractive index of the dispersed particles and media. This has been previously demonstrated for nanosilica and UV-curable acrylate monomers [25]. The results show that minimization of the Van der Waals forces and affinity of the monomer end group for the silica surface (for example hydrogen bonding) are the main parameters allowing high loading dispersions in the appropriate monomer and highly transparent dispersions having curing depths on the order of 10 mm in the UVA range. According to the V_{vdW} attraction, the interparticle attraction for two spherical particles of radius r separated by the distance h can be expressed by the effective Hamaker constant (A) [25]:

$$V_{vdW} = \frac{-Ar}{6\pi h} \quad (h \ll r) \tag{2.2}$$

The effective Hamaker constant is given by

$$A = a\left(\frac{\varepsilon_m - \varepsilon_p}{\varepsilon_m + \varepsilon_p}\right)^2 + b\frac{(n_m^2 - n_p^2)^2}{(n_m^2 + n_p^2)^{3/2}} \tag{2.3}$$

where ε is the dielectric constant, n is the refractive index and a and b are constants [25]. The subindices m and p refer to the dispersing medium and the dispersed particles, respectively. Equation (2.3) reveals that the dielectric constant and refractive index differences contribute to the Hamaker constant. Meanwhile, the dielectric constant depends on the complex refractive index (n_C) through Equation (2.4). Hence, the

refractive indices of the interacting media are matched, i.e., when $n_m = n_p$, the second term in Equation (3) vanishes as a result of reducing the Hamaker constant to a minimum.

$$\varepsilon = n_C^2 \tag{2.4}$$

The complex refractive index is defined by Equation (5) [27].

$$n_C = n + Ki \tag{2.5}$$

The real part of n_C, namely n, is the same as the normal refractive index [27]. The imaginary part of that, namely κ, is called the extinction coefficient. κ is directly related to the absorption coefficient α of the medium which is very low in a transparent material. The first term in Equation (3) may also become negligible when both the real and imaginary parts of the complex refractive indices (n_C) are matched [27] leading to a zero value of the Hamaker constant. Thus, the result of matching the refractive index in a colloidal system is effectively a minimization of the Van der Waals attraction. These form the base of our research which pertains to the possibility of silica nanoparticles (SiNPs) dispersion in a UV-curable monomer and its optical properties after the UV-cured film process.

In this chapter, highly loaded silica dispersions by matching refractive indices of the silica and a binder resin were prepared. A UV-curable acrylate monomer was chosen as the binder resin because its refractive index is close to that of SiNPs at the wavelength of 500 nm [22]. The dispersion of the SiNPs was coated on the glass substrate using a bar coater to prepare a thin solid silica-UV-cured film. The optical properties of the resulting films were then analyzed by a UV-visible spectrophotometer

and compared with the uncoated substrate in the range of 300-800 nm. The effect of the silica loading on the optical properties of the films was also investigated.

2.2 Experimental procedures

2.2.1 Materials

All solvents and chemicals were of reagent grade and used without further purification. The chemical formula of the used compounds are shown in Fig. 2.1. Silica nanoparticles, SO-C1, were purchased from Admatechs, Japan. An SEM image of the SiNPs used in this study is shown in Fig. 2.2. The particles have a spherical shape, and their size is in the range of 150-300 nm. The bulk density of SiNPs is 2.1 g/cm^3 as measured by a helium pycnometer. The UV-curable acrylate monomer was composed of two major components, dipentaerythritol penta-/hexa acrylate as an acrylic monomer and Irgacure 184 (1-hydroxycyclohexyl phenyl ketone) as a photo initiator supplied by the JSR Corporation, Japan. Methyl isobutyl ketone (MIBK; 99.5%) was purchased from Wako Pure Chemical Industries, Japan. The density of the MIBK is 0.802 g/cm^3. It was used as a reactive diluent in the composite monomer to adjust the viscosity and dispersibility.

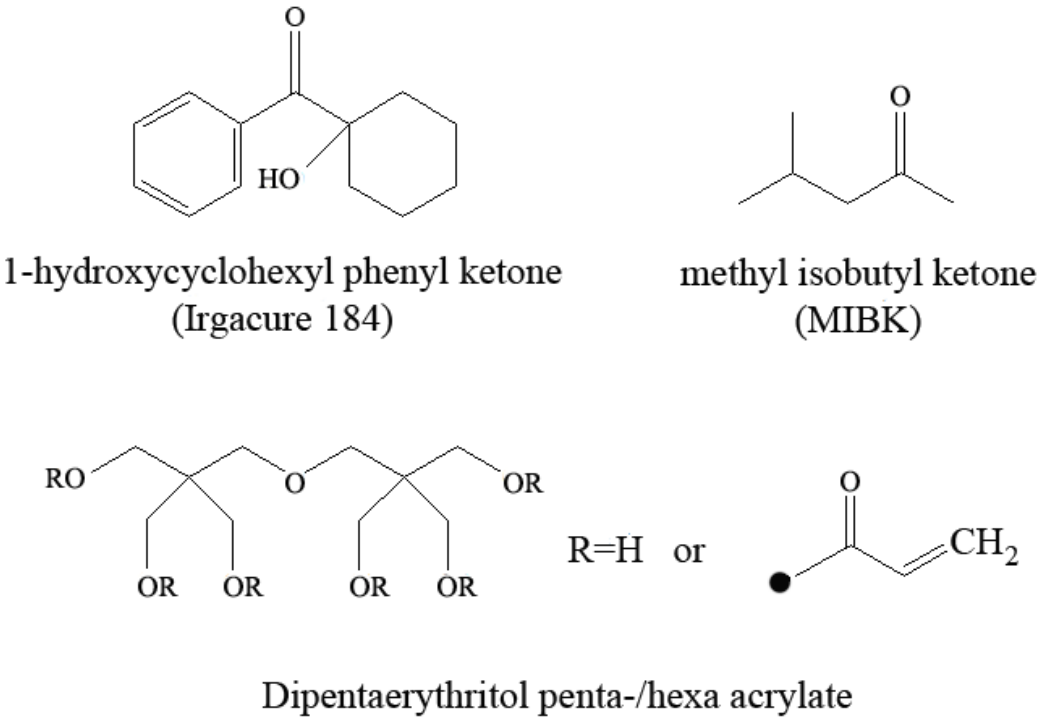

Fig. 2.1 Chemical formulas of the compounds used.

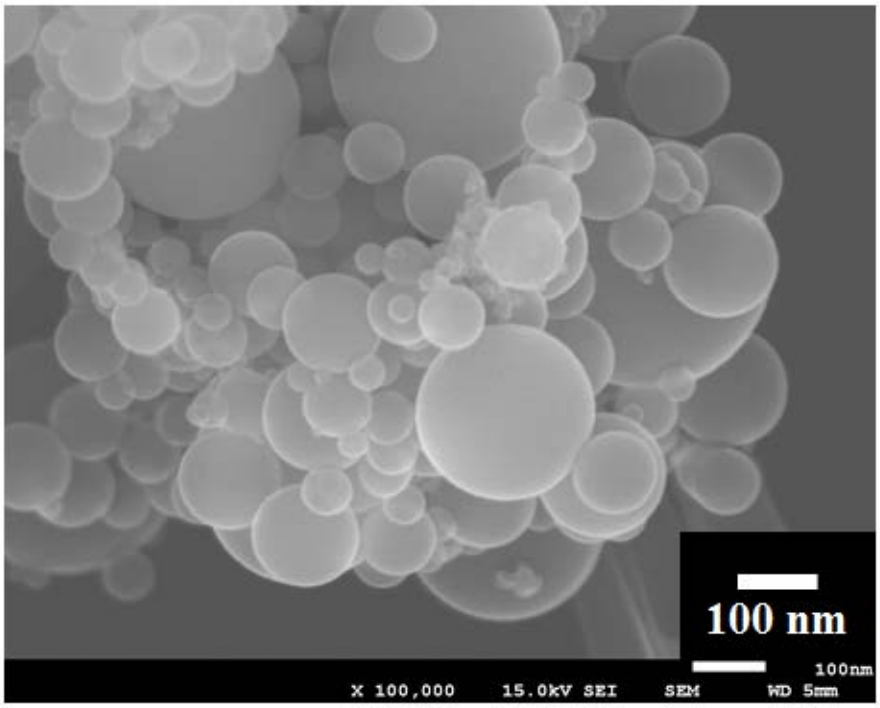

Fig. 2.2 FE-SEM image of the SiNPs as received.

2.2.2 Instrumentation

An Ultrapycnometer 1000T (Quantachrome Instruments) was used for measuring the bulk density of the SiNPs. Helium gas was used to precisely control the pressure of the pycnometer. The helium pycnometer was run in the multimode with a standard deviation of 0.05%. A Branson digital sonifier 450DA (Branson Ultrasonic Corp., JP) was used to disperse the SiNPs in the monomer solution. The digital sonifier was carried out using an ultrasonic horn. A planetary centrifugal deaeration mixer (ARE-930 Twin THINKY Mixer, JP) at a revolution speed of 1000 rpm under a vacuum of 20 kPa was used for removing air bubbles from the dispersions after the ultrasonic process. The particle size distribution of the SiNPs dispersions was determined by dynamic light scattering performed using a Malvern Zetasizer nano (Sysmex Company, JP). A VIBRO Viscometer SV-10 (A&D Co., JP) using the tuning fork vibration method equipped with small sample cup was used for measuring the viscosity of the dispersions. A 30 cm^3 volume of the dispersion was placed in the cup for measuring at 25°C. A refractometer (Multi-wavelength Abbe refractometer DR-M2; ATAGO Co., JP) with a 589 nm interference filter was used to determine the refractive index of the dispersions. The refractometer is capable of measuring in the range of 1.3000-1.7100 with a precision of ± 0.0002. A bar-coating machine (K101 Control Coater; RK PrintCoat Instruments, Ltd., UK) with a standard meter bar having the wire diameter of 0.76 mm and a constant speed of 2.0 cm/s was used to prepare the wet silica film. The wet silica film was cured by a UV-photo surface processor (PL16-110D; SEN LIGHTS Corp., JP) with a UV emission wavelength in the range of 254 nm and output of 110 W. The thicknesses of the wet and dry films were measured by a confocal laser scanning microscope (CLSM; LEXT 3D Measuring Laser Microscope CLS-4000; Olympus, JP) at a magnification of

5X. The surface morphology of the silica UV-cured films was examined using a field emission scanning electron microscope (FE-SEM; JSM7600F; JEOL, JP) equipped with COMPO detectors. The silica UV-cured films were directly dried on a hot plate at the temperature of 150°C for 2 h before being coated with osmium tetroxide in order to eradicate any unclear images caused by some residual solvent. A thin layer of the osmium tetroxide was coated on the dried sample by an osmium plasma coater (OPC60A; Filagen) prior to the imaging. It should be noted that the films were observed in the COMPO mode which uses back-scattered electrons [28]. They are a reflection from the sample due to elastic scattering. The intensity of the back-scattered electrons corresponds to the atomic number (Z) of the specimen. The optical properties of the prepared silica UV-cured films were measured by a UV-Vis-NIR spectrophotometer (UV3150; SHIMADZU, JP). The measurements were made in the wavelength range of 300-800 nm.

2.2.3 Preparation of silica UV-curable acrylate monomer dispersion

Dispersions containing 0.2-8.0 vol% of SiNPs were prepared by ultrasonication of the mixtures between the known masses of the silica powder and 20 wt% UV-curable monomer solutions by a digital sonifier at the amplitude of 40% and pulse on/off of 1 sec for 10 min in an ice bath to prevent polymerization throughout the dispersion process. The desired volume percentage of the SiNPs in the dispersion can be calculated by dividing the measured volume of the 20 wt% acrylate monomer solution (V_{sol}) by the volume of SiNPs (V_s). The calculated value is then converted to a percentage by multiplying by 100 and appending a percentage sign to the result.

$$Vol\%\ of\ SiNPs\ in\ dispersion = \frac{V_s}{V_s + V_{Sol}} \times 100 \qquad (2.6)$$

Using the average density of SiNPs and Equation (2.7), the volume of the SiNPs can be calculated.

$$V_s = \frac{M_s}{\rho_s} \tag{2.7}$$

where M_s is the mass of the SiNPs and ρ_s is the average density of the SiNPs, which was determined by the helium pycnometer. The calculated values are shown in the first column of Table 2.1.

Table 2.1 Amount of SiNPs in the dispersion and in the thin solid silica UV-cured film.

Amount of SiNPs in 20 wt% UV-curable acrylate monomer (vol%)	Amount of SiNPs in thin solid silica UV-cured film (vol%)
0.20	1
1.04	5
2.17	10
3.41	15
4.76	20
6.25	25
7.89	30

The second column of Table 2.1 lists the percentage volume content values of the SiNPs in the UV-cured films. The dry film basically consists of SiNPs dispersed throughout the continuous UV-cured acrylate film. The percentage volume content of

the SiNPs in the UV-cured films can be calculated by dividing the volume of the SiNPs by the total volume of all the solids. The calculated value with a decimal point is converted to a percentage by multiplying by 100 and appending a percentage sign to the result.

$$Vol\%\ of\ SiNPs\ in\ UV-cured\ film = \frac{V_S}{V_S+V_M} \times 100 \quad (2.8)$$

To know the volume of the acrylate resin (V_M) in the monomer solution, the measured volume of the acrylate monomer solution is multiplied by its density (ρ_{sol} = 0.855 g/cm^3) and then divided by the density of the acrylate monomer (ρ_M = 1.18 g/cm^3). It can be expressed as

$$V_M = V_{Sol} \times \frac{\rho_{Sol}}{\rho_M} \quad (2.9)$$

The air bubbles in the dispersions were removed by a planetary centrifugal deaeration mixer for 5 min in order to eliminate their effects on the optical properties of the resulting films. Dynamic light scattering (DLS) studies were conducted to measure the particle size distributions of the SiNPs in the dispersions. The viscosities of the dispersions were then measured by a viscometer. A refractometer was used to determine the refractive index of the dispersion. All the measurements were performed at 25°C.

2.2.4 Fabrication of thin solid silica UV-cured films on glass substrate

A clean glass substrate was coated by the silica dispersion using a commercial bar-coating machine to obtain a wet silica film. The glass substrate was ultrasonically cleaned successively in DI-water, ethanol and acetone for 10 min in each solvent. The wet silica film was initially dried at room temperature in the dark for 24 h before being

further cured by the UV-photo surface processor for 5 min to remove any organic compounds. The thin solid silica UV-cured film was then obtained with the solid content yield shown in Table 2.1. The thickness of both the wet and dry films was measured by the CLSM. The quantitative effect of the SiNPs on the optical properties of the thin solid silica UV-cured films was studied using the UV-Vis-NIR spectrophotometer. The transmittances of the coated substrates were then compared to that of the uncoated substrate in the wavelength range of 300-800 nm. The particle distributions on the film surfaces were also observed by the FE-SEM.

2.3 Results and Discussion

2.3.1 Physical properties of silica UV-curable acrylate monomer dispersion

The dispersions of the SiNPs in UV-curable acrylate monomer were successfully prepared. The amounts of the SiNPs in the dispersions were varied and the refractive indices of all the dispersions are illustrated in Fig. 2.3.

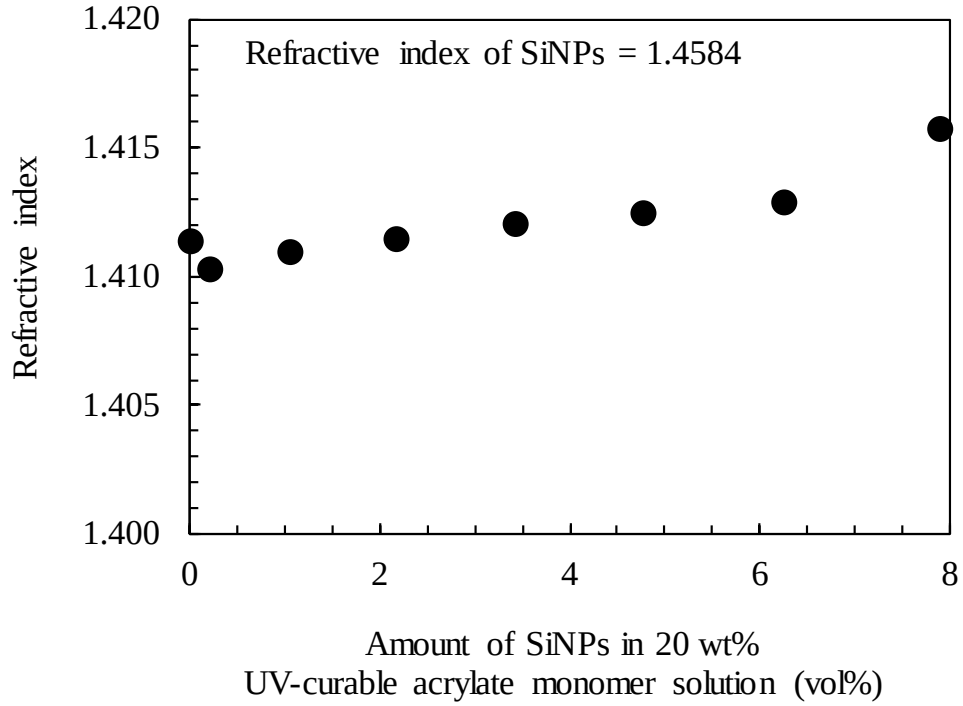

Fig. 2.3 Refractive indices of the modified UV-curable acrylate monomers for different amounts of SiNPs.

It can be seen that the presence of SiNPs in the UV-curable acrylate monomer significantly affects the refractive indices of the dispersions. Adding MIBK (n=1.3952 at 589 nm) to the UV-curable acrylate monomer solution makes its refractive index lower and closer to the refractive index of the SiNPs. The value of the refractive index of the SiNPs at 589 nm is about 1.4584 [29]. When the refractive indices of the dispersed particles and dispersing media are matched, it provides a transparent dispersion and allows a highly loaded dispersion [30-32]. To confirm the stability of the dispersion from the resultant of the matching refractive indices in a colloidal system, various amounts of the SiNPs in the dispersions at different times were studied.

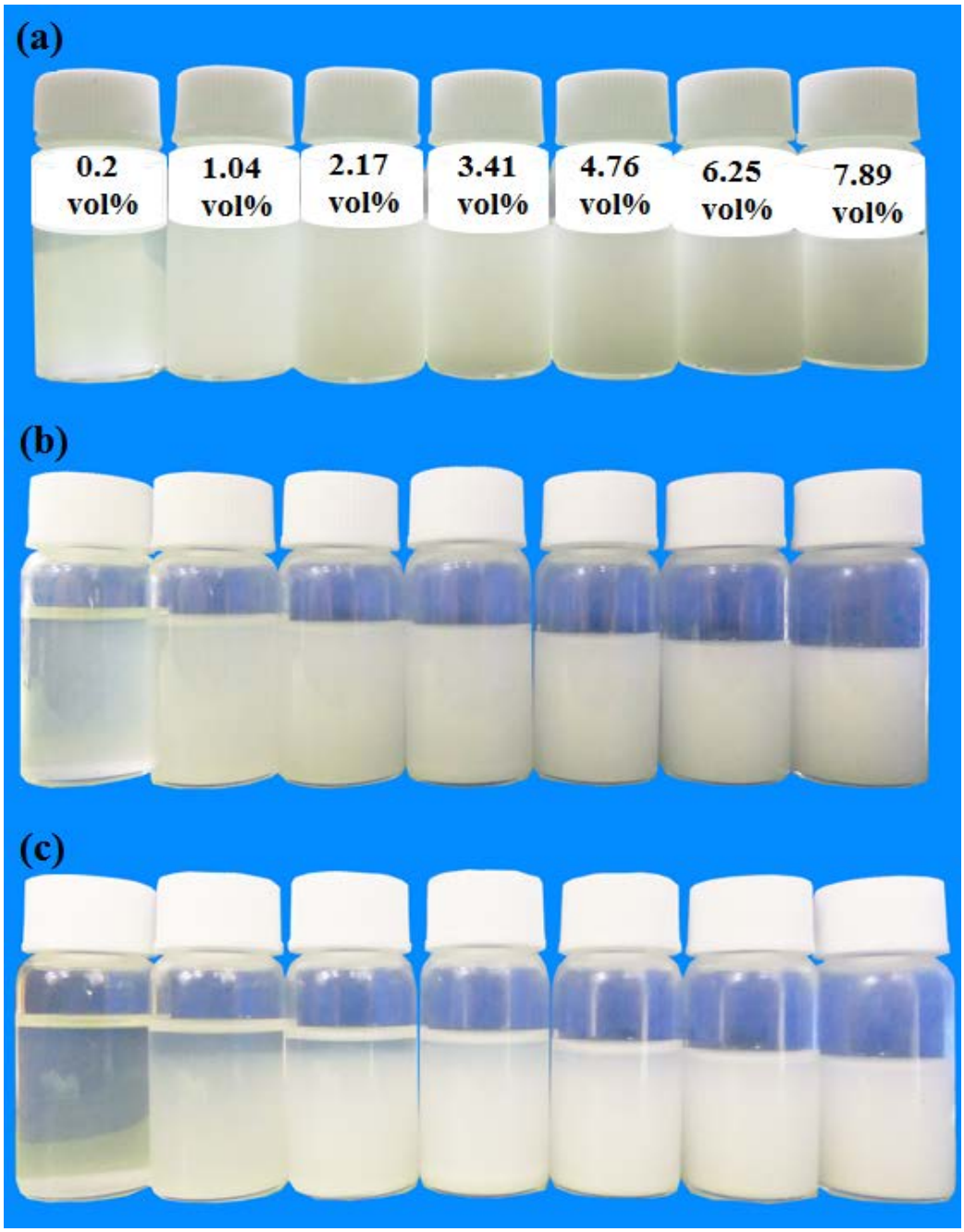

Fig. 2.4 Stability of silica UV-curable acrylate monomer dispersions

at different times such as (a) 0 h, (b) 1 h and (c) 24 h.

Fig. 2.4 shows images of the dispersions at the different times. The figure clearly reveals that the colloid dispersions with removed air bubbles (0 h) became turbid without any precipitation when the amount of the SiNPs increased from 0.20 to 7.89 vol%. Turbidity in the dispersions is caused by a high amount of dispersed particles. Besides, the stability of these colloidal dispersions during dark storage can be maintained for several hours by matching the refractive indices of the SiNPs and UV-curable monomer solution. However, a precipitate in the dispersions can be observed after 24 h as seen in Fig. 2.4 (c). The results suggest that the amount of MIBK in the dispersions of the silica UV-curable acrylate monomer may be sufficient to modify the interaction between the SiNPs resulting in the dispersion stability. This is consistent with some previous studies, which reported that the selected monomer with refractive index matching to the dispersed particles reduces the particle-particle attraction forces, especially the Van der Waals forces [25]. This leads to the dispersion containing a large amount of particles and having a long-term stability. The dispersion properties (like viscosity, pH and ionic strength), the dispersed particle properties (like particle size, particle volume fraction and specific surface area) and the presence of soluble polymers or surfactants [25] affect the particle interactions in the dispersion. To further understand the interaction of the particles in the dispersions, the silica loading effect on the viscosity of the dispersions was investigated. The results are shown in Fig. 2.5.

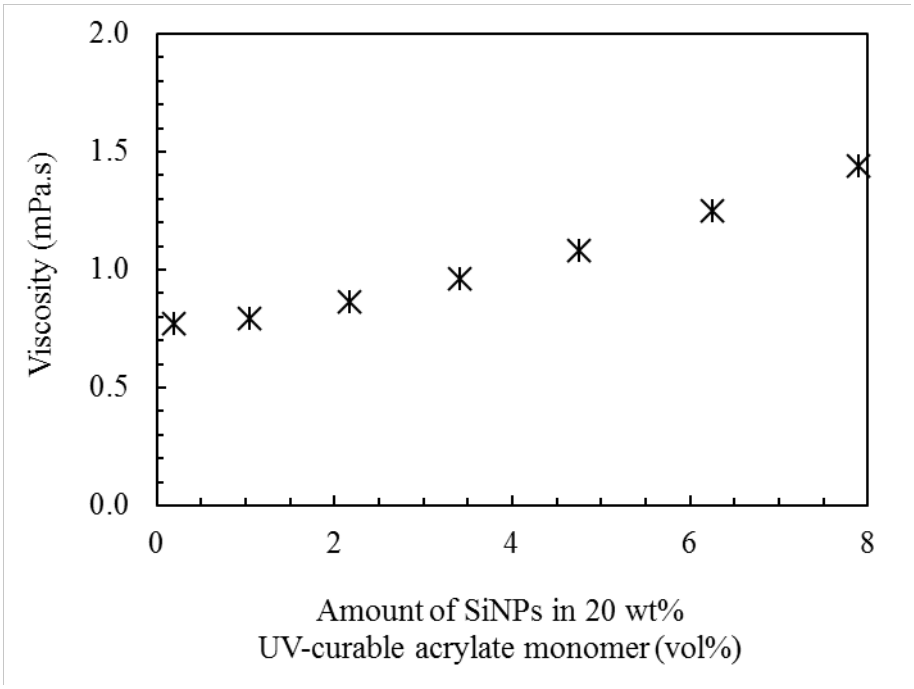

Fig. 2.5 Influence of silica loading on the viscosity.

The viscosity of the SiNPs dispersion gradually increases as the amount of the silica dispersed in the UV-curable acrylate monomer is increased corresponding to a previous study [33]. In a nonaqueous solution, the viscosity of a concentrated colloidal dispersion significantly depends on the interactions between the particles. Therefore, the lower the viscosity, the lower the interaction and the better is the given dispersant [34]. This is due to the structure of dipentaerythritol penta-/hexa acrylate that is OH terminated as shown in Fig. 2.1. This monomer is then able to form hydrogen bonding with the hydroxyl groups present on the silica surface and thereby increase the surface compatibility to the monomer which leads to particle aggregation [25, 35]. This is evident by the cumulative size distribution curve of the SiNPs dispersions as plotted on a log scale in Fig. 2.6.

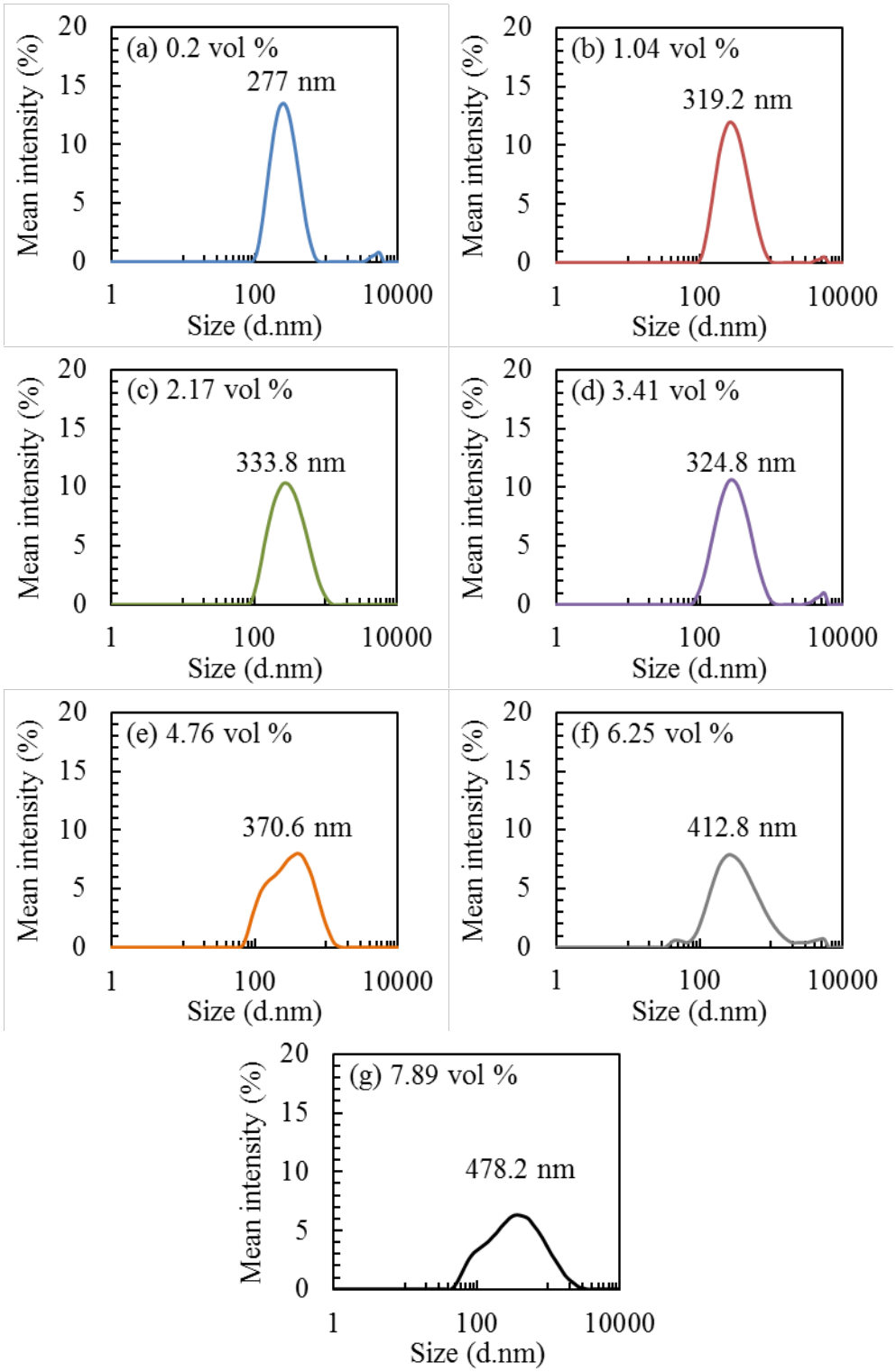

Fig. 2.6 The cumulative size distributions curve of SiNPs

dispersed in 20 wt% UV-curable acrylate monomer.

A larger size of the particles with a narrow distribution was obtained when the amount of the SiNPs in the UV-curable acrylate monomer was increased to 3.41 vol%. However, the larger size with a wider particle distribution was obtained when the amount of the SiNPs was higher than 3.41 vol%. These may be due to the fact that the SiNPs used here is hydrophilic and contains excess –OH groups on its surfaces [36]. The SiNPs also has a high surface area to volume ratio and therefore possesses a high surface energy. Consequently, it tends to aggregate so as to minimize the surface energies [37].

2.3.2 The optical properties of the thin solid silica UV-cured films

2.3.2.1 Optical transmittance of the thin solid silica UV-cured films

The dispersion of SiNPs in the UV-curable acrylate monomer was coated on a cleaned glass. The coated glass was then kept in the dark at room temperature for 24 h to prevent any premature polymerization. The wet silica film was exposed to 254 nm UV light for 5 min to induce the crosslinking polymerization. A thin solid silica UV-cured film was eventually obtained. The silica content in the films related to the final dry mass is shown in Table 2.1 To confirm the solvent removal by the UV-curing process, the thickness of the wet and dry silica films were measured by CLSM. The results are shown in Fig. 2.7 which shows that the average thicknesses of the UV-cured acrylate films doped and undoped with SiNPs are lower than those of the wet films. It indicates that the UV-curing process is capable for removing the solvent corresponding to the results from the COMPO mode in the FE-SEM characterization as will be shown later in Fig. 2.10. Besides, the increase in the amount of the SiNPs produces both thicker wet and dry films. This is due to the increasing amount of the particles that

affects the increasing viscosity of the dispersion (as seen in Fig. 2.5) corresponding to more formed silica aggregates [33].

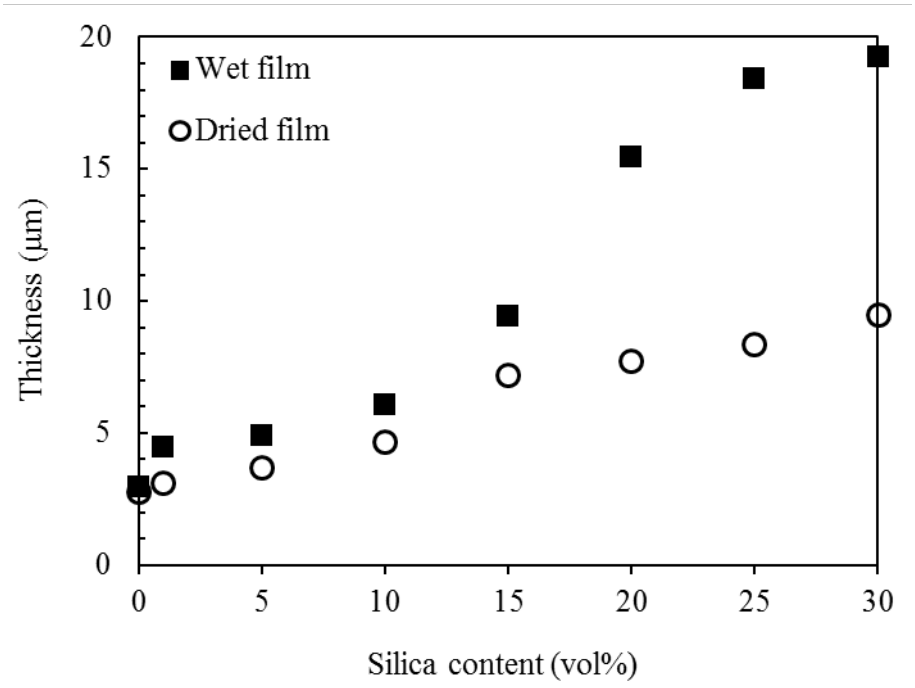

Fig. 2.7 Comparison of thicknesses of wet and dry films

with different SiNPs contents.

Therefore, the dispersion having high silica loading possibly contains a high number of particles with a bigger size and various shapes leading to the increased film thickness. In terms of the total transmittance, all the hybrid films were examined by UV-VIS in the wavelength range of 300-800 nm and the result is shown in Fig. 2.8.

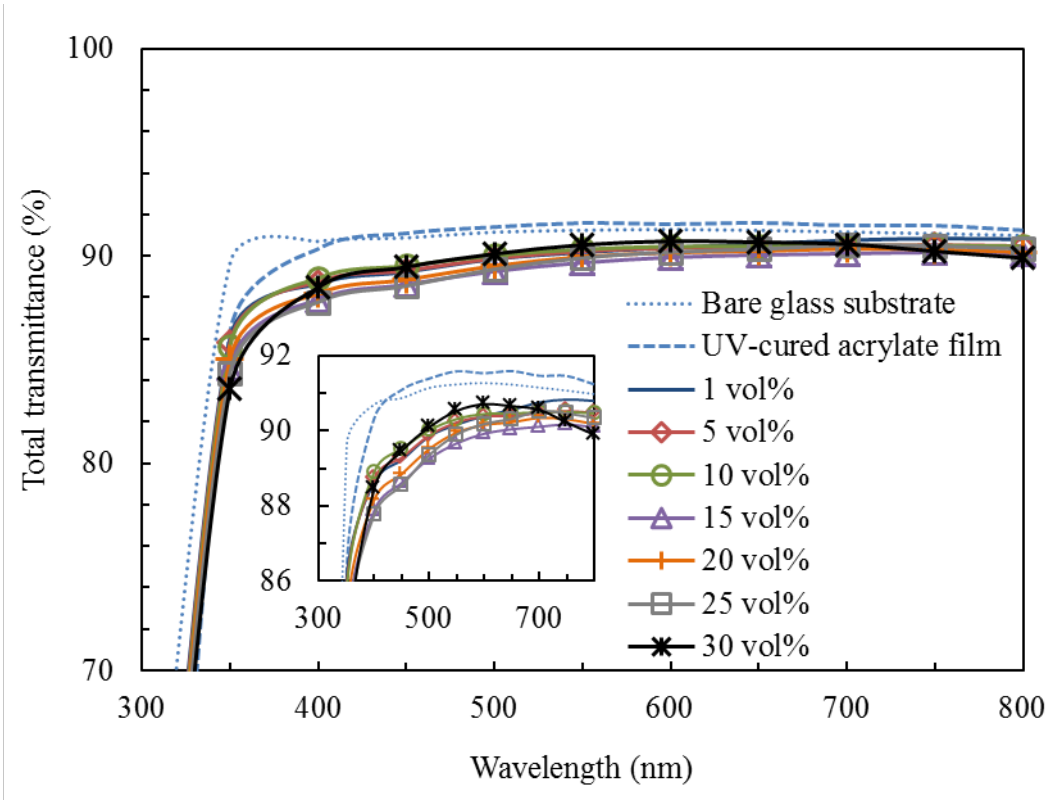

Fig. 2.8 Total transmittance of the modified UV-cured films with SiNPs coated on glass substrate.

In the visible region, the total transmittance of every coated glass is about 90% which is close to that of both the bare glass substrate [16] and the UV-cured acrylate film. These results confirmed that the highly transparent silica UV-cured films on the glass substrate were produced. A sharp absorption edge in the ultraviolet region due to the absorption of the glass substrate [16] was also observed. Interestingly, the edge shifts to a longer wavelength (red shift) for the pure UV-cured film. This behavior was also found in the UV-cured films containing SiNPs. This indicates that the UV-cured acrylate film may absorb light at a wavelength longer than the uncoated substrate.

2.3.2.2 Diffuse transmittance of the thin solid silica UV-cured films

The total light transmittance (T_t) and diffuse light transmittance (T_d) are usually used as indicators for estimating the light diffusing properties of diffuser plates in an LCD system [38]. The films with a high total transmittance and high diffuse transmittance tend to achieve a relatively excellent anti-glare and other optical properties [13]. They are thus suitable for a higher performance LCD in order to obtain the better final images. In this study, the thin solid silica UV-cured films with both a high total transmittance and high diffuse transmittance were prepared with various amounts of SiNPs.

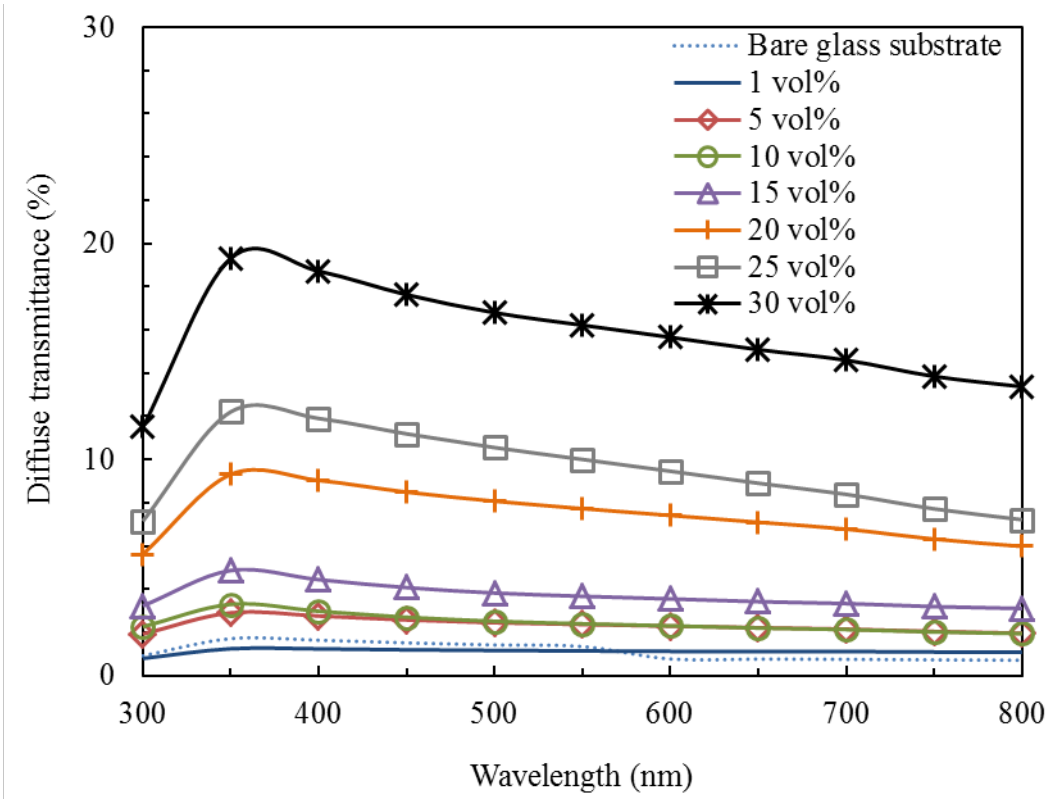

Fig. 2.9 Influence of silica quantity on the diffuse transmittance spectra of the thin solid silica UV-cured film coated on glass substrate.

The diffuse transmittance spectra of the films containing different amounts of SiNPs are shown in Fig. 2.9. They were measured using a spectrophotometer equipped with an integrating sphere. When compared to the bare glass, the samples containing SiNPs lower than 15 vol% showed slight increases in their diffuse transmittances, while those with 20 and 25 vol% SiNPs showed moderate increases. The highest diffuse transmittance of 20% was obtained at the 30 vol% level of SiNPs. However, the red shift was observed when the amount of SiNPs was greater than 20 vol%. The diffuse transmittance at a longer wavelength is decreased due to a lower interaction between the

light and particles when the wavelength is greater than the particle size. These results reveal that the diffuse transmittance of the film is attributed to the particle loading. When the polymer matrix is assumed to be transparent and homogeneous, the only scattering entity is then assumed to be the particles [39]. Therefore, the high number of particles in the film possibly provides a greater light scattering leading to a high diffuse transmittance. The refractive index of the film is evidence to confirm the light scattering occurrence. The average refractive index for cleaned glass substrates and UV-cured acrylate films is about 1.5232 and 1.5198, by, respectively. However, the refractometer cannot measure the refractive index of the UV-cured acrylate film containing the SiNPs due to the significant refractive line. The refractive line is quite difficult to visually focus the light as a result of an error in visual acuity. Thus, the refractive index for the thin solid silica UV-cured films cannot be defined. These results also support that a large amount of SiNPs in the UV-cured acrylate film may provide light scattering leading to the light refraction. Based on the Mie theory, when the light interacts with the high amount of particles with a size smaller than or comparable to the wavelength of the light, each particle is more illuminated by both the incident light and the secondary scattering than from other particles resulting in the increased diffuse transmittance of the film. This behavior is called multiple scattering which usually occurs in the film containing aggregated particles. If the aggregated particles in the media do not have a sufficient separation, the scattered light of each particle or cluster is assumed to be dependent on each other. At longer wavelengths, the diffuse transmittance drops because the interaction of the light with the particles decreases when the wavelengths become greater than the particles [40].

2.3.2.3 Morphology of the thin solid silica UV-cured films

To gain a better understanding of the quantitative effect of the SiNPs on the optical properties of the thin solid silica-UV-cured films, the surface morphology of the films were analyzed by FE-SEM.

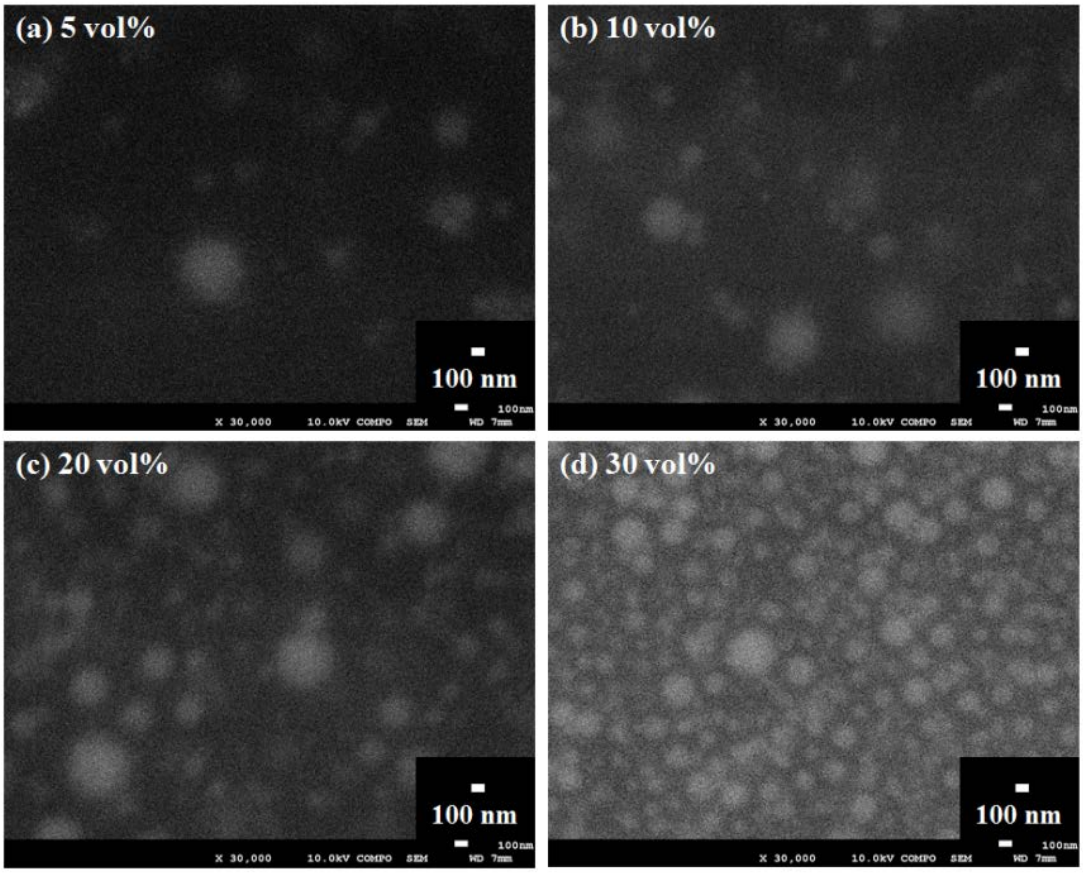

Fig. 2.10 FE-SEM surface images of the silica UV-cured film with different amounts of SiNPs (a) 5 vol%, (b) 10 vol%, (c) 20 vol% and (d) 30 vol%.

Fig. 2.10 illustrates the polymer surfaces containing carbon (C) atoms with a lower atomic number (as compared to silicon atom in silica) exhibit a dark background emission. This evidence confirms the existence of the SiNPs in these films. The films containing 5 and 10 vol% SiNPs as shown in Fig. 2.10 (a) and Fig. 2.10 (b) have low amounts of particles on the surface and have a random distribution. The observed particle size of the SiNPs is approximately 150 nm which is similar to that of the received particles (as seen in Fig. 2.2). These results suggest that only a small aggregation of particles occurs. However, the number of particles is increased in the film when the amount of SiNPs is increased to 20 vol% as illustrated in Fig. 2.10 (c). The size of the aggregates is in the range of 300 to 400 nm. It may be attributed to the strong interaction and strong adhesion between the particles [13]. The size of the aggregates corresponds to the cumulative size distribution of the SiNPs nanoparticles dispersed in the UV-curing resin as shown in Fig. 2.6. Interestingly, the thin solid silica UV-cured film with 30 vol% SiNPs exhibits a high particle distribution. The distribution is homogeneous and the particles form a greater aggregation as seen in Fig. 2.10 (d). Its diffuse transmittance is the highest (about 20%) as shown in Fig. 2.9 This indicates that the increased amount of SiNPs effectively improves the particle dispersion in the polymer film, and influences the morphology of the films corresponding to the increased optical properties of the films [13]. The reasonable explanation is the influence of multiple scattering. The multiple scattering occurs if the particles in the media are not sufficiently separated, thus the scattered light of each particle or cluster is dependent on each other [39]. In this case, both the incident and the secondary scattered light cause the illumination of each particle. Thus, the higher number of aggregated particles on the substrate more continuously traps the scattered

light resulting in both high total and diffuse transmittances. In addition, the increased SiNPs in the film exhibits a wide particle size distribution which improves the diffuse transmittance of the film at the longer wavelengths. The larger size of the aggregates allows the light with longer wavelengths to pass through.

2.4. Conclusion

A thin solid silica UV-cured film was successfully prepared by coating the SiNPs dispersion on a glass substrate, followed by UV exposure to induce crosslinking polymerization. The total transmittances of the films are close to the bare glass indicating the films transparency. Although the increased amounts of the SiNPs in the UV-cured films do not significantly affect their transmittances, the presence of SiNPs in the UV-cured films produces a significant difference in the diffuse transmittance. The thin solid silica UV-cured film containing 30 vol% SiNPs exhibits the diffuse transmittance of 20% which is higher than other films and the uncoated glass substrate. This is due to the increase in the multiple scattering by the particles in the film. The increased SiNPs in the UV-cured films also provides a good compatibility and good dispersion of the particles which is one of the main roles to improve the optical properties of the films. Therefore, the optical property of the thin solid silica UV-cured film depends on the amount and distribution of the silica nanoparticles.

References

[1] M. Misra, A. Guest and M. Tilley, Hybrid inorganic-organic UV-curable abrasion-resistant coatings, *Surf. Coat. Int.* **12** (1998) 594-595.

[2] L. Keller, C. Decker, K. Zahouily, S. Benfarhi, J.M. Le Meins and J. Miehe-Brendle, Synthesis of polymer nanocomposites by UV-curing of organoclay-acrylic resins, *Polymer* **45** (2004) 7437-7447.

[3] M.R. Haddon and T.J. Smith, The chemistry and applications of UV-cured adhesives, *Int. J. Adhes. Adhes.* **11** (1991) 183-186.

[4] D. Blanc, A. Last, J. Franc, S. Pavan and J.L. Loubet, Hard UV-curable organo-mineral coatings for optical applications, *Thin Solid Films* **515** (2006) 942-946.

[5] A. Milinavičiūtė, V. Jankauskaitė and P. Narmontas, Properties of UV-curable hyperbranched urethane-acrylate modified acrylic monomer coatings, *Mater. Sci. (Medžiagotyra)* **17** (2011) 378-383.

[6] R. Peters, V.M. Litvinov, P. Steeman, A.A. Dias, Y. Mengerink, R. van Benthem, C.G. de Koster, Sj. van der Wal and P. Schoenmakers, Characterisation of UV-cured acrylate networks by means of hydrolysis followed by aqueous size-exclusion combined with reversed-phase chromatography, *J. Chromatogr. A* **1156** (2007) 111-123.

[7] C.J. Chang, M.H. Tsai, P.C. Kao and H.Y. Tzeng, Optical and mechanical properties of jet printed and UV cured blue pixels with phosphated epoxy acrylate as the curing agent, *Thin Solid Films* **516** (2008) 5503-5507.

[8] K. Ohashi, K. Nakai, S. Kitayama and T. Kawaguchi, Mechanisms of hydrogen evolution and stabilization of UV-cured urethane acrylate resin for coating of optical fiber, *Polym. Degrad. Stab.* **22** (1988) 223-232.

[9] G. Harbers, S.J. Bierhuizen and M.R. Krames, Performance of High Power Light Emitting Diodes in Display Illumination Applications, *J. Display Technol.* **3** (2007) 98-108.

[10] Y. Du, L.E. Luna, W.S. Tan, M.F. Rubner and R.E. Cohen, Hollow Silica Nanoparticles in UV-visible Antireflection Coatings for Poly(methyl methacrylate) Substrates, *ACS Nano* **4** (2010) 4308-4316.

[11] Z. Wu, J. Walish, A. Nolte, L. Zhai, R.E. Cohen and M.F. Rubner, Deformable antireflection coatings from polymer and nanoparticle multilayers, *Adv. Mater.* **18** (2006) 2699-2702.

[12] Y. Jung, T.H. Yeo, W. Yang, Y. Kim, K. Woo and J. Moon, Direct photopatternable organic-inorganic hybrid materials as a low dielectric constant passivation layer for thin film transistor liquid crystal displays, *J. Phys. Chem. C* **115** (2011) 25056-25062.

[13] S. Song, Y. Sun, Y. Lin and B. You, A facile fabrication of light diffusing film with LDP/polyacrylates composites coating for anti-glare LED application, *Appl. Surf. Sci.* **273** (2013) 652-660.

[14] X.Y. Shang, Z.K. Zhu, J. Yin, and X.D. Ma, Compatibility of soluble polyimide/silica hybrids induced by a coupling agent, *Chem. Mater.* **14** (2002) 71-77.

[15] M. Giamberini and G. Malucelli, Hybrid organic-inorganic UV-cured films containing liquid-crystalline units, *Thin Solid Films* **548** (2013) 150-156.

[16] Y. Wang, H. Wang, X. Meng and R. Chen, Antireflective films with Si-O-P linkages from aqueous colloidal silica: Preparation, formation mechanism and property, *Sol. Energy Mater. Sol. Cells* **130** (2014) 71-82.

[17] Y.Y. Yu, C.Y. Chen and W.C. Chen, Synthesis and characterization of organic-inorganic hybrid thin films from poly(acrylic) and monodispersed colloidal silica, *Polymer* **44** (2003) 593-601.

[18] T. Ribeiro, C. Baleizão and J.P.S. Farinha, Functional Films from Silica/Polymer Nanoparticles, *Materials* **7** (2014) 3881-3900.

[19] D. Konjhodzic, H. Bretinger and F. Marlow, Structure and properties of low-n mesoporous silica films for optical applications, *Thin Solid Films* **495** (2006) 333-337.

[20] Y.Y. Yu, W.C. Chien and T.W. Tsai, High transparent soluble polyimide/silica hybrid optical thin films, *Polym. Test.* **29** (2010) 33-40.

[21] E. Spiller, I. Haller, R. Feder, J.E.E. Baglin and W.N. Hammer, Graded-index AR surfaces produced by ion implantation on plastic materials, *Appl. Opt.* **19** (1980) 3022-3026.

[22] K.C. Krogman, T. Druffel and M.K. Sunkara, Anti-reflective optical coatings incorporating nanoparticles, *Nanotechnology* **16** (2005) S338-S343.

[23] R. Barchini, J.G. Gordon II and M.W. Hart, Multiple light scattering model applied to reflective display materials, *Jpn. J. Appl. Phys.* **37** (1998) 6662-6668.

[24] S. Zürcher and T. Graule, Influence of dispersant structure on the rheological properties of highly-concentrated zirconia dispersions, *J. Eur. Ceram. Soc.* **25** (2005) 863-873.

[25] M. Wozniak, T. Graule, Y. Hazan, D. Kata and J. Lis, Highly loaded UV curable nanosilica dispersions for rapid prototyping applications, *J. Eur. Ceram. Soc.* **29** (2009) 2259-2265.

[26] J. A. Lewis, Colloidal Processing of Ceramics, *J. Am. Ceram. Soc.* **83** (2000) 234-2359.

[27] M. Fox, 2001, *Optical Properties of Solids*, Oxford University Press, New York, US.

[28] D. Kaczmarek, The method of increasing COMPO contrast by linearization of backscattering characteristic $\eta = f(Z)$, *Scann* **19** (1997) 310-315.

[29] I.H. Malitson, Interspecimen Comparison of the Refractive index of Fused Silica, *J. Opt. Soc. Am.* **55** (1965) 1205-1209.

[30] J. Kizling, B. Kronberg and J.C. Eriksson, On the formation and stability of high internal phase O/W emulsions, *Adv. Colloid Interface Sci.* **123-126** (2006) 295-302.

[31] S.Y. Kim and C.F. Zukoski, Particle Restabilization in Silica/PEG/Ethanol Suspensions: How Strongly do Polymers Need To Adsorb To Stabilize Against Aggregation?, *Langmuir* **27** (2011) 5211-5221.

[32] T. Chartier, C. Chaput, F. Doreau and M. Loiseau, Stereolithography of structural complex ceramic parts, *J. Mater. Sci.* **37** (2002) 3141-3147.

[33] D.M. Qi, Y.Z. Bao, Z.X. Weng and Z.M. Huang, Preparation of acrylate polymer/silica nanocomposite particles with high silica encapsulation efficiency via miniemulsion polymerization, *Polymer* **47** (2006) 4622-4629.

[34] L. Bergstrom, 1994, *Rheology of concentrated Suspensions, Surface and Colloid Chemistry in Advanced Ceramics Processing*, Marcel Dekker Inc., New York, US.

[35] C. Wang, Q. Wang and T. Wang, Simple Method for Preparation of Porous Polyimide Film with an Ordered Surface Based on in Situ Self-Assembly of Polyamic Acid and Silica Microspheres, *Langmuir* **26** (2010) 18357-18361.

[36] J.D. Cho and Y.B. Kim, The effects of silica nanoparticles on the photocuring behaviors of UV-curable polyester acrylate-based coating systems, *Macromol. Res.* **13** (2005) 362-365.

[37] W. Wu, Q. He and C. Jiang, Magnetic iron oxide nanoparticles: synthesis and surface functionalization strategies, *Nanoscale Res Lett* **3** (2008) 397-415.

[38] A. Kanemitsu, T. Sakamoto and H. Iyama, Light Diffuser Plates for LCD-TV Backlight Systems, R&D Report "*SUMITOMO KAGAKU*" **1** (2007) 1-10.

[39] A. Rastar, M.E. Yazdanshenas, A. Rashidi and S.M. Bidoki, Theoretical review of optical properties of nanoparticles, *J. Eng. Fiber Fabr.* **8** (2013) 85-96.

[40] H. Seel and R. Brendel, Optical absorption in crystalline Si films containing spherical voids for internal light scattering, *Thin Solid Films* **451-452** (2004) 608-611.

CHAPTER 3

MODIFICATION OF UV-CURED ACRYLATE FILMS BY SPHERICAL SILICA NANOPARTICLES FOR IMPROVING THEIR LIGHT DIFFUSING ABILITY

3.1 Introduction

There are two types of UV-curing resins, which are categorized by the curing mechanism, such as an acrylate radical polymerization and an epoxy cationic polymerization. Among these types, the UV-curable acrylate resin has a high UV-sensitivity and provides good mechanical and elastic properties such as modulus, strain hardening, tear strength, creep, and glass-rubber transition temperature after the UV-radiation curing [1-2]. For the UV-radiation curing, light hits the acrylate radical then stimulates a bonding process between molecules leading to the polymerizations. Consequently, the high cross-linked acrylate material is obtained by rapidly transforming a liquid resin into a solid material [3-4] called a UV-cured acrylate. The UV-cured acrylate is extensively used in many applications, for example, printed materials, optical surface protections, paints, durable ink, and acrylic sheets used for electronic display technologies [5-8]. In the case of the acrylic sheet, it exhibits a good transparency in the visible light range but it has a very low light diffusivity. The property of the light diffuser film is its homogeneous brightness by spreading the light that is essential for electronic display technologies to form excellent final images [9]. Many efforts have been devoted to increasing the light transmittance of the UV-cured polymer films along with increasing their light diffuse transmittance [8-10]. A variety of inorganic particles including titanium dioxide, copper oxide, aluminum hydroxide, alumina and silica are extensively used for the fabrication of light diffuser films due to their unique and enhanced mechanical, thermal, electrical and optical properties [8-11]. Among these materials, silica nanoparticles are very attractive to improve the optical properties of the polymer film because of their good light transmittance and diffusion

capacity, which may be promising candidates for light diffuser films in the electronic display industry [12-13].

In this chapter, spherical silica nanoparticles (SSiNPs) with dense structures were applied for modifying UV-cured acrylate films in order to improve their optical properties and light diffusing property. The films were coated on cleaned glass substrates using a bar coating machine. The transmittance and haze of all the modified films were analyzed by a UV-visible spectrophotometer and compared to the unmodified film coated on a glass substrate in the visible range (400-800 nm). The film having a higher haze value normally exhibits a better light diffusing ability [12]. Therefore, the light diffusing ability of the films was examined by an apparatus equipped with a 532 nm laser. The influence of silica content on the optical properties of the films was also investigated.

3.2 Experimental procedures

3.2.1 Materials

The spherical silica nanoparticles (SSiNPs) were purchased from Admatechs, Japan. The UV-curable acrylate monomer was supplied by the JSR Corporation, Japan. Methyl isobutyl ketone (MIBK; 99.5%), ethanol and acetone were purchased from Wako Pure Chemical Industries, Japan. All the glass substrates used in this study were ultrasonically cleaned in deionized water, ethanol and acetone for 10 min in each solvent to remove any contaminants. All solvents and chemicals were of reagent grade and used as received.

3.2.2 Fabrication of UV-cured acrylate films modified with spherical silica nanoparticles

The UV-curable acrylate monomer used in this study was composed of two major components such as dipentaerythritol penta-/hexa acrylate that acted as an acrylic monomer and Irgacure 184 (1-hydroxycyclohexyl phenyl ketone) that acted as a photo initiator. The monomer was diluted in the MIBK to 20 vol%, then mixed with a certain amount of the SSiNPs by the ultrasonic method. The suspension was coated on the cleaned glass substrates using a K101 control coater (RK PrintCoat Instruments, Ltd., United Kingdom). The coater using a standard meter bar having a 0.51 mm wire diameter was set at the constant speed of 2.0 cm/s. The obtained wet silica-acrylate film was stored in the dark at room temperature for 24 h to evaporate the solvent contained in the film. The dry silica-acrylate film was exposed to a 110 W UV lamp (254 nm) in a UV-photo surface processor (PL16-110D; SEN LIGHTS Corp., Japan) at ambient temperature. A variety of silica contents in the UV-cured acrylate films was fabricated by mixing different amounts of the SSiNPs in the 20 vol% UV-curable acrylate monomer. The silica contents of the UV-cured acrylate films were 1, 5, 10, 20 and 30 vol%.

3.2.3 Characterization

Thicknesses of all the dry and cured films were measured by a confocal laser scanning microscope (CLSM; LEXT 3D Measuring Laser Microscope CLS-4000; Olympus, Japan). Dispersibility of the SSiNPs on the surface of the UV-cured acrylate films with the various silica contents was also observed by the CLSM. A field emission scanning electron microscope (FE-SEM; JSM7600F; JEOL, Japan) was employed to

observe the morphologies of the SSiNPs. The FE-SEM was also used to observe the morphologies of the films. Prior to imaging by the FE-SEM, the films were directly dried on a hot plate at a temperature of 150°C for 2 h in order to eradicate any unclear images caused by some residual solvent. The dry samples were then coated by a thin layer of osmium tetroxide using an osmium plasma coater (OPC60A; Filagen). The coated samples were subjected to FE-SEM in order to observe their morphologies in the COMPO mode. The transmittance and haze of the films were measured by a UV-Vis-NIR spectrophotometer (UV3150; SHIMADZU, Japan). The haze value is defined as the ratio between the diffuse transmittance and total transmittance (Haze = $T_{diffuse}/T_{total}$) [14]. The haze value of the films was calculated at 532 nm corresponding to the wavelength of the laser used in the light diffusing study. The film having a higher haze value exhibits a better light diffusing ability [12]. The light diffusing ability of the films was examined by an apparatus equipped with a light source. The light source is a laser lamp with an emission of 532 nm (Z1M18B-F-532-PZ, Z-Laser, Germany). The films were placed in front of the laser light and the scattered light by the particles in the different films was obtained by a digital camera. The apparatus is illustrated by the schematic diagram in Fig. 3.1.

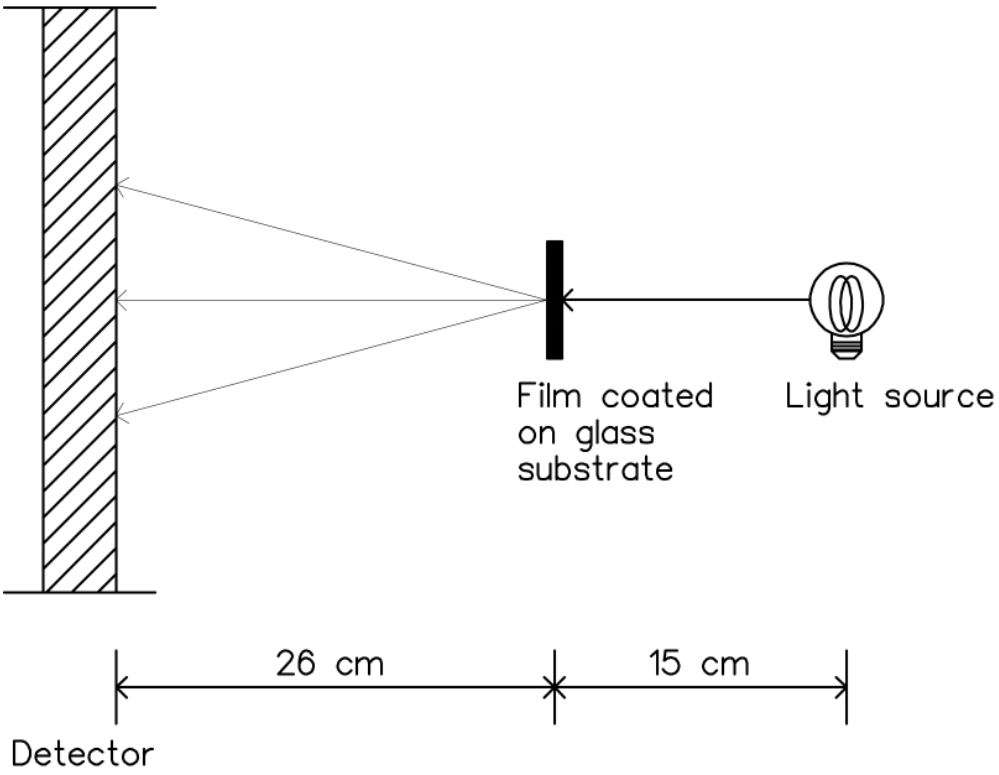

Fig. 3.1 Schematic illustration of the apparatus for achieving a scattered light image.

3.3 Results and Discussion

3.3.1 Morphologies of UV-cured acrylate films modified with spherical silica nanoparticles

The UV-cured acrylate films modified with the SSiNPs were successfully fabricated after subjecting the dry films to UV illumination for 10 min to induce the crosslinking polymerization. The film thicknesses of the cured films were then measured by the CLSM and compared to the dry films.

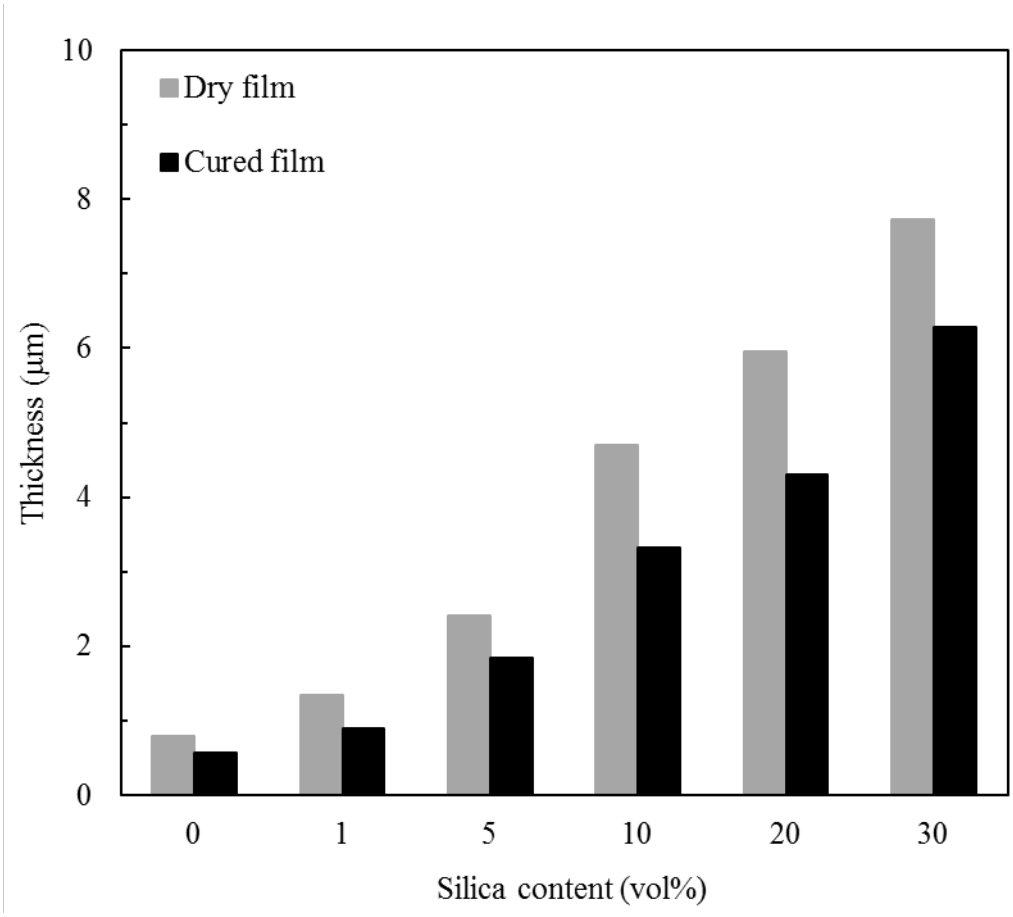

Fig. 3.2 Influence of silica content on the film thickness.

Fig. 3.2 shows the influence of the silica content on the film thickness. It can be seen that the average thickness of all the cured films is lower than that of all the dry films. Therefore, the time used for the UV-curing process is probably sufficient to transform the dry silica-acrylate films into the hardened UV-cured acrylate films. According its components, the UV-cured acrylate polymer is a high reactivity UV-curable resin, such as short reaction times on the order of seconds, offers a variety of monomers, and oligomers with functional end groups [15-16]. In addition, the UV intensity of the UV lamp used in this study was fixed at 110 W. Consequently, no more shrinkage of the UV-cured acrylate film was detected though the UV-curing time was longer than 10 min [17-18]. Interestingly, the thickness of both the dry and cured films gradually increased when the silica content was increased. This is due to the increased amount of particles that produces more aggregates on the film surfaces [19]. This was confirmed by the results from the CLSM images at the magnification of 100x. The middle in position of the UV-cured acrylate films modified with the SSiNPs was selected for observing the film surface.

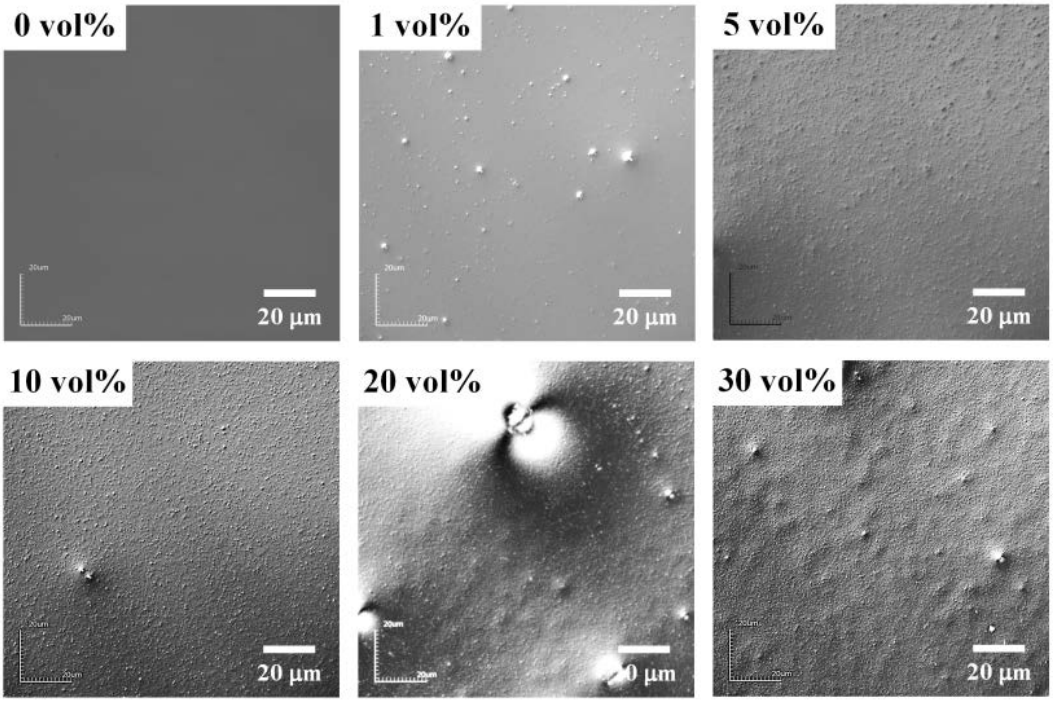

Fig. 3.3 CLSM images of the UV-cured acrylate films modified with the SSiNPs.

Fig. 3.3 shows the CLSM images of the UV-cured acrylate films modified with the SSiNPs. It was found that all the films coated on the glass substrates were uniform throughout the bar coating process. The unmodified film is smooth and no particles present. On the other hand, on the surface of all the modified films, it was observed that particles were clearly present. There is a low amount of particles on the film modified with 1 vol% SSiNPs. The particles have a random dispersion. When the silica content was increased from 5 and 10 vol%, the amount of the particles on the surface of the films moderately increased. Dispersibility of the particles on both films was quite good. The surface of these films seems to be rougher than the film modified with the 1 vol% SSiNPs. Nonetheless, the surface roughness of the films was still less than that of the

films modified with the 20 and 30 vol% SSiNPs. The result of the thickness and roughness analyses of all the modified films are consistent with some previous studies, which reported that the increased silica content produces films with a high thickness and roughness [20-21]. The observed particles on the films modified with the 20 and 30 vol% SSiNPs have a larger size and more aggregates.

However, visualization of the particles on all the modified films from the CLSM cannot accurately provide useful information about the size and form of the particles. It is due to some particles embedded in the films. Also, the magnification of the CLSM may be too low and insufficient to characterize when considering the original size of the SSiNPs. The image reveals that all particles are totally spherical and the particle size is in the approximate range of 100-250 nm.

An attempt to overcome these problems was made using the FE-SEM and the results are shown in Fig. 3.4. The SSiNPs containing silicon (Si) atoms with a higher atomic number as compared to the carbon (C) atom in the polymer surface exhibit bright spot emissions. These are due to the COMPO mode that provides the image contrast as a function of the elemental composition [22]. The results clearly confirm the existence of the silica particles in the films.

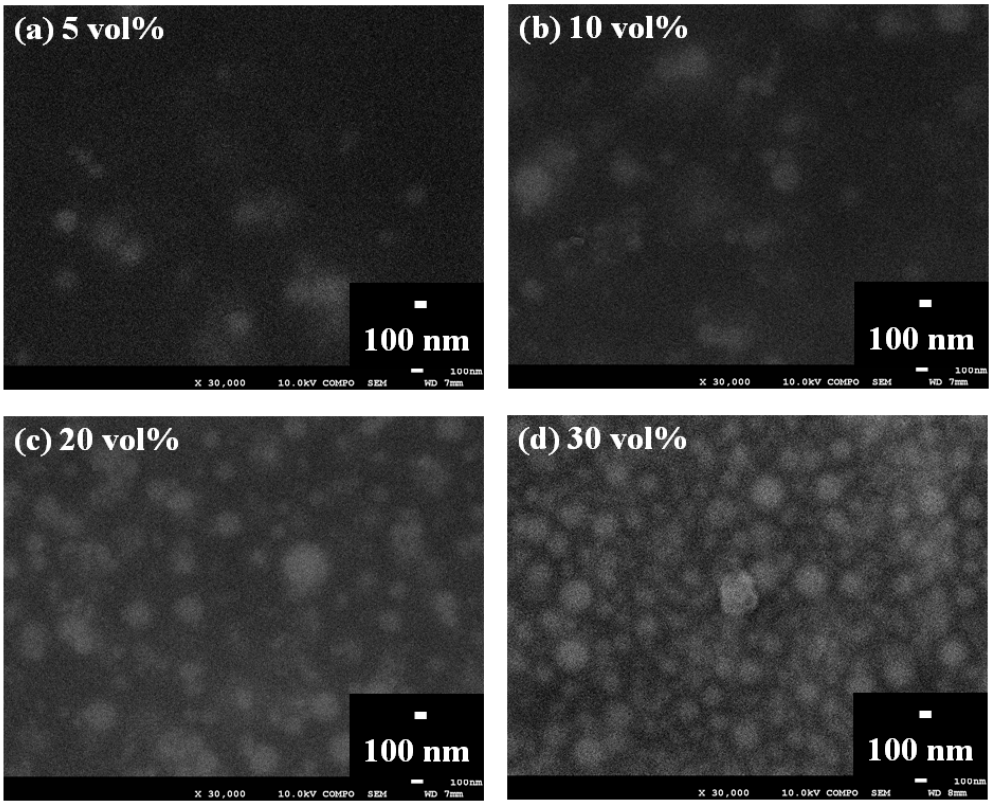

Fig. 3.4 FE-SEM images of the UV-cured acrylate films modified with various amounts of SSiNPs: (a) 5 vol%, (b) 10 vol%, (c) 20 vol% and (d) 30 vol%.

Figs. 3.4 (a) and (b) illustrate the FE-SEM images of the film surfaces modified with 5 vol% and 10 vol% SSiNPs; they show small amounts of the particles with random dispersions. The size of the observed particles is approximately 200 nm corresponding to the size of the received particles as shown in Fig. 3.5.

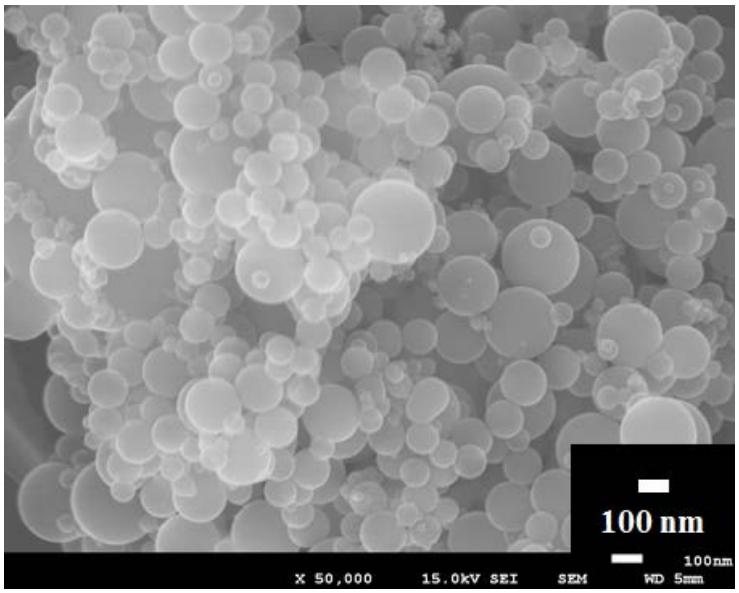

Fig. 3.5 FE-SEM image of the SSiNPs as received.

In addition, some of the particles on these film surfaces are close together as aggregates. When the silica content was increased to 20 vol%, the size of the aggregates is in the range of 300-500 nm as seen in Fig. 3.4 (c). This may be due to the fact that the SSiNPs used here are hydrophilic and contains silanol groups on their surface leading to the formation of hydrogen bonds between them [23]. The distances between the aggregates decrease that is caused by the loss of the liquid carrier during the UV-curing process [19]. This behavior is also found in the FE-SEM image of the surface of the film modified with 30 vol% SSiNPs as illustrated in Fig. 3.4 (d). The image shows the smallest distances between the aggregates and the best dispersion of particles when compared to the other images of the film surfaces with the lower silica content. Moreover, it exhibits the highest amount of the particles and aggregates. These results indicate that the increased silica content possibly provides a high number of particles

and a greater aggregation with a good dispersion leading to the increased thickness and roughness of the film. The increasing thickness and roughness of the films are responsible for the light diffusing ability of the films resulting in the enhanced haze value [24-25]. In addition, the presence of silica nanoparticles on the films can dramatically improve the optical properties of a polymer film because of their good light transmittance and diffusion capacity, which may be promising candidates for light diffuser films in the electronic display industry [12-13]. Thus, the optical properties of the UV-cured acrylate films modified with the SSiNPs were studied and further discussed in the following section.

3.3.2 Optical properties of UV-cured acrylate films modified with spherical silica nanoparticles

The transmittance of the UV-cured acrylate films modified with the SSiNPs was measured by the UV-Vis spectrophotometer in the visible region and compared to the unmodified film.

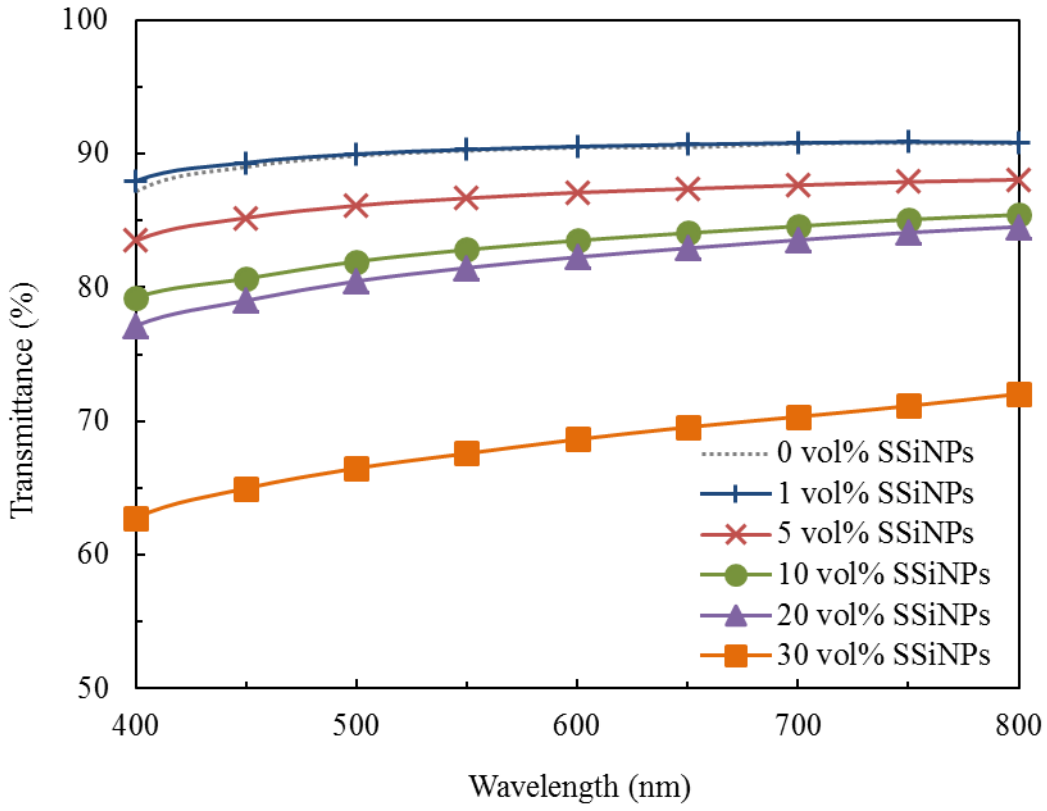

Fig. 3.6 Transmittance spectra of all films coated on the glass substrate.

Fig. 3.6 illustrates the transmittance spectra of all films coated on the glass substrate as a function of the wavelength. The transmittance spectra of the UV-cured acrylate film modified with 1 vol% overlap with the spectral characteristic of the unmodified film. Thus, the low silica content has no effect on the transmittance of the UV-cured acrylate film. In contrast, the transmittance of the modified films slightly decreases from 85 to 75 % when the silica content was increased from 5 to 20 vol%. The lowest transmittance obtained in the visible region was 60%, which is observed from the film modified with the highest SSiNPs (30 vol%). These results suggest that the films become more opaque when the silica content was increased [26]. When light

passes through heterogeneous films, the light scattering occurs due to the difference in the refractive indices between the heterogeneous phase (particles) and matrix [12]. Thus, the intensity of the light transmittance was attenuated. In principal, this type of light scattering is related to the size of the particles in the matrix [13]. If the size of the particles is much smaller than the wavelength of the incident light, the intensity of the light scattering is inversely proportional to the fourth power of the wavelength. This light scattering type is called Rayleigh scattering. On the other hand, if the size of the particles is independent of the wavelength of the incident light, the light scattering is classified as Mie scattering. Based on the Mie scattering, the intensity of the light scattering is independent of the wavelength of the incident light. In addition, the direction of the light scattering goes toward that of the incident light. Interestingly, the transmittance of the films modified with the SSiNPs slightly rises at a wavelength longer than 500 nm, thus the intensity of the light scattering during the SSiNPs is probably independent of the wavelength of the incident light. Therefore, the Mie scattering occurs in the films, and it can be inferred that the size of the particles or aggregated particles present inside the films is possibly larger than that of the wavelength of the incident light. Meanwhile, as received the particles are of various sizes with a high distribution (Fig. 3.5), and consequently, the various sizes of the observed particles on the film surfaces (Fig. 3.4) are almost smaller than 500 nm thus the Rayleigh scattering probably occurs on the film surfaces. These results are consistent with some previous studies [12]. It should be noted that the light scattering of the films corresponds to the Mie scattering interfering with the Rayleigh scattering.

The particle content in the films also plays a key role in their haze value, which is one of the main factors affecting the optical properties of the light diffuser films [12]. Therefore, the haze value of the UV-cured acrylate films modified with the SSiNPs was measured by a UV-Vis spectrophotometer and then calculated in order to investigate the effect of the silica content on the haze value.

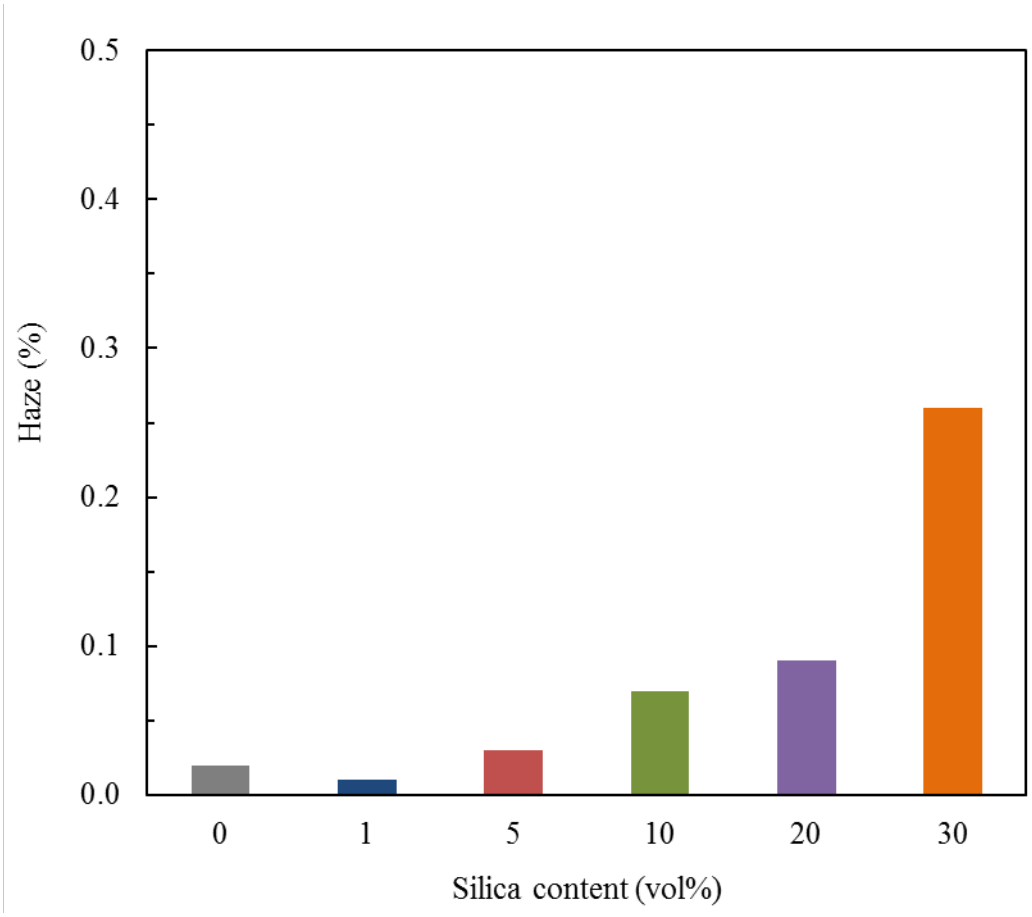

Fig. 3.7 Haze value of the UV-cured acrylate films modified with various silica contents.

Fig. 3.7 illustrates the haze value of the UV-cured acrylate films modified with various silica contents. The haze value slightly decreases as a result of the modification of the UV-cured acrylate film with 1 vol% SSiNPs. On the other hand, the haze gradually increases when the silica content was greater than 5 vol%. The film modified with 30 vol% SSiNPs has the highest haze value of about 0.26 although its transmittance is the lowest (as seen in Fig. 3.6). This might be due to the haze value that is considered using the light diffusion that depends on the light scattering from the particles. When the light interacts with the high number of particles with a size comparable or larger than the wavelength of the light, it is more possible that the scattered light leads to the high light diffusing ability of the film [27].

The light diffusing ability of the UV-cured films modified with the SSiNPs can be implied by their scattered light images. The scattered light images were visualized by the apparatus and subsequently taken by a digital camera.

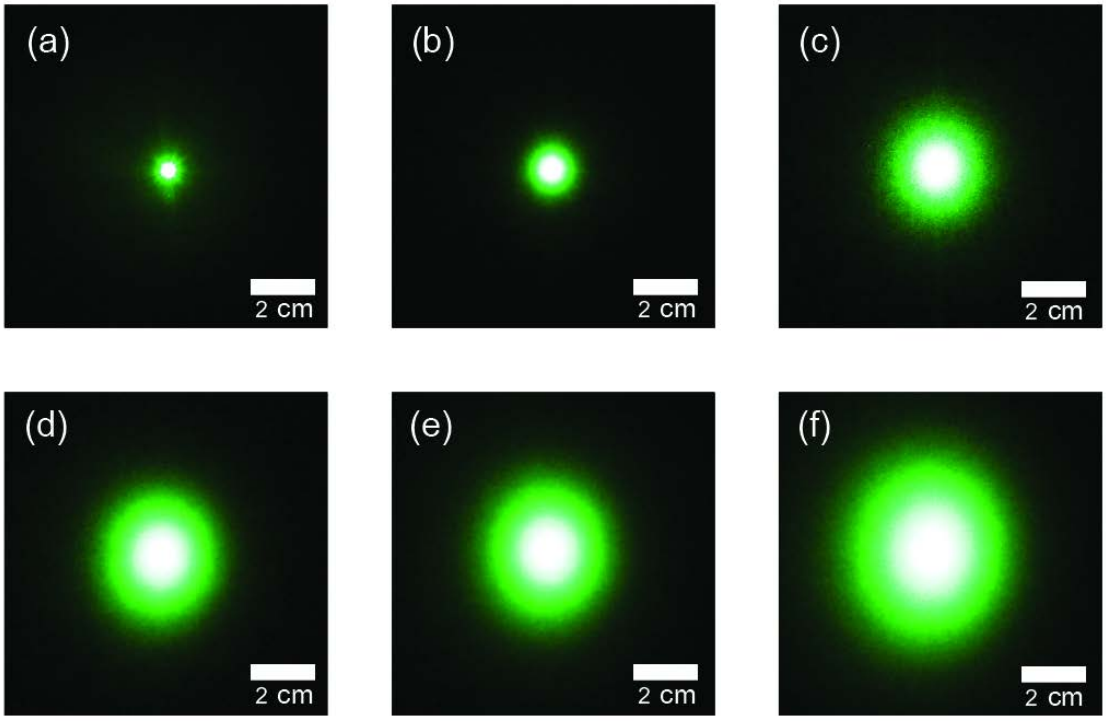

Fig. 3.8 The scattered light images of the UV-cured acrylate films containing various silica contents such as (a) 0 vol% (UV-cured acrylate film), (b) 1 vol%, (c) 5 vol%, (d) 10 vol%, (e) 20 vol% and (f) 30 vol%.

The scattered light images of all the samples are displayed in Fig. 3.8. Fig. 3.8 (a) shows the scattered light image of the unmodified film, which seems to be slightly lower than that of the film modified with 1 vol% SSiNPs (Fig. 3.8 (b)). The range of the scattered light by the particles in the film modified with 1 vol% SSiNPs is somewhat smaller by about five times than that of the films modified with silica of about 10 and 20 vol% as seen in Figs. 3.8 (c) and (d). The largest range of the scattered light by the particles is clearly observed in Fig. 3.8 (f),which shows the scattered light image of the film modified with the highest silica content (30 vol%). Based on the above mentioned results, it can be inferred that the light diffusing ability of the UV-cured acrylate film

increased when the silica content increased. This is due to the large number of silica nanoparticles that probably produce a high light scattering resulting in the enhancement of their light diffusing ability that corresponds to the haze value [12]. When the polymer matrix is assumed to be transparent and homogeneous, the particles are only assumed to produce the light scattering [27]. Moreover, the observed particles on the film surface as evidenced from the FE-SEM images (Fig. 3.4) seem to be close to each other. Thus, it can be implied that each particle is more illuminated by both the incident light and the secondary scattering than from other particles when the light interacts with the large amount of particles of a size comparable or larger than the wavelength of light. This behavior is called multiple scattering based on the Mie theory. The multiple scattering usually occurs when an aggregate is obtained in the film. Moreover, the aggregate does not have enough separation thus the scattered light of each particle or cluster is assumed to be dependent on each other. In addition, the scattered light continuously occurs in a film with a homogeneous dispersion of particles corresponding to the morphology of the UV-cured film with the high silica loading of 30 vol% presented in Fig. 3.4 (d). It is noteworthy that the image of the unmodified film (UV-cured acrylate film) in Fig. 3.8 (a) showed no light scattering effect. Furthermore, a more uniform distribution of scattered light was obtained with the UV-cured acrylate films modified with the SSiNPs. These results further prove the advantage of the SSiNPs for improving the light diffusing property of the UV-cured acrylate films. Thus, the films prepared in this study are promising candidates for light diffuser films.

3.4 Conclusion

The UV-cured acrylate films modified with the SSiNPs was successfully fabricated by coating suspension of silica-acrylate on cleaned substrates. The increasing silica content in the films reduces the transmittance of the films. The increasing silica content also provides a good compatibility and good dispersion of the particles which are some of the main ways to improve the optical properties of the films. The modified films have both a high haze and large range of scattered light. The largest range of the scattered light (transmittance 60% and haze 0.26) was obtained from the film modified with 30 vol% SSiNPs. The spherical silica nanoparticles may be utilized in the polymer films to obtain a high diffusing ability that is useful in the field of electronic display technologies.

References

[1] Z. Cui, 2009, *Nanofabrication: Principle, Capabilities and Limits, Springer Technology & Engineering*, New York, pp. 182.

[2] J.F. Rabek, 1993, *Radiation Curing in Polymer Science and Technology*, *Elsevier Applied Science*, London.

[3] L. Keller, C. Decker, K. Zahouily, S. Benfarhi, J.M. Le Meins and J. Miehe-Brendle, Synthesis of polymer nanocomposites by UV-curing of organoclay-acrylic resins, *Polymer* **45** (2004) 7437-7447.

[4] R. Peters, V.M. Litvinov, P. Steeman, A.A. Dias, Y. Mengerink, R. van Benthem, C.G. de Koster, Sj. van der Wal and P. Schoenmakers, Characterisation of UV-cured acrylate networks by means of hydrolysis followed by aqueous size-exclusion combined with reversed-phase chromatography, *J. Chromatogr. A* **1156** (2007) 111-123.

[5] A. Milinavičiūtė, V. Jankauskaitė and P. Narmontas, Properties of UV-curable hyperbranched urethane-acrylate modified acrylic monomer coatings, *Mater. Sci. (Medžiagotyra)* **7** (2011) 378-383.

[6] C.J. Chang, M.H. Tsai, P.C. Kao and H.Y. Tzeng, Optical and mechanical properties of jet printed and UV cured blue pixels with phosphated epoxy acrylate as the curing agent, *Thin Solid Films* **516** (2008) 5503-5507.

[7] K. Ohashi, K. Nakai, S. Kitayama and T. Kawaguchi, Mechanisms of hydrogen evolution and stabilization of UV-cured urethane acrylate resin for coating of optical fiber, *Polym. Degrad. Stab.* **22** (1988) 223-232.

[8] M. Giamberini and G. Malucelli, Hybrid organic-inorganic UV-cured films containing liquid-crystalline units, *Thin Solid Films* **548** (2013) 150-156.

[9] S. Song, Y. Sun, Y. Lin and B. You, A facile fabrication of light diffusing film with LDP/polyacrylates composites coating for anti-glare LED application, *Appl. Surf. Sci.* **273** (2013) 652-660.

[10] X.Y. Shang, Z.K. Zhu, J. Yin and X.D. Ma, Compatibility of soluble polyimide/silica hybrids induced by a coupling agent, *Chem. Mater.* **14** (2002) 71-77.

[11] Y. Wang, H. Wang, X. Meng and R. Chen, Antireflective films with Si-O-P linkages from aqueous colloidal silica: Preparation, formation mechanism and property, *Sol. Energy Mater. Sol. Cells* **130** (2014) 71-82.

[12] S. Guo, S. Zhou, H. Li and B. You, Light diffusing films fabricated by strawberry-like PMMA/SiO_2 composite microspheres for LED application, *J. Colloid Interface Sci* **448** (2015) 123-129.

[13] J. Hu, Y. Zhou, M. He and X. Yang, Novel multifunctional microspheres of polysiloxane@CeO_2-PMMA: Optical properties and their application in optical diffusers, *Opt. Mater.* **36** (2013) 271-277.

[14] Q.J. Jiang, J.G. Lu, J. Zhang, Y.L. Yuan, H. Cai, L. Hu, L.S. Feng, B. Lu, X.H. Pan and Z.Z. Ye, Texture-etched broad surface features of double-layered ZnO:Al transparent conductive films for high haze values, *J. Alloys Compd.* **596** (2014) 107-112.

[15] C. Decker, UV - radiation curing chemistry, *Pigment Resin Technol.* **30** (2001) 278.

[16] L.E. Schmidt, Y. Leterrier, J.M. Vesin, M. Wilhelm and J.A.E. Månson, Photorheology of fast UV-curing multifunctional acrylates, *Macromol. Mater. Eng.* **290** (2005) 1115-1124.

[17] S.S. Lee, A. Luciani and J.A.E. Månson, A rheological characterisation technique for fast UV-curable systems, *Prog. Org. Coat.* **38** (2000) 193-197.

[18] P.A.M. Steeman, A.A. Dias, D. Wienke and T. Zwartkruis, Polymerization and network formation of UV-curable systems monitored by hyphenated real-time dynamic mechanical analysis and near-infrared spectroscopy, *Macromolecules* **37** (2004) 7001-7007.

[19] M. Sumiya and K. Yamada, Development of filterability test method for gel retention performance for UV curable ink jet inks, in: *Proc. NIP30: The 30th International Conference on Digital Printing Technologies and Digital Fabrication*, PA, United States, 2014.

[20] W. Ming, D. Wu and R.V. Benthem, Superhydrophobic films from raspberry-like particles, *Nano Lett.* **5** (2005) 2298-2301.

[21] K. Senoo, Structure analysis of nanoparticle dispersed in transparent resin using synchrotron X-ray scattering, *Spring 8 Research Frontiers 2010 in Industrial Applications* (2010) 136-137.

[22] Y.J. Shin, S.H. Kim, D.H. Yang, H. Kwon and J.S. Shin, Amperometric glucose biosensor by means of electrostatic layer-by-layer adsorption onto polyaniline-coated polyester films, *J. Ind. Eng. Chem.* **16** (2010) 380-384.

[23] T. Nazir, A. Afzal, H.M. Siddiqi, Z. Ahmad and M. Dumon, Thermally and mechanically superior hybrid epoxy–silica polymer films via sol-gel method, *Prog. Org. Coat.* **69** (2010) 100-106.

[24] Q. Gao, H. Jiang, C. Li, Y. Ma, X. Li, Z. Ren, Y. Liu, C. Song and G. Han, Tailoring of textured transparent conductive SnO_2:F thin films, *J. Alloys Compd.* **574** (2013) 427-431.

[25] X. Yan, S. Venkataraj and A.G. Aberle, Wet-chemical surface texturing of sputter-deposited ZnO:Al films as front electrode for thin-film silicon solar cells, *Int. J. Photoenergy* **1** (2015) 1-10, DOI: 10.1155/2015/548984.

[26] B.Ö. Uysal and F.Z. Tepehan, Controlling the growth of particle size and size distribution of silica nanoparticles by the thin film structure, *J Sol-Gel Sci Technol* **63** (2012) 177-186.

[27] A. Rastar, M.E. Yazdanshenas, A. Rashidi and S.M. Bidoki, Theoretical review of optical properties of nanoparticles, *J. Eng. Fiber Fabr.* **8** (2013) 85-96.

CHAPTER 4

CHARACTERIZATION OF HOLLOW SILICA NANOPARTICLES AND THEIR APPLICATION IN LIGHT DIFFUSER FILMS

4.1 Introduction

Light diffuser films have both a high total and a diffuse transmittance since they are able to diffuse a point or line of light; for instance, adjusting the angle of incident light [1-2]. Consequently, the light diffuser films have homogeneous light penetration. Therefore, light diffuser films have attracted a lot of interest during recent years for applying in the backlight systems of several liquid crystal display (LCD) devices [2-5]. At present, two types of the light diffuser films are widely achieved as good optical diffusion in the LCDs. The first type is called surface-relief diffuser films, which are mainly dependent on the microstructures of the surface layers [6-9]. Most of the microstructures are fabricated by complicated processes using expensive equipment [2-3]. Another type, namely volumetric diffuser films, is simply prepared by coating a mixture of filler and binder resin on optical material. According to the production of those two light diffuser film types, the study of the volumetric diffusers has been conducted by many researchers. Moreover, the volumetric diffusers provide a uniform light scattering throughout the fillers, which play an important role in the optical properties of the volumetric diffusers [1, 4-5, 10-12]. There are many kinds of fillers; for example, organic particles [1], inorganic particles [2, 5, 13-14] and organic/inorganic composite particles [3-4, 15]. Principally, the filler-diffuser type films are related to the difference of refractive indices between the filler and the resin. When light passes through the interfaces of the filler and the resin, the refraction occurs as resulting in light scattering [2, 4-5].

In particular, polymer-inorganic hybrid nanocomposite materials are considered as excellent option for multifunctional materials [16-17]. This can be attributed to the fact

that they possess both polymers and inorganic nanoparticles. Moreover, such hybrid materials are capable of enhancing dispersion, which is advantageous for mixing fillers and binder resins [18]. In addition, an aggregation of a small number of inorganic particles is able to improve the bulk performance of polymer matrix for thermal, mechanical, and especially optical properties [2, 5, 13-14, 19-20]. Those properties significantly have an influence on the application of the filler-diffuser films [2]. Meanwhile, the microspherical structure of fillers is widely exploited in optical diffuser films in the LCD industry [3, 21-22]. However, using fillers which have a cubic structure in the fabrication of polymer-inorganic hybrid light diffuser films has not been reported in any involved research. Hollow silica nanoparticles (HSiNPs) comprise of a nano-sized hollow interior and a solid shell with the unique properties of low density, a high specific surface area, thermal insulation, and optical properties; for instance, light-weight filler [1, 5, 23-24]. Due to these properties, the HSiNPs have been much used as fillers light diffuser films. Their hollow structures can be expected to have a critical importance for light scattering as more light can penetrate into their hollow interior resulting in increasing light scattering [25].

In this chapter, silica nanoparticles with hollow structures (or hollow silica nanoparticles) were characterized. They were dispersed in a UV-curable acrylate monomer. The dispersion was coated on a cleaned glass substrate to fabricate a light diffuser film. The UV-curable acrylate monomer was used in this study because it has good mechanical and thermal properties; for instance, excellent optical properties [2, 26-28]. The composition of HSiNPs was initially investigated in order to eradicate any unexpected result, which may affect optical properties of the light diffuser films. The optical properties of the films containing different number of the particles were then

analyzed by a UV-visible spectrophotometer and compared to those of the cleaned glass in the visible region (400-800 nm). The quantitative effect of the particles on the optical properties of the films was also investigated.

4.2 Characterization of HSiNPs

4.2.1 Thermogravimetric analysis of HSiNPs

The thermogravimetric analysis (TGA, Thermo Plus TG-8120; Rigaku) was used to study the composition of HSiNPs. The sample was placed in a platinum crucible for each analysis and then heated in air to 800 ℃ at a heating rate of 10 ℃/min.

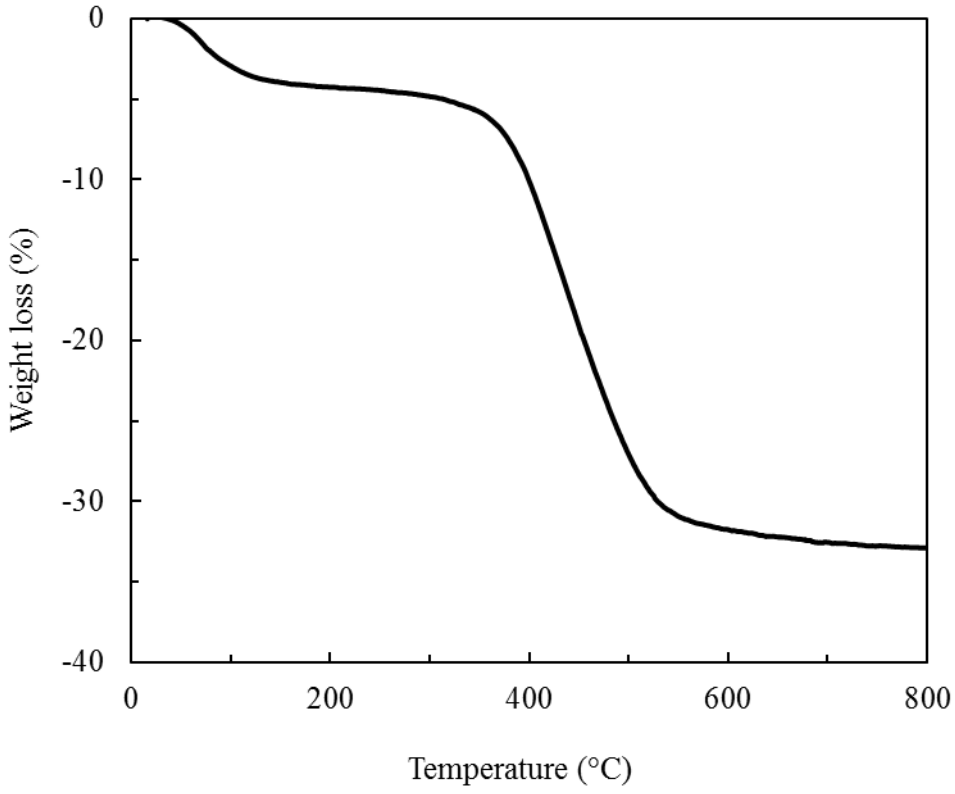

Fig. 4.1 TGA curve of the raw HSiNPs.

Fig. 4.1 shows the thermal decomposition of the raw HSiNPs. It reveals two regions of weight loss. The first region of weight loss is observed in the range of 40-150 °C because of the removal of bound water (5%). Another region of weight loss about 25% (300-520 °C) can be ascribed to the dehydration of Si-OH on the silicates or the loss of some residual reagent such as surfactant, which is used to produce the HSiNPs [29-30]. Moreover, the incombustible residue can be assumed to be silica as the results are consistent with other previous studies involving TGA for silica nanoparticles [31].

According to its TGA result, the raw HSiNPs was further calcined at temperature of 400 and 600 °C in order to eliminate some contamination which could lead to a flocculation of the HSiNPs. This formation is an undesirable in the preparation of highly loaded HSiNPs suspensions for a resulting film [32].

4.2.2 Morphologies of HSiNPs

The morphologies of HSiNPs before and after calcination were observed using a field emission scanning electron microscope (FE-SEM, JSM-7600F, JEOL Ltd.) at an acceleration voltage of 15 kV with secondary electron image (SEI) and transmission electron diffraction (TED). The samples were dispersed in ethanol (EtOH, 99% Wako Pure Chemical Industries, Ltd.) by an ultrasonication. Then, the suspensions were dropped on a microgrid (STEM150Cu, Oken Shoji) and dried in the air. The FE-SEM results are shown in Fig. 4.2.

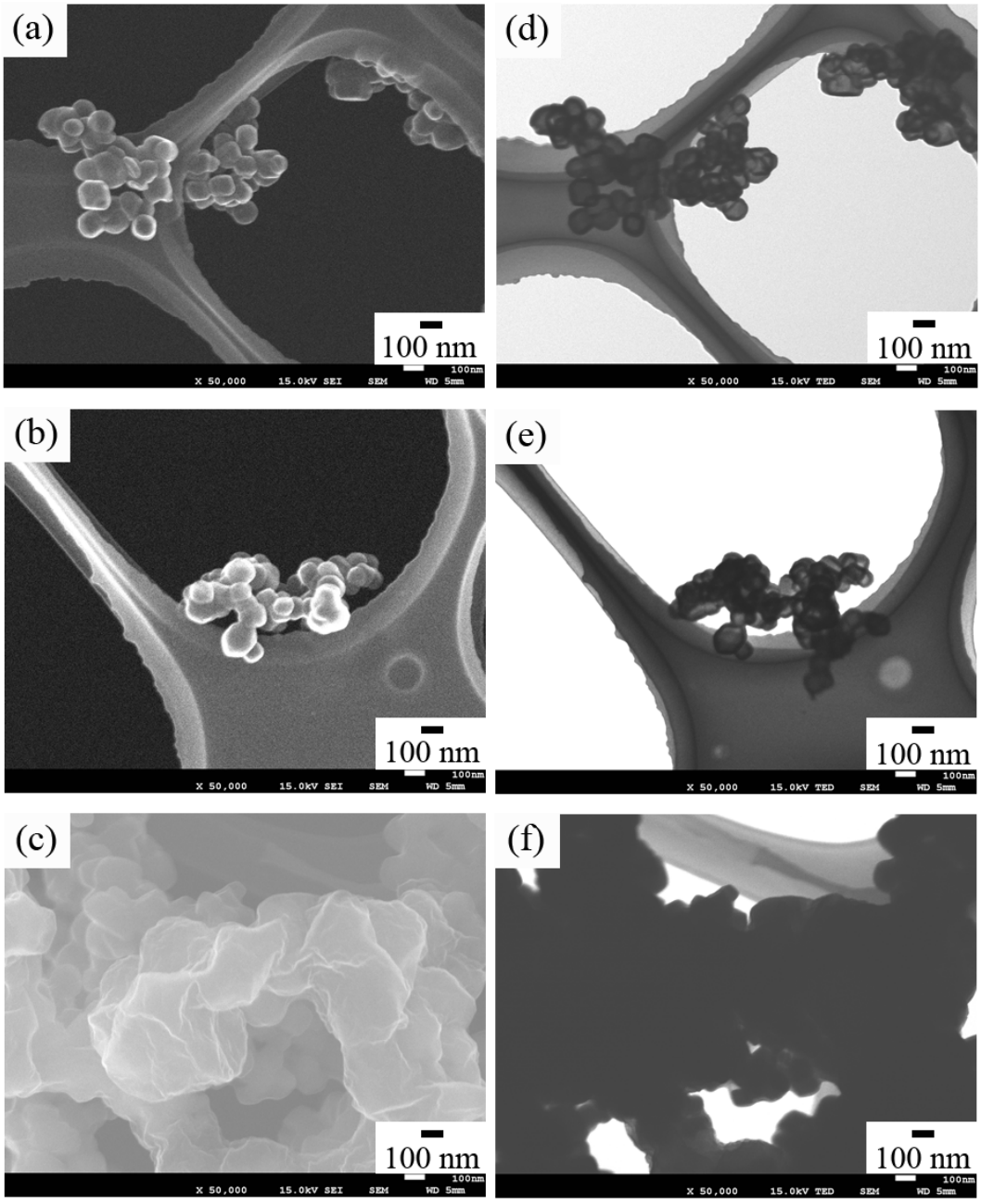

Fig. 4.2 FE-SEM images obtained from SEI and TED modes of HSiNPs before calcination for (a) and (d) and after calcination at temperature of 400 °C for (b) and (e), including to at temperature of 600 °C for (d) and (f).

Fig. 4.2 (a) shows the morphologies of the particles before calcination (raw) that clearly exhibits cubic shapes. The cubic shapes are also observed from the FE-SEM image obtained from SEI mode of the particles after calcination temperature at 400 °C as seen in Fig. 4.2 (b). However, no cubic shape is obtained from the particles after calcination temperature at 600 °C that is visibly shown in Fig. 4.2 (c). Meanwhile, the FE-SEM images obtained from TED mode of all particles were presented in Fig. 4.2 (d-f). The calcined particles at temperature of 400 °C (Fig. 4.2 (d)) contain a hollow interior the same as in the raw particles (Fig. 4.2 (e)). On the other hand, the morphologies of the calcined particles at temperature of 600 °C (Fig. 4.2 (f)) contain few hollow structures. These results indicate that the calcination temperature of 600 °C possibly changes hollow forms of the particles to dense forms. This is due to the mesoporous particle growth that increases condensation of silicon [33]. It results in a larger degree of Si-O-Si bonds and fewer Si-OH groups involving to typical nonporous Stöber particles. Therefore, the calcination temperature of 600 °C is not appropriate for preserving cubic shapes with hollow interiors of the HSiNPs. Consequently, the particles calcined at temperature of 400 °C were used to prepare a light diffuser film because they still exhibit the morphologies of the HSiNPs.

4.2.3 Density of HSiNPs

To get a better understanding of the effect of the calcination temperature on the morphologies of HSiNPs, the density of the powder samples was futher measured by a helium pycnometer (Ultrapycnometer 1000T, Quantachrome Instruments). The helium pycnometer was run in the multimode with a standard deviation of 0.05%. The samples

were dried under vacuum at temperature of 180 °C for 3 days in order to eradicate any error caused by some remaining air.

Table 4.1 Densities of HSiNPs before and after calcination.

Sample	Density (g/cm^3)
Raw HSiNPs	1.67
HSiNPs calcined at 400 °C	1.66
HSiNPs calcined at 600°C	1.78

Table 4.1 illustrates the densities of the HSiNPs before and after calcination. It reveals that the density of the HSiNPs calcined at 400 °C is considerably lower than that of the raw HSiNPs which is attributed to the contaminant removal. Meanwhile, the density of the HSiNPs calcined at 600 °C is obviously higher than that of the raw HSiNPs. Interestingly, the density of the HSiNPs at 600 °C is close to that of fumed silica nanoparticles (2.2 g/cm^3) [34-35]. Therefore, the temperature of 400 °C is much more suitable than 600 °C for removing the contamination in HSiNPs.

4.3 Experimental procedures

4.3.1 Facile fabrication of optical diffuser films with HSiNPs

Based on the results from the previous section, the calcined HSiNPs at temperature of 400 °C were used to prepare light diffuser films because the particles still maintain the original raw material morphologies. The number of the desired HSiNPs in the light diffuser films was studied as listed in the first column of Table 4.2.

Table 4.2 Amount of the calcined HSiNPs in light diffuser films

Amount of the calcined HSiNPs in light diffuser films (vol%)	Calcined HSiNPs in MIBK (g)	MIBK (g)	10 wt% UV-curable acrylate monomer solution (g)
5	0.415	20	36.05
10	0.830	20	33.10
15	1.245	20	30.15
20	1.660	20	27.20

The concentration of the suitable HSiNPs in the suspensions can be calculated using the equations on our previous study [26]. The calculated values are shown in the second column of Table 4.2. The known masses of the HSiNPs were dispersed in methyl isobutyl ketone (MIBK, 99.5% Wako Pure Chemical Industries, Ltd.) by the ultrasonication for 10 min. Meanwhile, UV-curable acrylate monomer supplied by the JSR Corporation was diluted by MIBK to 10 wt% UV-curable acrylate monomer solution. After that, each of the HSiNPs dispersions was combined with the 10 wt% monomer solution. Suspensions of the HSiNPs were obtained and then coated on cleaned glass substrates using a commercial bar coating machine (K101 Control Coater; RK PrintCoat Instruments, Ltd.) to obtain wet films. The cleaned glass substrates were obtained after successively cleaning in DI-water, EtOH, and acetone for 10 min in each solvent. The wet films were kept in the dark and then cured by a UV-photo surface processor (PL16-110D; SEN LIGHTS Corp.) for 5 min so as to induce photopolymerization. Consequently, the light diffuser films with different numbers of the HSiNPs as shown in the first column of Table 4.2 were obtained.

4.3.2 Characterization of optical diffuser films with HSiNPs

The morphologies of the obtained films were observed with the FE-SEM. Before the FE-SEM observation, the films were directly dried on a hot plate at the temperature of 150 °C for 2 h since some residual solvent containing in the films may cause of unclear images. The dried samples were further coated by a thin layer of osmium tetroxide using an osmium plasma coater (OPC60A; Filagen). The films were also studied for their optical transmittances in the visible region (400-800 nm) using a UV-Vis-NIR spectrophotometer (UV3150; SHIMADZU). The transmittance results of the films were then compared to those of a cleaned glass substrate. The light diffusing

ability of all films was inferred by their scattered light image. The scattered light image was recorded by a digital camera performed on the apparatus together with a 532 nm laser (Z1M18B-F-532-PZ; Z-Laser). The apparatus was invented based on our previous reports. A film coated on cleaned glass substrate was placed in front of the laser lamp in about 15 cm lengths from each other. Subsequently, a scattered light image of the film exhibits on the dark background, which has the distance between them about 26 cm.

4.4 Results and Discussion

4.4.1 Morphologies of the light diffuser films based on the HSiNPs as fillers

The HSiNPs calcined at 400 °C were used to fabricate the light diffuser films by coating their suspension on the cleaned glass substrates, then curing with the UV-photo surface processor. The optical images of obtained films were presented in Fig. 4.3.

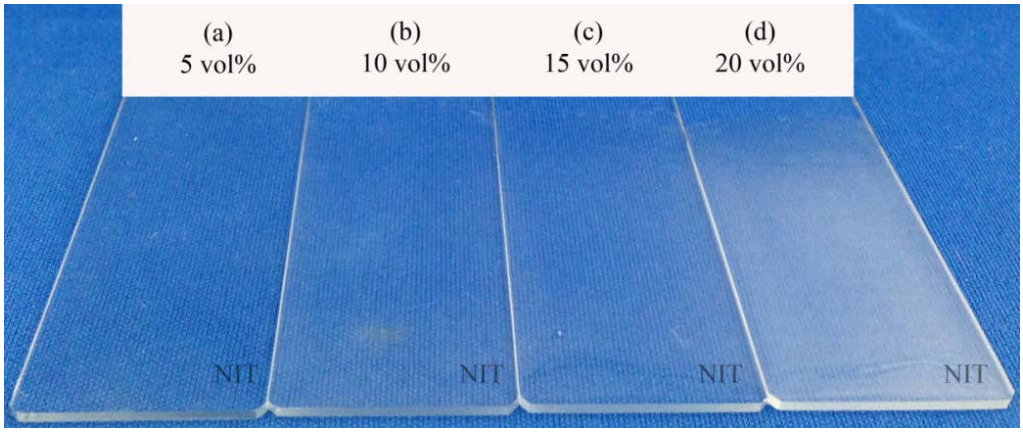

Fig. 4.3 Optical images of the light diffuser films containing different numbers of the HSiNPs such as (a) 5 vol%, (b) 10 vol%, (c) 15 vol% and (d) 20 vol%.

It distinctly shows that the obtained films were uniformly fabricated by the bar coating machine. Apparently, the films became slightly opaque when the number of the HSiNPs was increased from 5 to 20 vol%. The opacity in the films is attributed to a high number of fillers [36]. Moreover, the aggregated particles on the film surfaces possibly occur because of the solvent removal during the photopolymerization [37].

The FE-SEM with SEI mode was used to observe the morphologies of the light diffuser films based on the HSiNPs as fillers in order to study an effect of those particles.

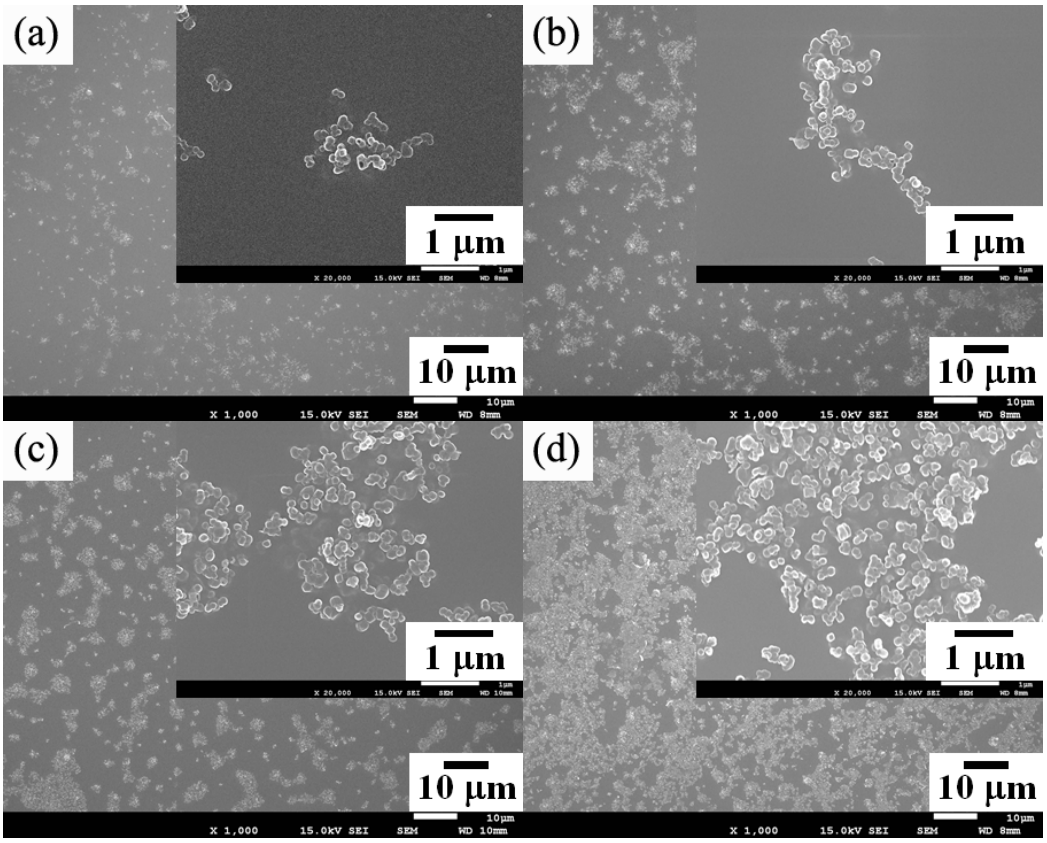

Fig. 4.4 FE-SEM images with (inset) high magnification of the light diffuser films containing different numbers of the HSiNPs such as (a) 5 vol%, (b) 10 vol%, (c) 15 vol% and (d) 20 vol%.

Fig. 4.4 shows the FE-SEM images with (inset) high magnification of the light diffuser films containing different numbers of the HSiNPs. The film surface containing 5 vol% the HSiNPs shown in Fig. 4.4 (a) has a small size of aggregated particles with a random dispersion. The size of about 1 μm of the aggregated particles can be roughly estimated by the high magnified FE-SEM image of the film as shown in inset Fig. 4.4 (a). From the enlarged FE-SEM image shown in the inset Fig. 4.4 (b), the film surface containing 10 vol% the HSiNPs exhibits a larger size of aggregated particles (~2 μm). Moreover, this film surface observed from the low magnified FE-SEM image (Fig. 4.4 (b) shows a good dispersion of the aggregated particles. Fig. 4.4 (c) shows the film surface containing 15 vol% the HSiNPs that exhibits a high number of aggregated particles. The aggregated particles observed are quite larger than 2 μm (as seen in inset Fig. 4.4 (c)) with a better dispersion as compared to the films containing lower number of the HSiNPs. Meanwhile, the film surface containing 20 vol% the HSiNPs illustrated in Fig. 4.4 (d) shows the highest number of aggregated particles as compared to the other films. The inset Fig. 4.4 (d) further reveals that the aggregated particles closely contact with the neighboring aggregated particles leading to a larger size (> 3 μm), which possess the entire film surface. When the film containing 20 vol% the HSiNPs was compared to the other films containing lower numbers of the HSiNPs, it suggests that the dispersion of aggregated particles on the film containing 20 vol% the HSiNPs exhibits the highest number of the particles with a homogeneous dispersion. All the results of the FE-SEM correspond to an order of the opacity of the film as shown in the Fig. 4.3. Moreover, the results indicate that the high number of the HSiNPs more probably provide a high number of those particles on the film surfaces with their high dispersion [18]. In addition, it can be concluded that both the size and dispersion of

fillers are the main factors, which have an influence on the optical performance of light diffuser films [2, 18].

4.4.2 Optical properties of the optical diffuser films with the HSiNPs

4.4.2.1 Total transmittance of the light diffuser films based on the HSiNPs as fillers

The total transmittance of the light diffuser films based on the HSiNPs as fillers was measured by the UV-Vis-NIR spectrophotometer in the visible region (400-800 nm), then compared to the cleaned glass substrate, which is demonstrated in Fig. 4.5.

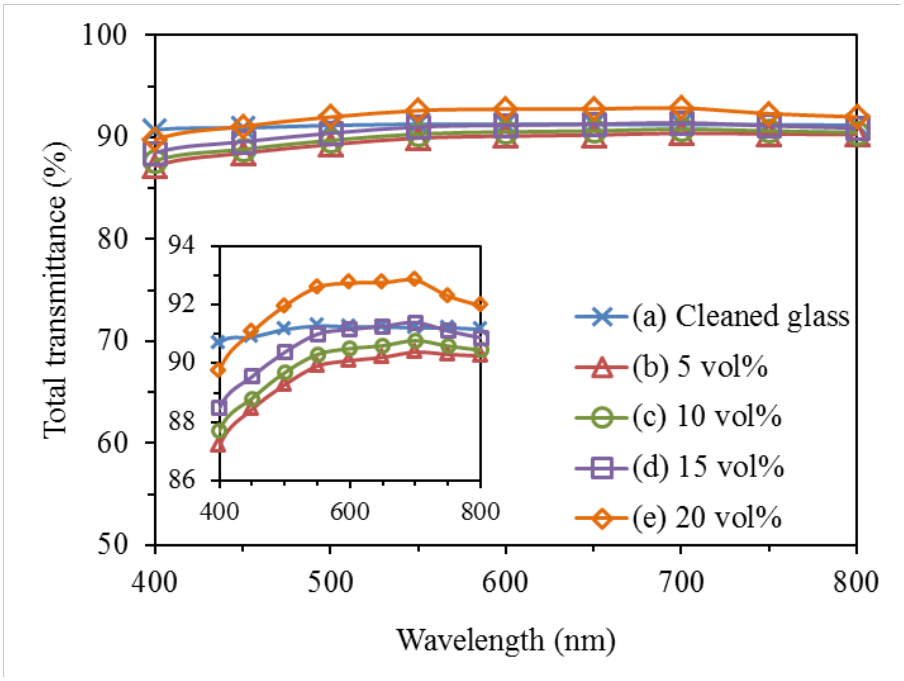

Fig. 4.5 Total transmittance spectra of the cleaned glass (a) and the light diffuser films containing different numbers of the HSiNPs such as (b) 5 vol%, (c) 10 vol%, (d) 15 vol% and (e) 20 vol%.

It can be found that the transmittance spectra of every coated glass is over 87%, which approaches that of the uncoated glass (cleaned glass) [38]. The results indicate that the high transparency of the light diffuser films coated on the glass substrate was fabricated. Interestingly, the transmittance spectra of the film containing 20 vol% the HSiNPs (Fig. 4.5 (d)) is over than that of the cleaned glass (Fig. 4.5 (a)) at the wavelength longer than 450 nm. Therefore, the film containing 20 vol% the HSiNPs possibly has an anti-reflection property [38]. Moreover, the total transmittance of the light diffuser films slightly decreases with the decreasing number of the HSiNPs as fillers in those films. These results disagree with the optical images of the films as shown in Fig. 4.4. It is due to the difference in refractive indices between particles and films [10]. Larger aggregated HSiNPs with a high refractive index possibly result in optical scattering and opacity of material.

4.4.2.2 Diffuse transmittance of the light diffuser films based on the HSiNPs as fillers

The diffuse transmittance of the light diffuser films containing different numbers of the HSiNPs was measured using the spectrophotometer equipped with an integrating sphere and then compared to that of the cleaned glass.

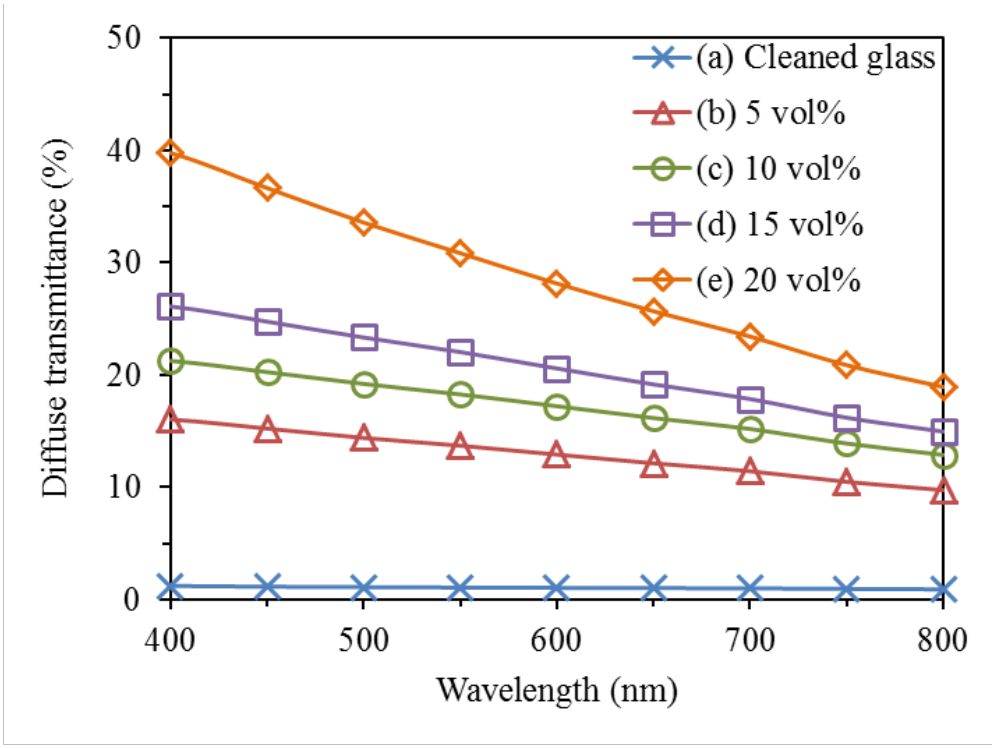

Fig. 4.6 Diffuse transmittance spectra of the cleaned glass (a) and the light diffuser films containing different numbers of the HSiNPs such as (b) 5 vol%, (c) 10 vol%, (d) 15 vol% and (e) 20 vol%.

Fig. 4.6 demonstrates the diffuse transmittance spectra of the films and the cleaned glass. It was found that the diffuse transmittance of the films is more than that of the cleaned glass. The results reveal that the films based on the HSiNPs dramatically improve diffuse transmittance of the glass substrate. Also, the diffuse transmittance of the films gradually increases with the increasing number of the particles in those films [3-5]. The enhanced diffuse transmittance relates to the different refractive indices between particles and homogeneous film, which can be explained by the Rayleigh scattering [4]. The Rayleigh scattering defined that the light scattering depends on the

size of the particles, which is very small in relation to the wavelength of incident light. And the intensity of the scattering is inversely proportional to the fourth power of the wavelength. Also, the Rayleigh scattering has a significant influence on the longer wavelength of the light. This relates to the abrupt reduction of the diffuse transmittance at the longer wavelength, which can be seen in all diffuse transmittance of the films (Fig. 4.6 (b)-(e)). The results can be inferred that almost aggregated particles inside the films are smaller than the wavelength of the incident light and the size of the observed aggregated particles on the film surfaces (as can be seen in the FE-SEM images of the film surfaces in Fig. 4.4) [10]. Meanwhile, the aggregated particles on the film surfaces possibly occur throughout the Rayleigh scattering interfering with the Mie scattering. In the case of the Mie scattering, the size of the particles is comparable or larger than the wavelength of the incident light [10, 39]. The intensity of the light scattering is independent to the size of the particles. Moreover, the direction of the light scattering is towards that of the incident light. The light scattering on the film surfaces significantly has an influence on the enhancement of the total and diffuse transmittance of those films. It is evidently confirmed by the sequence of the diffuse transmittance of the films, which corresponds to the order of the total transmittance of those films.

4.4.2.3 Light diffusing ability of the light diffuser films based on the HSiNPs as fillers

The Mie scattering not only play a key role in the transmittances of the films but also influences on homogenization of the incident light. The homogenization is one of the main factors in achieving good light diffuser films [2]. The homogenization of the light penetrated throughout the light diffuser films containing different numbers of the HSiNPs can be examined using the apparatus. The results are shown in the scattered

light image of the films as exhibited in Fig. 4.7, which imply the light diffusing ability of those films.

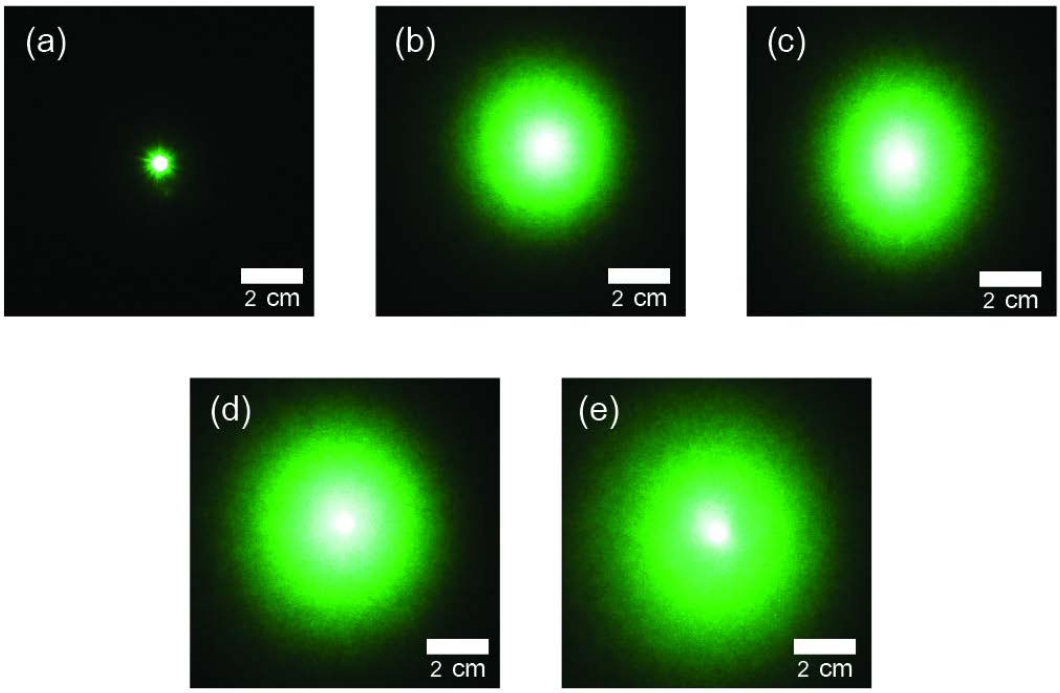

Fig. 4.7 The scattered light images of the cleaned glass (a) and the light diffuser films containing different numbers of the HSiNPs such as (b) 5 vol%, (c) 10 vol%, (d) 15 vol% and (e) 20 vol%.

In comparison of the scattered light images in Fig. 4.7, they reveal that the size of the scattered light images of the films is larger than that scattered light image of the cleaned glass. The films can diffuse the point and the line light source resulting in homogeneous surface lighting [2]. It can be implied that the films exhibit their high light diffusing ability. These are due to the production of the scattered light by the

particles. The scattered light is caused by the particles only, when the polymer matrix is assumed to be transparent and homogeneous [40]. Consequently, the high number of particles loaded in the films probably provides a greater light scattering leading to a high diffuse transmittance. As could be seen in Fig. 4.7 (b)-(e), the size of the scattered light image of the film dramatically increases with the increasing number of the HSiNPs. The scattered light images of the films exhibit fairly uniform pattern. This suggests that the HSiNPs used as fillers leads to the uniform pattern of the scattered light [4, 11-12]. In addition, the aggregated particles on the film surfaces (as observed from the FE-SEM images in Fig. 4.4) do not have a sufficient separation; therefore, they probably produce multiple scattering based on the Mie scattering [40]. The multiple scattering usually occurs in the film containing aggregated particles because the scattered light of each particle or cluster is supposed to be dependent on each other. Consequently, the film containing the highest number of aggregated particles (20 vol% the HSiNPs) more continually provides the scattered light leading to both high transmittances and homogeneous light. These properties play a significant role in a high performance of a light diffuser film [2]. Therefore, the films containing a high number of the HSiNPs have a great potential to be light diffuser films, especially manufactured multifunctional light diffuser films in the LCD industry. A schematic illustration of applying the light diffuser film based on the HSiNPs as fillers in the LCD is shown in Fig. 4.8.

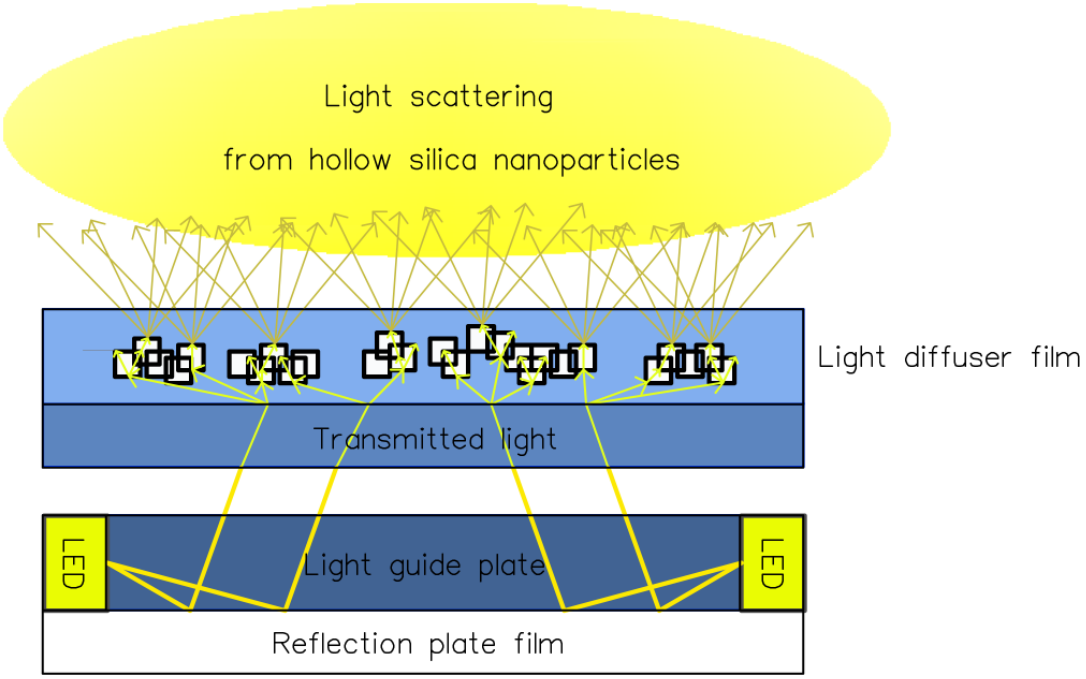

Fig. 4.8 Schematic illustration of applying the light diffuser film based on the HSiNPs as fillers in the LCD.

4.5 Conclusion

The light diffuser films based on HSiNPs as fillers were facilely fabricated by coating the suspension of the HSiNPs calcined at temperature of 400 °C and the UV-curable acrylate monomer solution. The number of the particles in the films was varied from 5 to 20 vol%. The films became opaque when the number of the HSiNPs was increased. Meanwhile, the films containing different numbers of the particles exhibit various total transmittances and they are also close to the cleaned glass. The diffuse transmittance of the films increases as the number of particles increases that are also obviously higher than that of the cleaned glass. Interestingly, a film based on 20 vol% HSiNPs gives the highest total transmittance (93%) and diffuse transmittance (40%)

when comparing to other films in this study. The film also exhibits the largest size of the scattered light image which indicates its highest light diffusing ability. In conclusion, the increased number of the HSiNPs in light diffuser films improves both transmittances and light diffusing ability; therefore, the HSiNPs are potentially applied for fillers in light diffuser films of backlight unit in the LCD industry

References

[1] S. Song, Y. Sun, Y. Lin and B. You, A facile fabrication of light diffusing film with LDP/polyacrylates composites coating for anti-glare LED application, *Appl. Surf. Sci.* **273** (2013) 652-660.

[2] X. Sun, N. Li, J. Hang, L. Jin, L. Shi, Z. Cheng and D. Shang, Nano-silica reinforced hybrid light-diffusing films with enhanced mechanical and thermal properties, *Opt Appl* **45** (2015) 393-404.

[3] J. Hu, Y. Zhou and X. Sheng, Optical diffusers with enhanced properties based on novel polysiloxane@CeO_2@PMMA fillers, *J. Mater. Chem. C* **3** (2015) 2223-2230.

[4] J. Hu, Y. Zhou, M. He and X. Yang, Novel multifuntional microspheres of polysiloxane@CeO_2-PMMA: Optical properties and their application in optical diffusers, *Opt. Mater.* **36** (2013) 271-277.

[5] J. Hu, Y. Zhou and T. Zhang, The novel optical diffusers based on the fillers of boehmite hollow microspheres, *Mater. Lett.* **136** (2014)114-117.

[6] J.H. Wang, S.Y. Lien, J.R. Ho, T.K. Shih, C.F. Chen, C.C. Chen and W.T. Whang, Optical diffusers based on silicone emulsions, *Opt Mater* **32** (2009) 374-377.

[7] T.C. Huang, J.R. Ciou, P.H. Huang, K.H. Hsieh and S.Y. Yang, Fast fabrication of integrated surface relief and particle-diffusing plastic diffuser by use of a hybrid extrusion roller embossing process, *Opt Express* **16** (2008) 440-447.

[8] S.J. Liu and Y.C. Huang, Manufacture of dual-side surface-relief diffusers with various cross angles using ultrasonic embossing technique, *Opt Express* **17** (2009) 18083-18092.

[9] D. Sakai, K. Harada, S. Kamemaru, M.A. El-Morsy, M. Itoh and T. Yatagai, Direct fabrication of surface relief holographic diffusers in azobenzene polymer films, *Opt Rev* **12** (2005) 383-386.

[10] S. Guo, S. Zhou, H. Li and B. You, Light diffusing films fabricated by strawberry-like PMMA/SiO_2 composite microspheres for LED application, *J. Colloid Interface Sci* **448** (2015) 123-129.

[11] H. Butt, K.M. Knowles, Y. Montelongo, G.A.J. Amaratunga and T.D. Wilkinson, Devitrite-Based Optical Diffusers, *ACS Nano* **8** (2014) 2929-2935.

[12] S. Ahn and G.H. Kim, An electrosprayed coating process for fabricating hemispherical PMMA droplets for an optical diffuser, *Appl Phys A* **97** (2009) 125-131.

[13] L.E. Mcneil and R.H. Frenceh, Multiple scattering from rutile TiO_2 particles, *Acta Materialia* **48** (2000) 4571-4576.

[14] Y. Zhao, P. Ding, C. Ba, A. Tang, N. Song, Y. Liu and L. Shi, Preparation of TiO_2 coated silicate micro-spheres for enhancing the light diffusion property of polycarbonate composites, *Displays* **35** (2014) 220-226.

[15] K. Shin, H.N. Kim, J.C. Cho, S.J. Moon, J.W. Kim and K.D. Suh, Fabrication of monodisperse polymer/silica hybrid microparticles for improving light diffusion properties, *Macromol Res* **20** (2012) 385-390.

[16] T. Wang, T.T. Isimjan, J. Chen and S. Rohani, Transparent nanostructured coatings with Uv-shielding and superhydrophobicity properties, *Nanotechnology* **22** (2011) 265708.

[17] M. H. Tsai, C.J. Chang, P.J. Chen and C.J. Ko, Preparation and characteristics of poly(Amide-Imide)/titania nanocomposite thin films, *Thin Solid Films* **516** (2008) 5654-5658.

[18] M.E. Calvo, J.R. Castro Smirnov and H. Míguez, Novel approaches to flexible visible transparent hybrid films for ultraviolet protection, *J. Polym. Sci. Pol. Phys.* **50** (2012) 945-956.

[19] Y. Tu, L. Zhou, Y.Z. Jin, C. Gao, Z.Z. Ye, Y.F. Yang and Q.L. Wang, Transparent and flexible thin films of ZnO-polystyrene nanocomposite for UV-shielding applications, *J. Mater. Chem.* **20** (2010) 1594-1599.

[20] L. Qi, A. Sehgal, J.C. Castaing, J.P. Chapel, J. Fresnais, J.F. Berret and F. Cousin, Redispersible hybrid nanopowders: Cerium oxide nanoparticle complexes with phosphonated-peg oligomers, *ACS Nano* **2** (2008) 879-888.

[21] H.P. Kuo, M.Y. Chuang and C.C. Lin, Design correlations for the optical performance of the particle-diffusing bottom diffusers in the LCD backlight unit, *Powder Technol.* **192** (2009) 116-121.

[22] L. Mingyan, W. Daming, Z. Yajun and Z. Jian, Optimization and design of LCD diffuser plate with micro-semisphere structure, *Procedia Eng.* **16** (2011) 306-311.

[23] Y. Liaoa, X. Wu, H. Liu and Y. Chen, Thermal conductivity of powder silica hollow spheres, *Thermochim. Acta* **526** (2011) 178-184.

[24] Y. Du, L.E. Luna, W.S. Tan, M.F. Rubner and R.E. Cohen, Hollow silica nanoparticles in UV-visible antireflection coatings for poly(methyl methacrylate) substrates, *ACS Nano* **4** (2010) 4308-4316.

[25] M.C. Tsai, J.Y. Lee, P.C. Chen, Y.W. Chang, Y.C. Chang, M.H. Yang, H.T. Chiu, I.N. Lin, R.K. Lee and C.Y. Lee, Effects of size and shell thickness of TiO_2 hierarchical hollow spheres on photocatalytic behavior: An experimental and theoretical study, *Appl. Catal., B* **147** (2014) 499-507.

[26] W. Suthabanditpong, R. Buntem, C. Takai, M. Fuji and T. Shirai, The quantitative effect of silica nanoparticles on optical properties of thin solid silica UV-cured films, *Surf. Coat. Technol.* **279** (2015) 25-31.

[27] A. Milinavičiūtė, V. Jankauskaitė and P. Narmontas, Properties of UV-curable hyperbranched urethane-acrylate modified acrylic monomer coatings, *Mater. Sci. (Medžiagotyra)* **17** (2011) 378-383.

[28] C.J. Chang, M.H. Tsai, P.C. Kao and H.Y. Tzeng, Optical and mechanical properties of jet printed and UV cured blue pixels with phosphated epoxy acrylate as the curing agent, *Thin Solid Films* **516** (2008) 5503-5507.

[29] H. Wanyika, E. Gatebe, P. Kioni, Z. Tang and Y. Gao, Synthesis and characterization of ordered mesoporous silica nanoparticles with tunable physical properties by varying molar composition of reagents, *Afr. J. Pharm.* **5** (2011) 2402-2410.

[30] D. Das, Y. Yang, J. S. O'Brien, D. Breznan, S. Nimesh, S. Bernatchez, M. Hill, A. Sayari, R. Vincent and P. Kumarathasan, Synthesis and Physicochemical characterization of mesoporous SiO_2 nanoparticles, *J Nanomater.* **2014** (2014) Article ID 176015.

[31] R.V.R. Virtudazo, M. Fuji, C. Takai and T.Shirai, Fabrication of unique hollow silicate nanoparticles with hierarchically micro/mesoporous shell structure by a simple double template approach, *Nanotechnology* **23** (2012) 485608.

[32] A. Liberman, N. Mendez, W.C. Trogler and A.C. Kummel, Synthesis and surface functionalization of silica nanoparticles for nanomedicine, *Surf Sci Rep.* **69** (2014)132-158.

[33] Y. Chen, H. Chen, L. Guo, Q. He, F. Chen, J. Zhou, J. Feng and J. Shi, Hollow/rattle-type mesoporous nanostructures by a structural difference-based selective etching strategy, *ACS Nano* **4** (2009) 529-539.

[34] S. Rimdusit, K. Punson, I. Dueramae, A. Somwangthanaroj and S. Tiptipakorn, Rheological and thermomechanical characterizations of fumed silica-filled polybenzoxazine nanocomposites, *ENGINEERING JOURNAL* **15** (2011) 27-38; DOI:10.4186/ej.2011.15.3.27.

[35] V.M. Gun'ko, L.S. Andriyko, V.I. Zarko, A.I. Marynin, V.V. Olishevskyi and W. Janusz, Effects of dissolved metal chlorides on the behavior of silica nanoparticles in aqueous media, *Cent. Eur. J. Chem.* **12** (2014) 480-491.

[36] T. Otsuka and Y. Chujo, Poly(methyl methacrylate) (PMMA)-based hybrid materials with reactive zirconium oxide nanocrystals, *Polym. J.* **42** (2010) 58-65.

[37] T. Ribeiro, A. Fedorov, C. Baleizão and J.P.S. Farinha, Formation of hybrid films from perylenediimide-labeled core-shell silica-polymer nanoparticles, *J. Colloid Interface Sci.* **401** (2013) 14-22.

[38] J. W. Leem, Y. Yeh and J.S. Yu, Enhanced transmittance and hydrophilicity of nanostructured glass substrates with antireflective properties using disordered gold nanopatterns, *Opt Express* **20** (2012) 4056-4066.

[39] R. Barchini, J.G. Gordon II and M.W. Hart, Multiple Light Scattering Model Applied to Reflective Display Materials, *Jpn. J. Appl. Phys.* **37** (1998) 6662-6668.

[40] A. Rastar, M.E. Yazdanshenas, A. Rashidi and S.M. Bidoki, Theoretical review of optical properties of nanoparticles, *J. Eng. Fiber Fabr.* **8** (2013) 85-96.

CHAPTER 5

CONTROLLING STRUCTURE OF HOLLOW SILICA NANOPARTICLES THROUGH CORE-TEMPLATE REMOVAL PROCESS WITH ACID AND APPLYING THEIR STRUCTURE FOR LIGHT DIFFUSER FILMS

5.1 Introduction

Recently, liquid crystal display (LCD) has dramatically become a dominant product in the display market. Therefore, the backlight unit as an essential part of LCDs has been gradually developed by many approaches. The backlight unit supplies light for LCDs, which cannot emit the light by themselves [1]. This unit mainly composes of a light emitter, a light guide plate, a reflection film, one or two brightness enhancement film (s), and one or two light diffuser film (s). Remarkably, the light diffuser film has a function of scattering and homogenizing the light source over a wide angle in order to achieve comfortable and wide view-angle image from LCDs [2-6]. At present, there are two types of light diffuser films achieved for applying in LCDs which are volumetric diffuser type [1, 2] and surface-relief diffuser type [3-6]. Since the surface-relief diffuser type is fabricated by complicated process using expensive equipment, many researchers are much attracted to study the volumetric diffuser type which is more simply fabricated by coating a mixture of filler and binder resin on optical material [7-12]. The light scattering in this diffuser type is caused by fillers, which are mainly organic or inorganic particles. Based on the utilization of the light diffuser in LCDs, inorganic particles are much attractive because of their thermal stability [8, 10]. However, the particles tend to approach each other leading to agglomeration problem. It is a cause of low transmittance of the light diffuser films. Meanwhile, number of the particles in the diffusers is one of the main factors of number of backlight unit in LCDs. This is related to the energy consumption and the weight of screens [7, 8]. To overcome these problems, hollow structure of the particles has shown a great promise to solve them.

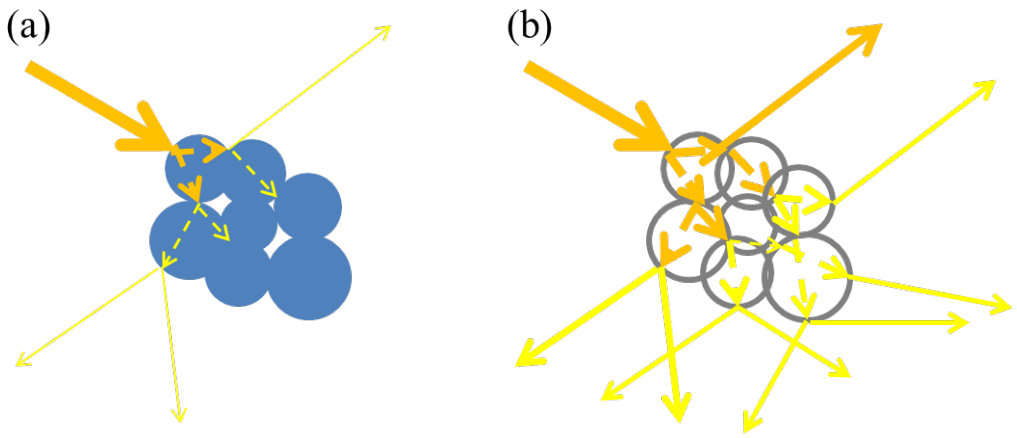

Fig. 5.1 Schematic illustration of light scattering occurred by (a) dense particles and (b) hollow particles.

Hollow particles fundamentally comprise of hollow interiors and solid shells surrounding the hollow interiors [13-15]. Due to their unique characteristic, these particles have many interesting properties; for example, low density [8], high specific surface area [8, 14], thermal insulation [16, 17], optical properties [7, 8, 18], light-weight filler [8], and etc. Therefore, the hollow particles are extensively applied for many applications, such as catalysis [19, 20], bio-technology [21-24] and optical diffuser [8]. However, the utilization of the hollow particles in the field of light diffuser films is particularly much more attractive as these particles probably allow light penetration through their hollow interiors and slightly absorb the light with their solid shells. It can be illustrated by Fig. 5.1, which implies that the light scattering is more possibly occurred by hollow particles (Fig. 5.1 (b)) than by dense particles (Fig. 5.1 (a)). Meanwhile, the power consumption may be reduced when the light pass through hollow particle [8, 18, 20]. Moreover, the difference of refractive indices between the hollow

interior and the solid shell more probably produces more light refraction in the light diffuser films [8]. According to these reasons, morphologies and surface properties of hollow particles significantly affect the efficiency of light diffuser films. Therefore, one of the effective approaches to obtain suitable hollow particles is a synthesis of hollow silica nanoparticles via inorganic particle template method incorporated with removing core-template by the acid dissolution [13, 15, 25, 26]. The hollow silica nanoparticles (HSiNPs) have many essential properties for light diffuser films; for instance, low density, thermal insulation, prominent optical material, and light-weight filler [9, 17, 18]. Meanwhile, the method is neither additional toxic chemicals nor a calcination process.

In this chapter, HSiNPs were synthesized using calcium carbonate ($CaCO_3$) as the inorganic core- template which was removed by HCl. The pH of HCl was varied as 1, 2 and 5. The aim of this process was to control structure (e.g. shell thickness, hollow interior). The obtained particles were expectedly suitable for fabricating silica-UV-cured polymer composite films with high optical properties. The morphologies and surface properties of the synthesized HSiNPs at different pH were characterized. The silica/UV-cured polymer composite films were fabricated by coating dispersions of each HSiNPs in a UV-curable acrylate monomer and then cured by a UV-lamp. The optical transmittances, light diffusing ability and morphologies of the composite films were then studied. An effect of the morphological HSiNPs on the optical properties of the composite films was also discussed.

5.2 Experimental procedures

5.2.1 Materials

Calcium carbonate ($CaCO_3$, Homocal D) was obtained from Shiraishi Calcium Kaisha, Ltd. The appearance of the $CaCO_3$ is in cubic shapes with the particle size of about 80 nm, which was determined by field emission scanning electron microscopy (FE-SEM) observation as shown in Fig. 5.2.

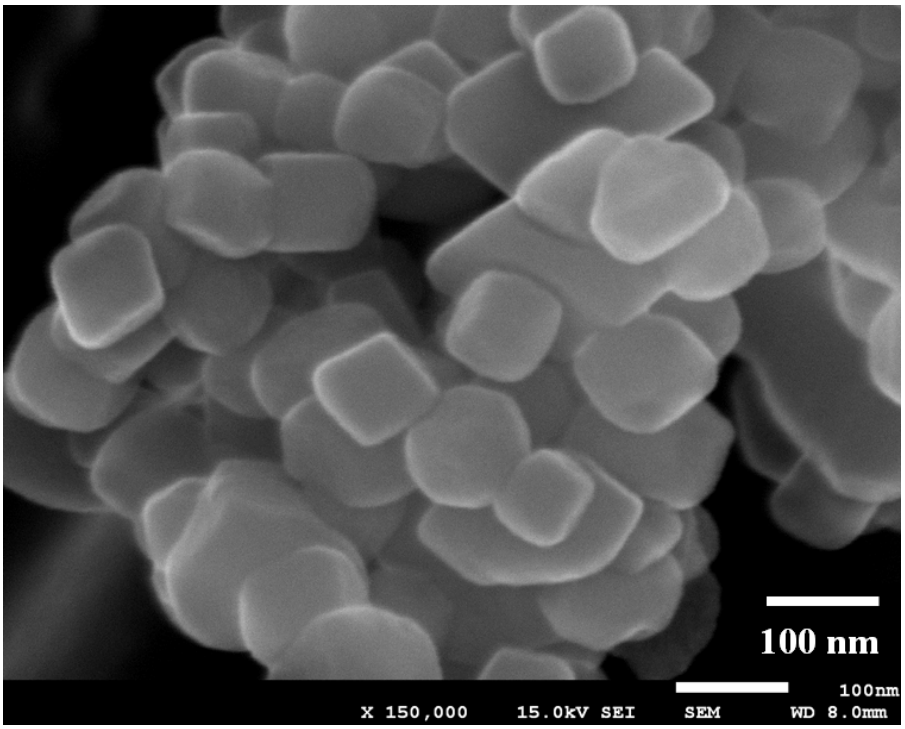

Fig. 5.2 FE-SEM image of the raw $CaCO_3$ nanoparticles.

Diglyme (Dg, Wako Pure Chemical Industries, Ltd.) was dissolved in deionized water (DI-water) to obtain 69.0% diglyme aqueous solution (Dg aq.). The 69% Dg aq. was used as a solvent to prepare HSiNPs. For HSiNPs, tetraethoxysilane (TEOS, Wako Pure Chemical, Ltd.) as silica sources, ammonia water (NH_3 aq., 25% Wako Pure Chemical Industries, Ltd.) as a catalyst for sol-gel reaction and hydrochloric acid (HCl, Wako Pure Chemical, Ltd.) as an acid treatment were used as received.

UV-curable acrylate monomer (JSR Corporation) and methyl isobutyl ketone (MIBK, 99.5% Wako Pure Chemical Industries, Ltd.) were mixed to be binder resin for fabricating silica/UV-cured polymer composite films. All glass substrates were ultrasonically cleaned successively in DI-water, ethanol (EtOH, 99% Wako Pure Chemical Industries, Ltd.) and acetone (Wako Pure Chemical Industries, Ltd.) for 10 min in each solvent before being used as optical materials for coating the composite films.

5.2.2 Synthesis of hollow silica nanoparticles

HSiNPs were synthesized based on our previous reports, which used $CaCO_3$ nanoparticles as the template [25] and HCl as the acid treatment [13]. The synthesized method was modified so as to get the appropriate morphologies of HSiNPs morphologies for fabricating silica/UV-cured polymer composite film with high optical properties. The $CaCO_3$, D_g aq., TEOS and 25.0% NH_3 aq. were mixed and stirred for 90 min at room temperature in the ratio of $CaCO_3$:D_g aq.:TEOS:NH_3 aq. = 2:29:1.6:0.45 in order to obtain core-shell particles. After that, the milky white solution was centrifuged and filtrated. Precipitates were washed with EtOH twice times and then dried under vacuum. The dried powders were further treated with HCl to remove

$CaCO_3$ template. During the removal template process, pH of HCl was varied as 1, 2, and 5 in order to modify the morphologies and surface properties of HSiNPs. The samples removed core-templates were washed several times with EtOH/H_2O solution until they became neutral before being dried under vacuum. Consequently, the synthesized HSiNPs at pH 1, 2 and 5, namely, HSiNPs-1, HSiNPs-2 and HSiNPs-5 by respectively, were obtained.

5.2.3 Fabrication of silica/UV-cured polymer composite films

Each of the HSiNPs was dispersed in MIBK by a Branson digital sonifier (450DA, Branson Ultrasonic Corp.) equipped with an ultrasonic horn at the amplitude of 40% and pulse on/off of 1 sec for about 10 min. The UV-curable acrylate monomer was diluted in MIBK to 20 vol% UV-curable acrylate monomer solution. Each of the HSiNPs dispersions was then mixed with the monomer solution at the ratio of 1:1 by the sonifier for 10 min in the ice bath. After that, a planetary centrifugal deaeration mixer (ARE-930 Twin THINKY Mixer) at a revolution speed of 1000 rpm under a vacuum of 20 kPa was used for removing air bubbles in the dispersions about 5 min. As a result, the HSiNPs in UV-curable acrylate monomer dispersions were obtained and coated on the cleaned glass substrates using a bar-coating machine (K101 Control Coater; RK PrintCoat Instruments, Ltd.). The wet silica composite films were initially dried at room temperature in the dark for 24 h before being further cured by a UV-photo surface processor (PL16-110D; SEN LIGHTS Corp.). The dried films were cured at room temperature for 5 min to induce polymerization. Consequently, the silica/UV-cured polymer composite films coated on glass substrate were obtained.

5.2.4 Characterization

The synthesized HSiNPs were characterized by a X-ray diffraction (XRD, Model RINT 1100; Rigaku) with Cu Kα radiation (λ = 1.54056 Å). The XRD was operated at scanning rate of 2 $°s^{-1}$ (5°-60°, 2θ) with an operating voltage of 40 kV and emission current 40 mA. The surface morphologies of the samples were observed by a field emission scanning electron microscope (FE-SEM, JSM7600F; JEOL Ltd.) at an acceleration voltage of 15 kV. Prior to imaging by the FE-SEM, the samples were dispersed in EtOH by an ultrasonication. The suspensions were then dropped on a microgrid (STEM150Cu; Oken Shoji) and dried in the air. The interior morphologies of the samples were studied using a transmission electron microscope (TEM, JEM-Z2500; JEOL Ltd.) at 200 kV. The surface properties of the samples were examined by the Brunauer-Emmett-Teller (BET) method and the Bareett-Joyner-Halenda (BJH) method. These methods were studied using an automatic surface area analyzer (BELSORP-miniII-CM) with Nitrogen gas (N_2) adsorption desorption isotherm recorded at 77 K.

The optical transmittances of the silica/UV-cured polymer composite films were measured by a UV-Vis-NIR spectrophotometer (UV3150; SHIMADZU) in the visible region (400-800 nm). The transmittances of the composite films were then compared to those of the UV-cured polymer film. For further understanding the effect of the particle aggregation, the cumulative size distribution of the HSiNPs in UV-curable acrylate monomer dispersions were studied using a Dynamic light scattering (DLS, Malvern Zetasizer nano; Sysmex Company). Meanwhile, the light diffusing ability of all films was examined by an apparatus equipped with a 532 nm laser (Z1M18B-F-532-PZ; Z-Laser). The films were placed in front of the laser light about 15 cm. Then, a scattered

light image of the films shows on a dark background, which is far from them about 26 cm. The surface morphologies of the silica/UV-cured polymer composite films were studied using the FE-SEM. Before the FE-SEM observation, the films were directly dried on a hot plate at the temperature of 150 °C for 2 h as some residual solvent containing in the films may cause of unclear images. The dried samples were further coated by a thin layer of osmium tetroxide using an osmium plasma coater (OPC60A; Filagen).

5.3 Results and Discussion

5.3.1. Morphologies and surface properties of hollow silica nanoparticles

The X-ray diffraction patterns (XRD) of the $CaCO_3$ and the synthesized HSiNPs at different pH of HCl are shown in the Fig. 5.3.

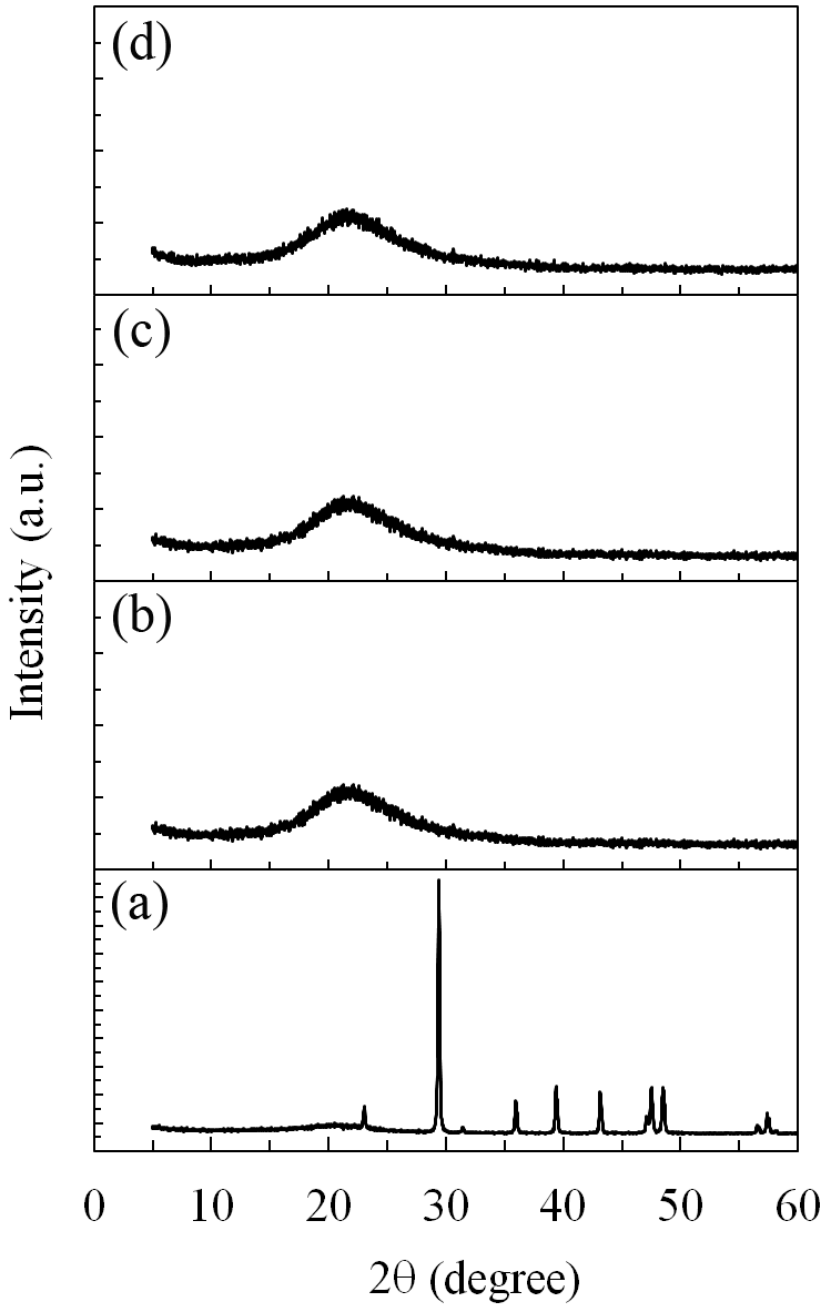

Fig. 5.3 XRD patterns of (a) raw $CaCO_3$ nanoparticles,

(b) HSiNPs-1, (c) HSiNPs-2 and (d) HSiNPs-5.

The XRD pattern of the $CaCO_3$ showed in Fig. 5.3 (a) presents the diffraction angle which is identified as calcite [14]. In contrast, no diffraction pattern of the calcite is observed in Figs. 5.3 (b), (c) and (d), which show the XRD results of the HSiNPs. It confirms that the $CaCO_3$ core-template was completely removed by HCl during acid treatment [14]. Moreover, all diffraction patterns observed in Figs. 5.3 (b-d) reveal that the synthesized particles are amorphous [27]. The morphologies of the obtained HSiNPs after the acid treatment were observed by the FE-SEM.

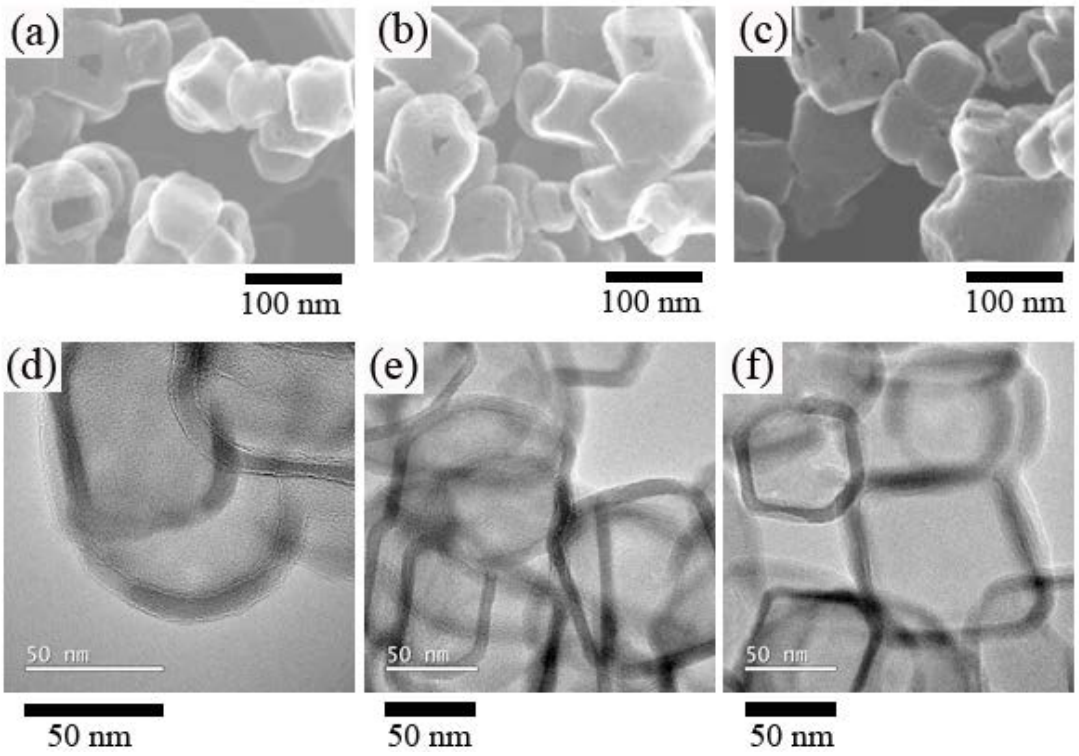

Fig. 5.4 FE-SEM images of (a) HSiNPs-1, (b) HSiNPs-2 and (c) HSiNPs-5 and their TEM images as following shown in (d), (e) and (f), by respectively.

Figs. 5.4 (a), (b) and (c) show FE-SEM images of the HSiNPs removed core-template by HCl at pH of 1, 2, and 5 respectively. They reveal that shape of the HSiNPs at the different pH still retains cubic and is similar to that of $CaCO_3$ core-template (as can be seen in Fig. 5.2). Therefore, the shape of the samples was not modified by the acid treatment [13, 14, 28]. The surface roughness of the samples gradually increases with increasing pH of HCl. Meanwhile, window cavities are fragmentary observed on some cubic particles in each sample. It may be due to a number of silica that may insufficiently coat on some faces of core-templates [28].

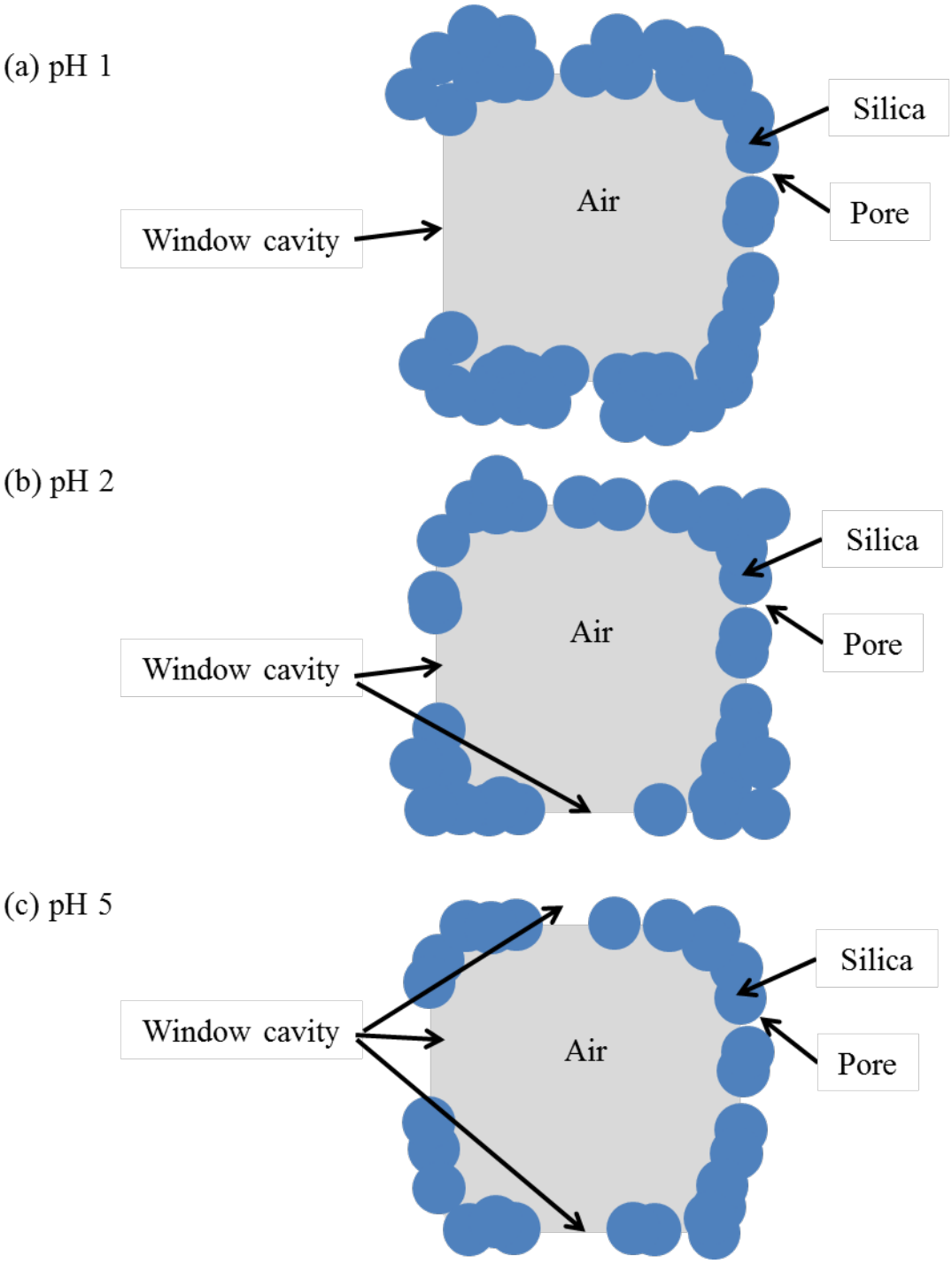

Fig. 5.5 Schematic illustration of silica growth

around air produced by removing core-template at pH of (a) 1, (b) 2, and (c) 5.

Moreover, the cubic calcites as the core-template probably have high surface energy at their vertexes and edges so SiOH may preferentially adsorb on those area to decrease their surface energy [25]. This behavior can be illustrated in Fig. 5.5. As a result, the window cavities were produced on faces of the cubic silica nanoparticles. The results indicate that the different pH of HCl significantly provide the distinctive morphologies of the HSiNPs. Consequently, it further has an effect on the morphologies of films that affects the optical properties of those [7].

Figs. 5.4 (d), (e) and (f) respectively illustrate TEM images of HSiNPs-1, HSiNPs-2 and HSiNPs-5. All the images obviously show hollow interior that completely confirm the core-template removal and a formation of silica surrounding the core-templates [13-15, 28]. The silica shell seems to be thicker when the pH of HCl decreases because the low pH of HCl (high number of H^+) more probably induces more aggregation [14].

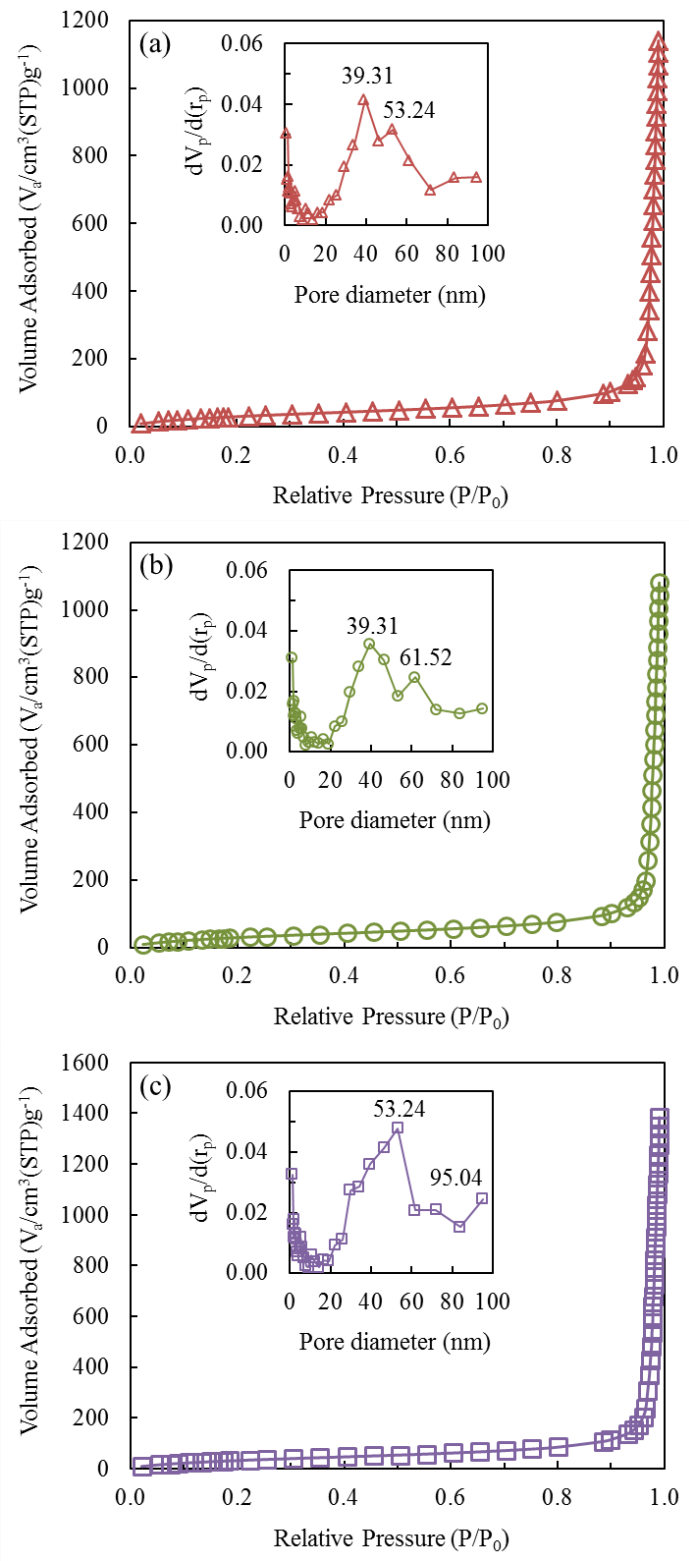

Fig. 5.6 N_2-adsorption isotherm with (inset) pore size distribution of (a) HSiNPs-1, (b) HSiNPs-2 and (c) HSiNPs-5.

Figs. 5.6 (a), (b) and (c) demonstrate the result of nitrogen adsorption isotherm at 77 K with (inset) the pore size distribution of HSiNPs-1, HSiNPs-2 and HSiNPs-5. All of the adsorption isotherms present the type II isotherm in the IUPAC classification scheme which is considered as the characteristic of nonporous materials [29]. The abrupt growth of the adsorptions at high relative pressure (P/P_0~0.9-1.0) is obviously observed. It is attributed to the adsorption of macropores [29]. The pores existed within shells and hollow interiors are composed of the HSiNPs [26]. The BJH method was applied to determine pore size distribution of the various HSiNPs and the results are demonstrated in inset Fig. 5.6 (a, b and c). The pore of the HSiNPs-1 (inset Fig. 5.6 (a) is around 39.31 and 53.24 nm. Inset Fig. 5.6 (b) displays the pore of the HSiNPs-2 that is about 39.31 and 61.52 nm. The pore size distribution of the HSiNPs-2 appears to be slightly larger than that of the HSiNPs-1. Meanwhile, the pore of the HSiNPs-5 (inset Fig. 5.6 (c)) is approximately 53.24 and 95.04 nm which is much larger than that of the HSiNPs-1 and of the HSiNPs-2. This can be explained that the size of the hollow interior of the HSiNPs-5 is quite larger than that of the HSiNPs-1 and HSiNPs-2, which corresponds to the TEM results. The pore size of all HSiNPs is slightly different from the hollow interior size of those. It evidently confirms that the pore and the cavity pore (window cavity) are probably within the shell of the HSiNPs resulting in the growth of nitrogen molecules penetration [14]. This explanation is also evidently supported by the FE-SEM results (as shown in Figs. 5.4 (a), (b) and (c)). The BET specific surface area of the HSiNPs-1, HSiNPs-2 and HSiNPs-5 is approximately 128.74, 131.65 and 143.15 m^2/g, by respectively. It can be inferred that the specific surface area increases when the pore size increases [30].

5.3.2 Optical properties and morphologies of the silica/UV-cured polymer composite films

5.3.2.1 Optical properties of the silica/UV-cured polymer composite films

The total transmittance of the UV-cured polymer film and the silica/UV-cured polymer composite films embedded with different HSiNPs were measured by the UV-Vis spectrophotometer in the visible region (400-800 nm). The results are shown in Fig. 5.7.

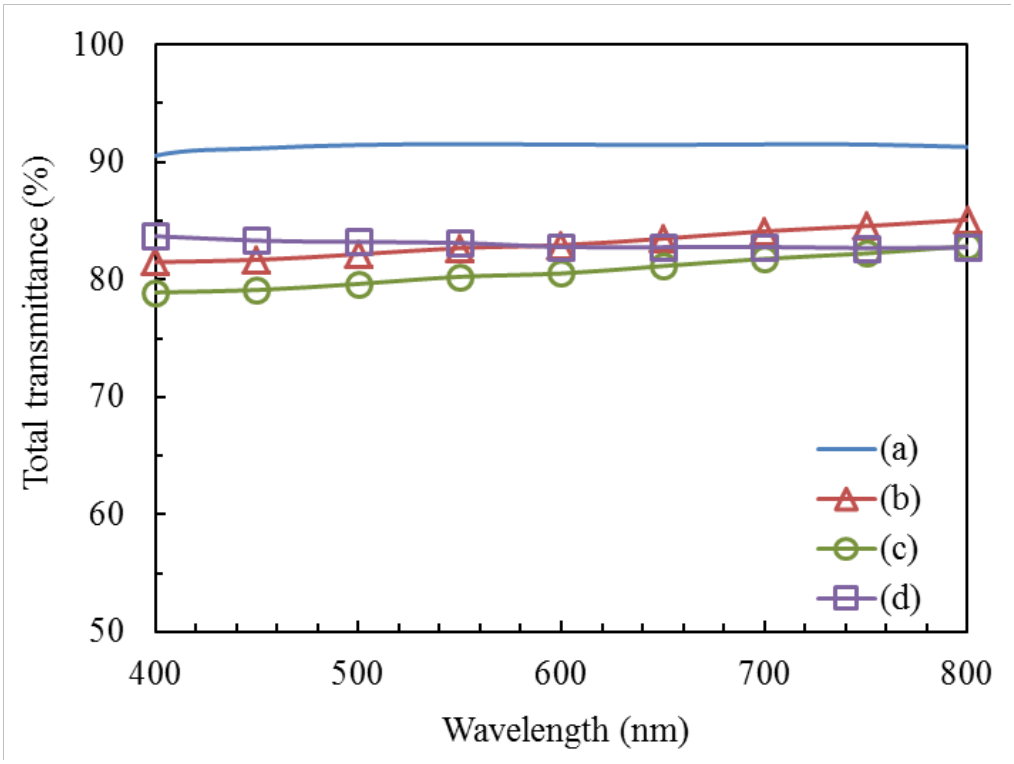

Fig. 5.7 Total transmittance spectra of the UV-cured polymer film (a) and the silica/UV-cured polymer composite films embedded with (b) HSiNPs-1, (c) HSiNPs-2 and (d) HSiNPs-5.

Figs. 5.7 (b), (c) and (d) consecutively display the total transmittance spectra of the composite films embedded with HSiNPs-1, HSiNPs-2 and HSiNPs-5. They can be seen that their transmittance spectra is lower than the total transmittance spectra of the UV-cured polymer film as shown in Fig. 5.7 (a). This is due to the transmitted light that is less absorbed by silica shell of the embedded particles [20]. Therefore, the intensity of the transmitted light attenuates. On the other hand, almost the transmitted light can propagate toward the particles. As a result, the transmittance of the composite films is still over than 80% indicating their transparency. The transmitted light then interacts with the particle shell and consequently passes through hollow interior of the particles leading to inner light scattering [8]. The inner light scattering is possibly increased by the different refractive indices between the solid shell and hollow interior of the particles. The light scattering during different refractive indices between materials relates to Rayleigh scattering [9]. The Rayleigh scattering happens if size of the scattering particles (heterogeneous phase) is much smaller than the incident light wavelength [31]. Consequently, the intensity of the light scattering is directly proportional to $1/\lambda^4$ (λ, wavelength of the incident light). In addition, the Rayleigh scattering affects an enhancement of the transmittance at longer wavelength [9-10, 32]. The enhancement of the transmittance at longer wavelength visibly exhibits in the total transmittance spectra of the composite films embedded with HSiNPs-1 and HSiNPs-2 as respectively shown in Figs. 5.7 (b) and (c). Nonetheless, the transmittance of the silica/UV-cured polymer composite film embedded with HSiNPs-5 maintains above about 80% at longer wavelength. It can be implied that Mie scattering potentially contributes in the HSiNPs-5 composite film. Based on the Mie scattering, intensity of the light scattering is independent to wavelength of the light propagation if size of the

scattering particles is comparable or larger than the wavelength [9, 33]. The light scattering greatly penetrates toward direction of the incident light.

To enhance more comprehension of the effect of scattering particle size, the cumulative size distribution of the different HSiNPs in UV-curable acrylate monomer dispersions was measured using the DLS. The results are shown in Fig. 5.8.

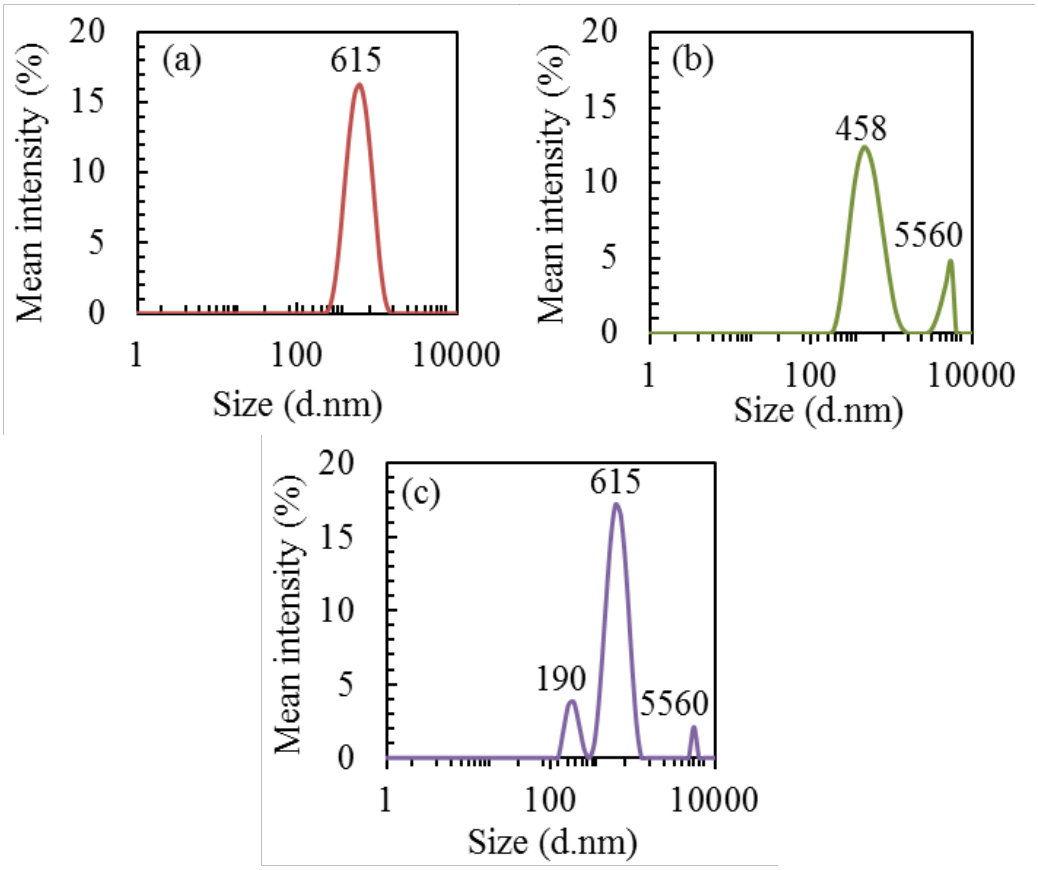

Fig. 5.8 The cumulative size distribution pattern of the HSiNPs in UV-curable acrylate monomer dispersions prepared by (a) HSiNPs-1, (b) HSiNPs-2 and (c) HSiNPs-5.

Fig. 5.8 (a) illustrates the size distribution of the HSiNPs-1, which is around 615.10 nm with a narrow distribution. Fig. 5.8 (b) displays the size distribution of the HSiNPs-2 that is obviously distinguished to two peaks. Such distinguished peaks are detected around 458.70 and 5560 nm. Fig. 5.8 (c) presents the size distribution of the HSiNPs-5 and exhibits the distinguished peak. According to the Fig. 5.8, there are three distinguished peaks that are respectively observed at 190.10, 615.10 and 5560 nm. When comparing the size distribution of the different HSiNPs, the HSiNPs-5 tends to provide a larger cumulative size therefore the surface properties of the particles possibly affect the cumulative size distribution of the particles in the dispersions. Based on the BET determination, the specific surface area of the HSiNPs-5 is about 143.15 m^2/g, which is the highest surface area to volume ratio as compared to other HSiNPs. The high surface area to volume expectedly contains high surface energy. The particles with high surface energy greatly tend to aggregate for minimizing their surface energies [34]. As a result, the cumulative size of the HSiNPs is in order of HSiNPs-1, HSiNPs-2 and HSiNPs-5 corresponding to the specific surface area results, while the cumulative size of the HSiNPs is also attributed to the strong interaction and strong adhesion between the particles [7]. The cumulative size of the HSiNPs can be inferred that almost the particles in the dispersions should be in aggregation forms. Consequently, the aggregation has an influence on the film formation with different roughness and morphologies which leads to distinctive optical properties and light diffusing properties [7]. Interestingly, the obtained particle sizes correspond to the size of scattering particles based on both Mie and Rayleigh scatterings. This can be implied that silica/UV-cured polymer composite films embedded with different HSiNPs probably exhibit both good light transmittance and good light diffusivity [10].

The diffuse transmittance of the silica/UV-cured polymer composite films embedded with different HSiNPs was studied using the spectrophotometer equipped with an integrating sphere. The results are shown in Fig. 5.9.

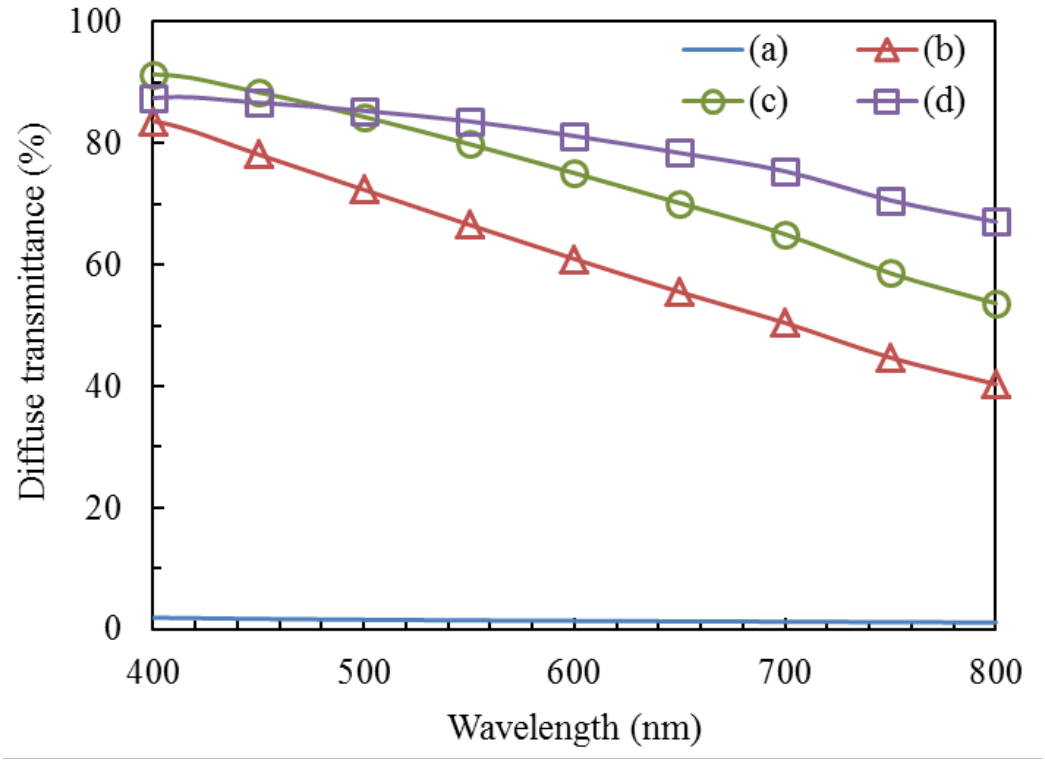

Fig. 5.9 Diffuse transmittance of the UV-cured polymer film (a) and the silica/UV-cured polymer composite films embedded with (b) HSiNPs-1, (c) HSiNPs-2 and (d) HSiNPs-5.

Figs. 5.9 (b), (c) and (d) are consecutively demonstrated the diffuse transmittance spectra of the composite films embedded with HSiNPs-1, HSiNPs-2 and HSiNPs-5. They reveal that the diffuse transmittance spectra of the composite films are significantly higher than that of the UV-cured polymer film (as shown in Fig. 5.9 (a)). It obviously proves that the presence of the HSiNPs improves the light diffusivity of the films. The improvement of the light diffusivity could be attributed to the inner light scattering [7, 9-10]. The inner light scattering is probably occurred by window cavities with in the shell and hollow interior structure of the HSiNPs [20]. In principle, the inner light scattering relates to the Mie scattering interfere with the Rayleigh scattering [8-10]. Meanwhile, the enhancement of the light diffuse transmittance also relates to the difference of refractive indices between top surface of the composite films and air (Rayleigh scattering) [9]. The Rayleigh scattering more contributes to longer wavelength of the light as compared to the Mie scattering [9-10]. Therefore, the simultaneous reduction of diffuse transmittance at the longer wavelength of the composite films embedded with HSiNPs-1, HSiNPs-2 as seen in the Fig. 5.9 (b) and (c) may be attributed to the Rayleigh scattering. Moreover, these results can be inferred that the diffuse transmittance of those composite films depends on wavelength of incident light. On the contrary, the characteristic is not detected in the HSiNPs-5 composite film (as seen in Fig. 5.9 (d)). The HSiNPs-5 composite film still maintains the high diffuse transmittance at longer wavelength so the wavelength of the incident light slightly affects it. This can be implied that the Mie scattering more probably occurs in the HSiNPs-5 film as compared to other composite films. Interestingly, at wavelength of 400 nm, the diffuse transmittance of the composite films embedded with HSiNPs-1, HSiNPs-2 and HSiNPs-5 (as shown in Fig. 5.9 (b), (c) and (d)) is approximately 84, 91

and 87 %, by respectively. They appear to be more than their total transmittance (as shown in Fig. 5.7 (b), (c) and (d)). It is more possibly that all the composite films have an anti-reflection property. According to the optical transmittances results, the silica UV-composite film embedded with HSiNPs-5 exhibits both of the high transparency and high diffusivity. Meanwhile, the morphologies results from the previous section, the HSiNPs-5 particles have thinner shell and larger hollow interior size as compared to other HSiNPs. Therefore, the composite film embedded with the particles which shell are thinner and the hollow interior are larger is more properly used to be fillers for optical diffusers in the LCD industry.

The Mie scattering not only supports the transmittance of the light but also enhances homogenization of the incident light [9]. The homogenization of the UV-cured polymer film and the silica/UV-cured polymer composite films embedded with different HSiNPs were studied using the apparatus equipped with the digital camera. The results, as shown in Fig. 5.10, are further used to be inferred the light diffusing ability of those films.

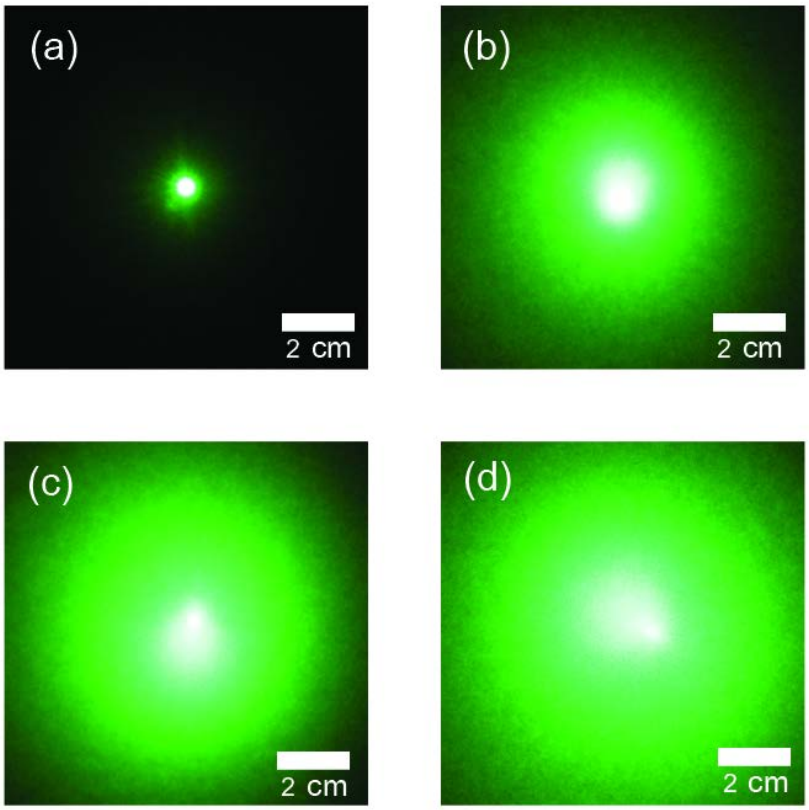

Fig. 5.10 The scattered light image of the UV-cured polymer film (a) and the silica/UV-cured polymer composite films embedded with (b) HSiNPs-1, (c) HSiNPs-2 and (d) HSiNPs-5.

Fig. 5.10 (a) shows the scattered light image of the UV-cured polymer film that present a small light spot among the dark area. The image can be inferred that the laser light propagation forms to small light spot with a little diffusing and other part apart from light is almost dark. On the contrary, the scattered light image of all composite films (as seen in Fig. 5.10 (b), (c) and (d)) is obviously larger than that of the UV-cured film. The images also reveal that the light scattering occurred by the HSiNPs in the films is able to occur at different angles of the incident light [8] before reforming by

itself [7]. The size of the scattered light image of the HSiNPs-1 composite film appears to be the smallest of the composite films, while the scattered light image size of the HSiNPs-5 composite film is largest and slightly larger than that of the HSiNPs-2 composite film. However, the appearance of the scattered light image of the HSiNPs-2 resembles to that of the HSiNPs-5 composite film. This is attributed to the surface morphologies of those films [35]. Meanwhile, the hollow interior size of the HSiNPs-2 and HSiNPs-5 particles is quite similar. Such similar size possibly allows the penetration of the light scattering to the films with the resemble characteristic. The sequence of the scattered light image size corresponds to the order of the diffuse transmittance of the composite films (Fig. 5.9 (b), (c) and (d)) due to the shell thickness of the HSiNPs. The range of the light scattering emerged from the composite film embedded with HSiNPs containing thicker shell (HSiNPs-1) is probably smaller than that with the HSiNPs containing thinner shell (HSiNPs-2 and HSiNPs-5). This is because the thicker shell can possibly absorb more the light scattering [20]. Consequently, the smaller range of the light scattering assembles to a smaller size of light spot homogenization [7] corresponding to the scattered light image of the HSiNPs-1 composite film in Fig. 5.10 (a). The distinct size of the scattered light images can be implied that the light diffusing ability of the films is significant different. The larger size of the scattered light image of the composite film should exhibit the higher light diffusing ability. Additionally, the results visibly confirm that the presence of the hollow silica nanoparticles existed of window cavities effectively improves the light diffusing ability of the UV-cured polymer film. Therefore, the hierarchical structure of the silica is one of the most effective light-weight fillers to apply for production of light diffuser films, especially in the LCD industry [7-9]. Consequently, the hierarchical

silica probably decreases the number of backlight unit in LCD resulting in energy-saving [8]. A schematic illustration of utilizing the hollow silica nanoparticles as fillers in light diffuser films in the LCD is shown in Fig. 5.11.

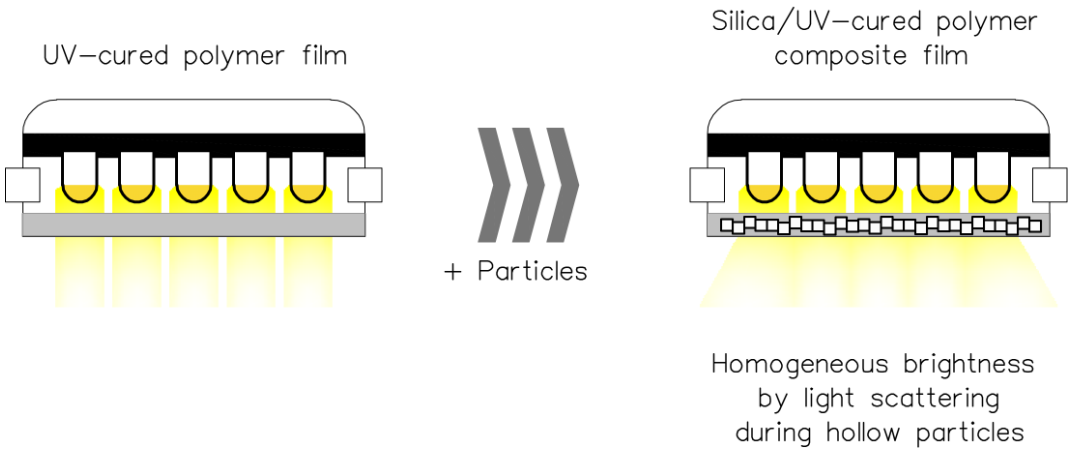

Fig. 5.11 schematic illustration of utilizing the hollow silica nanoparticles to be fillers in light diffuser films in the LCD.

5.3.2.2 Morphologies of the silica/UV-cured polymer composite films

A variety of optical transmittances and scattered light image size of the composite film possibly attributes to the morphologies of composite films [7-9, 32, 35, 36]. The morphologies of the composite films were therefore studied using the FE-SEM observation as shown in Fig. 5.12.

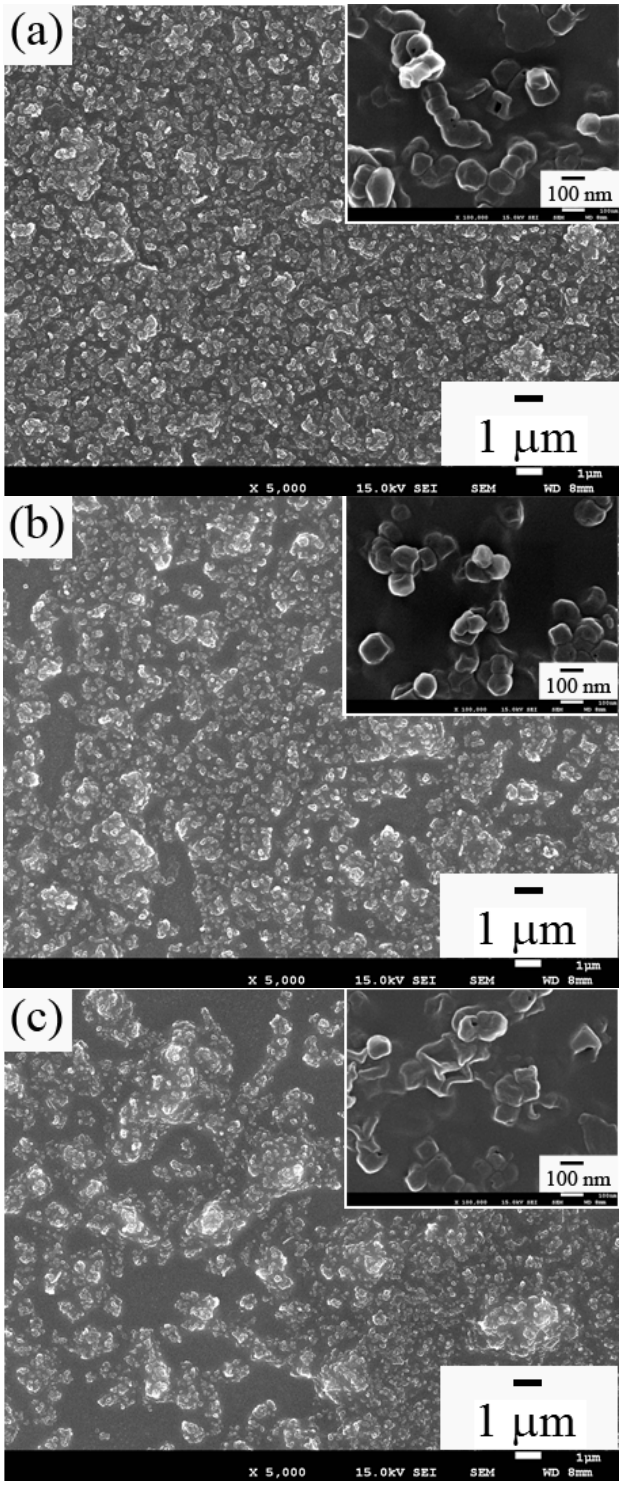

Fig. 5.12 The FE-SEM images of the UV-cured polymer film embedded with (a) HSiNPs-1, (b) HSiNPs-2 and (c) HSiNPs-5.

Fig. 5.12 (a) demonstrates the morphologies of the HSiNPs-1 composite film. It exhibits that the observed size of aggregates on the film surface is uniformly about 1 μm, which is obviously much larger than that of the HSiNPs-1 aggregates in the dispersion as shown in Fig. 5.8 (a). This result can possibly occur when the solvent has evaporated through the UV-curing process [37]. Moreover, the size of the aggregates is a random distribution. On the other hand, the observed size of aggregates obtained from the HSiNPs-2 composite film (as shown in Fig. 5.12 (b)) is a wide distribution with a good dispersibility. Fig. 5.12 (c) presents the FE-SEM image of the HSiNPs-5 composite film that reveals a wide distribution of aggregate size. The morphologies of the film are quite similar to those of the HSiNPs-2 composite film. The similarity of the morphologies is supported the evidence of the analogous scattered light image pattern of the HSiNPs-2 and HSiNPs-5 composite film [35]. Furthermore, multiple scattering probably occurs in all films embedded with HSiNPs because the particles almost appear in aggregate forms or clusters [38]. Therefore, the light scattering of each particle or cluster is dependent to each other. Consequently, both the incident light and the secondary light scattering cause the illumination of each particle. According to these behaviors, it can be inferred that the higher number of aggregates on the films, the more of multiple scattering provides. This leads to improve both total and diffuse transmittances. This reasonable explanation supports the high diffuse transmittance and larger size of the scattered light image of the HSiNPs-2 and HSiNPs-5 composite films. According to the film morphologies results, they can be implied that the HSiNPs-2 and HSiNPs-5 particles are more possibly used to fabricate silica UV-cured polymer composite film for the appropriate morphologies. Meanwhile, the synthesized HSiNPs contain window cavities on their shell, which is one of the hierarchical structures.

Therefore, it can be concluded that the hierarchical structure of HSiNPs possibly improves optical properties of the silica UV-cured polymer composite films, while the hierarchical hollow silica nanoparticles are potentially applied for fillers in optical diffusers in the LCD industry.

5.4 Conclusion

The morphologies and surface properties of the HSiNPs were successfully modified by HCl at different pH. The high pH of HCl produces HSiNPs with thinner shells, small window cavities and high specific surface area. The presence of the hierarchical structure of HSiNPs within the composite film improves both total and diffuse transmittances of the UV-cured polymer film. Remarkably, the silica/UV-cured polymer composite film embedded with HSiNPs-5 containing larger size of hollow interior, thinner shell and high specific surface area exhibits higher total transmittance (~80%) and higher diffuse transmittance (~80%) when comparing to other composite films. Its properties still maintain at longer wavelength. Moreover, the film gives the largest size of the scattered light image indicating its high light diffusing property. This is due to a good dispersibility of aggregates on the film surface. These results indicate that the distinct morphologies and surface properties of the HSiNPs are key factors to improve optical properties of the silica/UV-cured polymer composite films. Furthermore, HSiNPs-5 is more properly applied for fabricating the silica/UV-cured polymer composite films in order to achieve high optical transmittances and light diffusing property. In conclusion, HSiNPs with hierarchical structures are potentially to apply in the inorganic fillers in light diffuser films of backlight unit of LCDs. The utilization of

the hierarchical HSiNPs in LCDs probably reduces number of backlighting unit in the LCD industry leading to energy-saving and subsequently light-weight LCDs.

References

[1] H.P. Kuo, M.Y. Chuang and C.C. Lin, Design correlations for the optical performance of the particle-diffusing bottom diffusers in the LCD backlight unit, *Powder Technol.* **192** (2009) 116-121.

[2] B.T. Liu and Y.T. Teng, A novel method to control inner and outer haze of an antiglare film by surface modification of light-scattering particles, *J. Colloid Interface Sci*. **350** (2010) 421-426.

[3] J.H. Wang, S.Y. Lien, J.R. Ho, T.K. Shih, C.F. Chen, C.C. Chen and W.T. Whang, Optical diffusers based on silicone emulsions, *Opt Mater* **32** (2009) 374-377.

[4] T.C. Huang, J.R. Ciou, P.H. Huang, K.H. Hsieh and S.Y. Yang, Fast fabrication of integrated surface relief and particle-diffusing plastic diffuser by use of a hybrid extrusion roller embossing process, *Opt Express* **16** (2008) 440-447.

[5] S.J. Liu and Y.C. Huang, Manufacture of dual-side surface-relief diffusers with various cross angles using ultrasonic embossing technique, *Opt Express* **17** (2009) 18083-18092.

[6] D. Sakai, K. Harada, S. Kamemaru, M.A. El-Morsy, M. Itoh and T. Yatagai, Direct fabrication of surface relief holographic diffusers in azobenzene polymer films, *Opt Rev* **12** (2005) 383-386.

[7] S. Song, Y. Sun, Y. Lin and B. You, A facile fabrication of light diffusing film with LDP/polyacrylates composites coating for anti-glare LED application, *Appl. Surf. Sci.* **273** (2013) 652-660.

[8] J. Hu, Y. Zhou and T. Zhang, The novel optical diffusers based on the fillers of boehmite hollow microspheres, *Mater. Lett.* **136** (2014) 114-117.

[9] S. Guo, S. Zhou, H. Li and B. You, Light diffusing films fabricated by strawberry-like PMMA/SiO_2 composite microspheres for LED application, *J. Colloid Interface Sci* **448** (2015) 123-129.

[10] J. Hu, Y. Zhou, M. He and X. Yang, Novel multifunctional microspheres of polysiloxane@CeO_2-PMMA: Opitcal properties and their application in optical diffusers, *Opt. Mater.* **36** (2013), 271-277.

[11] H. Butt, K.M. Knowles, Y. Montelongo, G.A.J. Amaratunga and T.D. Wilkinson, Devitrite-Based Optical Diffusers, *ACS Nano* **8** (2014) 2929-2935.

[12] S. Ahn and G.H. Kim, An electrosprayed coating process for fabricating hemispherical PMMA droplets for an optical diffuser, *Appl Phys A* **97** (2009) 125-131.

[13] M. Fuji, T. Shin, H. Watanabe and T. Takei, Shape-controlled hollow silica nanoparticles synthesized by an inorganic particle template method, *Adv. Powder Technol.* **23** (2012) 562-565.

[14] M. Fuji, C. Takai, Y. Tarutani, T. Takei and M. Takahashi, Surface properties of nanosize hollow silica particles on the molecular level, *Adv. Powder Technol.* **18** (2007) 81-91.

[15] C. Takai, T. Ishino, M. Fuji and T. Shirai, Rapid and high yield synthesis of hollow silica nanoparticles using an NH_4F catalyst, *Colloids Surf., A* **446** (2014) 46-49.

[16] Q. Yue, Y. Li, M. Kong, J. Huang, X. Zhao, J. Liu and R.E. Willifor, Ultralow density hollow silica foams produced through interfacial reaction and their exceptional properties for environmental and energy applications, *J. Mater. Chem.* **21** (2011) 12041-12046.

[17] Y. Liao, X. Wu, H. Liu and Y. Chen, Thermal conductivity of powder silica hollow spheres, *Thermochim. Acta* **526** (2011) 178-184.

[18] Y. Du, L.E. Luna, W.S. Tan, M.F. Rubner and R.E. Cohen, Hollow silica nanoparticles in UV-visible antireflection coatings for poly(methyl methacrylate) substrates, *ACS Nano* **4** (2010) 4308-4316.

[19] S.W. Kim, M. Kim, W.Y. Lee and T. Hyeon, Fabrication of hollow palladium spheres and their successful application to the recyclable heterogeneous catalyst for Suzuki coupling reactions, *J. Am. Chem. Soc.* **124** (2002) 7642-7643.

[20] M.C. Tsai, J.Y. Lee, P.C. Chen, Y.W. Chang, Y.C. Chang, M.H. Yang, H.T. Chiu, I.N. Lin, R.K. Lee and C.Y. Lee, Effects of size and shell thickness of TiO_2 hierarchical hollow spheres on photocatalytic behavior: An experimental and theoretical study, *Appl. Catal., B* **147** (2014) 499-507.

[21] S.M. Marinakos, M. F. Anderson, J.A. Ryan, L.D. Martin and D.L. Feldhein, Encapsulation, permeability, and cellular uptake characteristics of hollow nanometer-sized conductive polymer capsules, *J. Phys. Chem. B* **105** (2001) 8872-8876.

[22] P. Tartaj, M.P. Morales, S. Veintemillas-Verdaguer, T. Gonalez-Carreno and C. J. Serna, The preparation of magnetic nanoparticles for applications in biomedicine, *J. Phys. D* **36** (2003) R182-R197.

[23] Y. Jiao, J. Guo, S. Shen, B. Chang, Y. Zhang, X. Jiang and W. Yang, Synthesis of discrete and dispersible hollow mesoporous silica nanoparticles with tailored shell thickness for controlled drug release, *J. Mater. Chem.* **22** (2012) 17636-17643.

[24] Y. Hu, Q. Zhang, J. Goebl, T. Zhang and Y. Yin, Control over the permeation of silica nanoshells by surface-protected etching with water, *Phys. Chem. Chem. Phys.* **12** (2010) 11836-11842.

[25] C. Takai, M. Fuji and K. Fujimoto, Skeletal Silica Nanoparticles Prepared by Control of Reaction Polarity, *Chem. Lett.* **40** (2011) 1346-1348.

[26] R.V.R. Virtudazo, H. Watanabe, T. Shirai, M. Fuji and M. Takahashi, Simple preparation and initial characterization of semi-amorphous hollow calcium silicate hydrate nanoparticles by ammonia-hydrothermal-template techniques, *J Nanopart Res* **15** (2013) 1604-1612.

[27] R. Filipović, D. Lazić, M. Perušić and I. Stijepović, Oil absorption in mesoporous silica particles, *Processing and Application of Ceramics* **4** (2010) 265-269.

[28] Z.Z. Li, L.X. Wen, L. Shao and J.F. Chen, Fabrication of porous hollow silica nanoparticles and their applications in drug release control, *J. Controlled Release* **98** (2004) 245-254.

[29] K.C.W. Wu, *Synthesis of Multi-functionalized Mesoporous Silica Nanoparticles for Cellulosic Biomass Conversion, in Heterogeneous Catalysis for Today's Challenges: Synthesis, Characterization and Application*; The Royal Society of Chemistry, 2015, DOI: 10.1039/9781849737494-00001.

[30] C. L. Mangun, M.A.Daley, R.D. Braatz and J. Economy, Effect of pore size on adsorption of hydrocarbons in phenolic-based activated carbon fibers, *Carbon* **36** (1998) 123-131.

[31] L.E. Mcneil and R.H. French, Multiple scattering from rutile TiO_2 particles, *Acta mater.* **48** (2000) 4571-4576.

[32] S.E. Yancey, W. Zhong, J.R. Heflin and A.L. Ritter, The influence of void space on antireflection coatings of silica nanoparticle self-assembled films, *J. Appl. Phys.* **99** (2006) 034313.

[33] R. Barchini, J.G. Gordon II and M.W. Hart, Multiple Light Scattering Model Applied to Reflective Display Materials, *Jpn. J. Appl. Phys.* **37** (1998) 6662-6668.

[34] W. Wu, Q. He and C. Jiang, Magnetic Iron Oxide Nanoparticles: Synthesis and Surface Functionalization Strategies, *Nanoscale Res Lett* **3** (2008) 397-415.

[35] J. Hegmann, M. Mandl and P. Löbmann, Sol-gel derived scattering layers as substrates for thin-film photovoltaic cells, *Thin Solid Films* **564** (2014) 201-205.

[36] J. Yoo, J. Lee, S. Kim, K. Yoon, I.J. Park, S.K. Dhungel, B. Karunagaran, D. Mangalaraj and J. Yi, High transmittance and low resistive ZnO:Al films for thin film solar cells, *Thin Solid Films* **480-481** (2005) 213-217.

[37] M. Sumiya and K. Yamada, Development of filterability test method for gel retention performance for UV curable ink jet inks, in: *Proc. NIP30: The 30th International Conference on Digital Printing Technologies and Digital Fabrication*. PA, United States, 2014.

[38] A. Rastar, M.E. Yazdanshenas, A. Rashidi and S.M. Bidoki, Theoretical review of optical properties of nanoparticles, *J. Eng. Fiber Fabr.* **8** (2013) 85-96.

CHAPTER 6

CONCLUDING REMARKS AND

POTENTIAL DIRECTION FOR FUTURE RESEARCH

6.1 Concluding remarks

This work successfully applied silica nanoparticles with a variety of structure for fabricating high optical properties films. The parameters on silica structure, a UV-curable acrylate monomer for balancing transmittance and haze of the films were mainly investigated. The hollow silica nanoparticles were synthesized by inorganic particle template method before further modifying their morphologies and surface properties to achieve a proper structure for being fillers in the films. A bar coating machine and a UV-photo surface processor were used for the film fabrication. The summary and conclusion of this thesis work are itemized as the following:

Chapter 2, a facile method to prepare the highly loaded silica nanoparticle dispersions is matching refractive indices of the silica nanoparticles and a UV-curable acrylate monomer. This method provides a long-term stability of silica dispersions during dark storage because of the reduction of particle-particle attraction forces. Therefore, the films prepared by coating these dispersions contain a high number of silica nanoparticles. Moreover, the total transmittances of the obtained films which are close to the bare glass indicate the films transparency. Although the multiplication of the silica nanoparticles in the UV-cured films does not significantly affect their transmittances, the presence of silica nanoparticles in the UV-cured films produces a significant difference in the diffuse transmittance. The thin solid silica UV-cured film containing 30 vol% silica nanoparticles exhibits the highest diffuse transmittance in this study, which is about 20%. This is due to the increase in the multiple scattering by the particles in the film. The increase of the silica nanoparticles in the UV-cured films also provides a good compatibility and good dispersion of the particles which is one of the main roles to improve the optical properties of the films. Therefore, it can be said that

the optical property of the thin solid silica UV-cured film depends on the amount and distribution of the silica nanoparticles.

In chapter 3, spherical silica nanoparticles containing dense structures were used to modify UV-cured acrylate films. The films were successfully fabricated by coating suspensions of silica-acrylate on cleaned glass substrates. The results revealed that the modified films had a high haze and large range of scattered light. The largest range of the scattered light was obtained from the film modified with 30 vol% spherical silica nanoparticles, which exhibited the transmittance about 60% and the haze about 0.26. The spherical silica nanoparticles may be utilized in the polymer films to obtain a high diffusing ability which is useful in the field of electronic display technologies.

In chapter 4, silica nanoparticles containing hollow structures which incorporated with UV-cured acrylate film were successfully done. The films were facilely fabricated with the suspension of hollow silica nanoparticles calcined at temperature of 400 °C and a UV-curable acrylate monomer solution was coated. The films become opaque when the amount of the hollow silica nanoparticles increases. The increased amount of hollow silica nanoparticles improves both of the optical properties and the light diffusing ability of the films. Interestingly, a film based on 20 vol% hollow silica nanoparticles gives the highest total transmittance (93%) and diffuse transmittance (40%) when comparing to other films in this study. Its total transmittance is also higher than that of the cleaned glass substrate. Meanwhile, the high amount of hollow silica nanoparticles in the films provides a larger size of the scattered light image. This can be implied that the films are able to diffuse the point or the line of the light source. Accordingly, the films based on the hollow silica nanoparticles as fillers are potentially applied for light diffuser films in LCDs.

In chapter 5, the morphologies and surface properties of hollow silica nanoparticles were prosperously controlled by varying pH of HCl in the core-template removal process. The low pH of HCl produces the thicker shell and larger window cavities of the hollow silica nanoparticles while the high pH of HCl provides the higher specific surface area of those. Meanwhile, the presence of hollow silica nanoparticles, which contain larger size of hollow interiors, thinner shells, larger window cavities and high specific surface area, in the silica/UV-cured polymer composite film exhibits higher total transmittance (~80%) and higher diffuse transmittance (~80%) when comparing to other composite films and still maintains at longer wavelength. Moreover, the film gives the largest size of the scattered light image indicating its high light diffusing property. Therefore, the distinct morphologies and surface properties of the hollow silica nanoparticles significantly affect the optical properties and the morphologies of the resulting films. According to these results of the study, the hollow silica nanoparticles with hierarchical structure are one of the effective inorganic fillers for light diffuser films.

Based on the above mentioned results, they can be concluded that the structures and morphologies of silica, including its aggregation size are main factors to improve optical transmittances and light diffusing ability of UV-cured acrylate films. These are due to all silica structures provides more light refraction event inside the films than orginal UV-cured acrylate films. Meanwhile, the silica containing a hollow structure more possibly allows light penetration via its hollow interior. It slightly absorbs light on its solid shell. Furthermore, the hollow structure of silica, which has a window cavity, a thin shell, a large hollow interior, dramatically improves diffuse transmittance and light diffusing ability of the films that are better than those of the films embedded with the

dense structure of silica. Therefore, the hollow silica nanoparticles with hierarchical structure are one of the effective inorganic fillers for light diffuser films. The films can be applied for optical diffusers of the backlight unit of liquid crystal display (LCD) screens. Consequently, utilizing the hierarchical hollow silica nanoparticles in the field of optical diffusers probably reduce the number of backlight unit in the LCD industry leading to energy saving and subsequently light-weight LCD screens.

6.2 Potential directions for future research

The accomplishment of the different structures of silica nanoparticles which utilized for fabricating high optical properties films has provided opportunities to tune their morphologies and surface properties. These advantages have in turn exploration of light interaction in a film with respect to apply as a light diffuser film of back light unit in the LCD industry. The light diffuser film not only requires high optical performance, but also need other proper properties; for example, mechanical, thermal, UV-shielding, fluorescence, well NIR absorption and durability. Therefore, silica surface of both dense and hollow structures should be developed for further research in order to match with other binder resins for serving with diverse electronic devices.

RESEARCH ACTIVITIES

Publications

Chapter 2

[1] **W. Suthabanditpong**, R. Buntem, C. Takai, M. Fuji and T. Shirai, The quantitative effect of silica nanoparticles on optical properties of thin solid silica UV-cured films, *Surf. Coat. Technol.* **279** (2015), 25-31.

Chapter 3

[2] **W. Suthabanditpong**, C. Takai, M. Fuji, R. Buntem and T. Shirai, Studies of optical properties of UV-cured acrylate films modified with spherical silica nanoparticles, *Adv. Powder Technol.*, Article in press, DOI: 10.1016/j.apt.2016.01.022.

Chapter 4

[3] **W. Suthabanditpong**, M. Tani, C. Takai, M. Fuji, R. Buntem and T. Shirai, Facile fabrication of light diffuser films based on hollow silica nanoparticles as fillers, *Adv. Powder Technol.,* Article in press, DOI: 10.1016/j.apt.2016.01.028.

Oral/poster presentation

2015

[1] "Studies on optical properties of UV-cured acrylate films modified by dense silica nanoparticles" (Oral)

W. Suthabanditpong, M. Fuji, R. Buntem, C. Takai and T. Shirai

The 11th International Conference on Ceramic Materials and Components for Energy and Environmental Applications (CMCEE), Vancouver, Canada, Jun. 14-19, 2015.

ACKNOWLEDGEMENTS

This dissertation could not have been accomplished if it had not been contributed by people surrounding this project. I therefore would like to thank those.

First, I deeply appreciate and admire my supervisor, Prof. Masayoshi Fuji, for his patience and professional advices throughout the completion of this dissertation. I am also thankful for his invaluable guidance, kind and moral supports concerning all my complications apart from the studies during my stay in Japan.

I am thankful to committee members- Prof. Takashi Ida and Prof. Nobuyasu Adachi for their valuable insights and constructive comments on the earlier version of my work to make it more scientifically relevant.

I wish to express my deepest gratitude to Assoc. Prof. Takashi Shirai and Dr. Chika Takai who constant help and generous support with invaluable advice during the progress of my doctoral studies. They always gave good comments and responded with great compliments towards my experimental works especially during our end-report seminar presentation. I also wish to convey my sincere thanks to Dr. Hadi Razavi-Khosroshahi for his invaluable help for observing my hollow silica particles in TEM during entire periods of my research.

Many thanks to all the colleagues in Advanced Ceramics Research Center (ACRC) for their supporting including for the lively and enthusiastic discussions on food, daily news, the intricacies of the Japanese language and cultures. Those memorable moments are what made the ACRC my second home.

Also, I cannot forget the kindness of the office secretaries of ACRC, Mrs Shiho Yoshinaga, Mrs Tomomi Hayashi, Mrs Michiko Michimura and Mrs Kumiko Wakai, for the supporting during my stay in Japan and for the fast execution and processing of my pertinent official documents.

I wish to thank the Advanced Low Carbon Technology Research and Development Program (ALCA) of the Japan Science and Technology Agency (JST), and Research Assistantship offered in the Processing Group of ACRC for financial support of my research work. I am also thankful to the JSR Corporation for supplying UV-curable acrylate monomer, and to the Admatechs, Co. Ltd. for supplying the silica nanoparticles. Many thanks are extended to the GRANDEX, Co. Ltd. for providing the hollow silica nanoparticles, and to the Shiraishi Calcium Kaisha, Ltd. for providing the calcium carbonate.

My deep appreciation is extended to Asst. Prof. Dr. Radchada Buntem for her encouragement in taking-up further studies. A special thank goes to all of my lovely friends for their everlasting supports/prayers.

Finally, I am deeply indebted and grateful to my parents, my brothers and my sisters, for their unconditional love and moral support, and for being the greatest family on earth. The love and encouragements kept me going during challenging times in Japan.

Walaiporn Suthabanditpong